UNIVERSITY OF OKLAHOMA

GRADUATE COLLEGE

CONSIDERATION OF LIE SYMMETRY GROUPS IN COMPUTATIONAL FLUID DYNAMICS

A DISSERTATION

SUBMITTED TO THE GRADUATE FACULTY

in partial fulfillment of the requirements for the

Degree of

DOCTOR OF PHILOSOPHY

By

ERSIN OZBENLI

Norman, Oklahoma

2018

CONSIDERATION OF LIE SYMMETRY GROUPS IN COMPUTATIONAL FLUID DYNAMICS

A DISSERTATION APPROVED FOR THE
SCHOOL OF AEROSPACE AND MECHANICAL ENGINEERING

BY

Dr. Prakash Vedula, Chair

Dr. M. Cengiz Altan

Dr. Wilson E. Merchán-Merchán

Dr. Jivtesh Garg

Dr. Dimitrios Papavassiliou

This dissertation is dedicated to my parents and grandparents for their unconditional love and support:

Mehmet Özbenli (Father)
Ayşe Özbenli (Mother)
Remzi Özbenli (Grandfather)
Züleyha Özbenli (Grandmother)

Acknowledgements

I would like to express my sincere gratitude to my committee chair and adviser Dr. Prakash Vedula, who has set an example of excellence as a mentor and role model, for his invaluable guidance and support throughout the development of this dissertation. I will be forever thankful not only for the extra hours he took from his busy schedule just to help me overcome problems related to my research, but also for his persistent effort in preparing me for the life in academia. Without his guidance, this dissertation would have not been possible. I would also like to express my deepest appreciation to my committee member Dr. M. Cengiz Altan for his invaluable contributions to my development as a researcher. His dedication to research and persistent efforts to mentor graduate students were truly inspirational to me. Further, I would like to thank my outside committee member Dr. Dimitrios Papavassiliou and other committee members Dr. Wilson E. Merchán-Merchán and Dr. Jivtesh Garg not only for participating in my dissertation committee but also for their valuable comments and feedback. I will be forever grateful. I also want to thank the Ministry of National Education of Turkey for providing me with a scholarship that simply funded me throughout my graduate life. And last but not least, I would like to express my deepest appreciation and sincere gratitude to my parents, for their unconditional love and support, and my wife for her persistent encouragement, support, and love.

Contents

Acknowledgements **v**

List of Tables **ix**

List of Figures **xi**

Abstract **xvi**

1 Introduction **1**
1.1 Motivation 1
1.2 Historical Preface of Group Theory 2
1.3 Lie Symmetry Groups 4
1.4 Symmetry Preservation in Numerical Schemes 6
1.5 Scope of the Dissertation 11

2 Lie Symmetry Analysis of Differential Equations **16**
2.1 Scope of the Chapter 16
2.2 Introduction to Lie symmetry Analysis 16
2.3 Applications and Discussion 23
2.3.1 Chemically Reactive Boundary Layer flow 23
2.3.2 Boundary Layer flow over a Wedge with Slip 29
2.3.3 Analysis of Stagnation Point Conditions in an Inviscid, Compressible Blunt-Body Flow 33

3 Numerical Solution of Modified Differential Equations based on Symmetry Preservation **40**
3.1 Scope of the Chapter 40
3.2 Mathematical Formulation and Moving Frames 41
3.3 Method of Modified Equations 44
3.3.1 Linear Advection Equation 44
3.3.2 Inviscid Burgers' Equation 47
3.4 Construction of Invariant Modified Schemes 48
3.4.1 Linear Advection Equation in 1D 48
3.4.2 Linear Advection Equation in 2D 52
3.4.3 Inviscid Burgers' Equation 54
3.5 Numerical Experiments 57
3.5.1 Linear Advection Equation in 1D 57
3.5.2 Linear Advection Equation in 2D 61

3.5.3 Inviscid Burgers' Equation . . . 63
3.6 Chapter Summary . . . 67

4 High Order Accurate Finite Difference Schemes based on Symmetry Preservation 70
4.1 Scope of the Chapter . . . 70
4.2 Construction of High Order Invariant Schemes . . . 72
4.2.1 Linear Advection-Diffusion Equation in 1D . . . 73
4.2.2 Inviscid Burgers' Equation . . . 77
4.2.3 Viscous Burgers' Equation . . . 84
4.2.4 Linear Advection-Diffusion Equation in 2D . . . 86
4.3 Numerical Experiments . . . 91
4.3.1 Linear Advection-Diffusion Equation in 1D . . . 91
4.3.2 Inviscid Burgers' Equation . . . 94
4.3.3 Viscous Burgers' Equation . . . 98
4.3.4 Linear Advection-Diffusion Equation in 2D . . . 100
4.4 Chapter Summary . . . 102

5 Construction of Invariant Compact Finite Difference Schemes 106
5.1 Scope of the Chapter . . . 106
5.2 Mathematical Formulation . . . 107
5.2.1 Construction of Compact Schemes . . . 107
5.2.2 Invariantization of Compact Schemes . . . 109
5.3 Development of Invariant Compact Schemes . . . 110
5.3.1 Inviscid Burgers' Equation . . . 110
5.3.2 Linear Advection-Diffusion Equation in 1D . . . 114
5.3.3 Viscous Burgers' Equation . . . 116
5.3.4 Linear Advection-Diffusion Equation in 2D . . . 118
5.4 Results and Discussion . . . 120
5.4.1 Inviscid Burgers' Equation . . . 121
5.4.2 Linear Advection-Diffusion Equation in 1D . . . 123
5.4.3 Viscous Burgers' Equation . . . 124
5.4.4 Linear Advection-Diffusion Equation in 2D . . . 129
5.5 Chapter Summary . . . 131

6 Construction of Invariant Schemes for Euler Equations 135
6.1 Scope of the Chapter . . . 135
6.2 Introduction . . . 136
6.3 Mathematical background and Symmetry Methods . . . 138
6.3.1 Euler Equations in 1D . . . 138
6.3.2 Euler Equations in 2D . . . 140
6.4 Invariant schemes . . . 141
6.4.1 Invariant Lax-Friedrichs Scheme . . . 142

6.4.2 Invariant van Leer Flux Splitting scheme 145
6.5 Results and Discussion 146
6.6 Chapter Summary 157

7 Summary and Future Work **158**
7.1 Scope of the Chapter 158
7.2 Research Highlights 158
7.2.1 Chapter Summaries 159
7.3 Future Research 162
7.3.1 Extensions of Scope to Address Limitations 162
7.3.2 Extensions to More General Problems 163

Bibliography **168**

Appendix A An Invariant MUSCL Scheme for Solution of Euler Equations in 1D **181**

Appendix B Lie Symmetry Groups of Euler Equations in 3D **185**

Appendix C Lie Symmetry Groups of Incompressible Navier-Stokes Equations **188**

List of Tables

3.1 Root mean square error (RMSE) and L_∞ error in numerical solutions of advection equation obtained from various numerical schemes for $\tau = 0.01,\ h = 0.2,$ and $\alpha = 1$. 60
3.2 Root mean square error (RMSE) and L_∞ error in numerical solutions of inviscid Burgers' equation obtained from various schemes, with $\tau = 0.01,$ and $h = 0.05$ 63
3.3 Root mean square error (RMSE) and L_∞ error in numerical solutions of inviscid Burgers' equation (in the case of a Riemann problem) obtained from various schemes for $\tau = 0.01,$ and $h = 0.05$ 66

4.1 Root mean square error (RMSE) and L_∞ error associated with numerical solutions for linear advection-diffusion equation. 92
4.2 Root mean square error (RMSE) and L_∞ error associated with numerical solutions for inviscid Burgers' equation. 95
4.3 Root mean square error (RMSE) and L_∞ error associated with numerical solutions for the viscous Burgers' equation. 99

5.1 Root mean square error (RMSE) and L_∞ error associated with numerical solutions (based on compact schemes) for the inviscid Burgers' equation. 121
5.2 Root mean square error (RMSE) and L_∞ error associated with numerical solutions (based on compact schemes) for the one-dimensional linear advection-diffusion equation. 124
5.3 Root mean square error (RMSE) and L_∞ error associated with numerical solutions (based on compact schemes) for the viscous Burgers' equation. 126
5.4 Variation of RMSE and L_∞ errors associated with numerical solutions presented in figure 5.7 (left) with respect to the Galilean parameter c. 127
5.5 Variation of RMSE and L_∞ errors associated with numerical solutions presented in figure 5.7 (right) with respect to the Galilean parameter c. 127
5.6 Root mean square error (RMSE) and L_∞ error associated with numerical solutions (based on compact schemes) for two-dimensional linear advection-diffusion equation. 129

6.1 Initial configurations for one-dimensional Euler equations. 147
6.2 L_∞ and RMSE errors (based on velocity u) for Euler equations in 1D. 148
6.3 Two-dimensional Euler equations. Initial data for *case* 1. 153
6.4 Two-dimensional Euler equations. Initial data for *case* 2. 154

6.5 Two-dimensional Euler equations. Initial data for *case* 3. 155
6.6 Two-dimensional Euler equations. Initial data for *case* 4. 156

A.1 Initial configurations for one-dimensional Euler equations. 182

List of Figures

2.1 Mapping of points on a curve from a source space to a target space. . 18
2.2 Stream function (F), velocity (F'), and concentration (G) versus the distance from the surface (α). Parameter settings: $left: S = 0,\ \gamma = 0,\ \beta = 0.1,\ Sc = 0.7,\ right: S = 0.1,\ \gamma = 0.1,\ \beta = 0.1,\ Sc = 0.7$ 28
2.3 Boundary layer flow over a Wedge. 30
2.4 Representation of stagnation point in a blunt-body flow. 34

3.1 Advection equation (1D). Comparison of profiles of u (at $t = 2$) obtained from the exact solution, first order upwind scheme, and proposed invariant scheme is shown in the left figure. Spatial distributions of percentage errors are shown in the right figure. Parameter settings: $\tau = 0.05,\ h = 0.2,\ \alpha = 1,$ and $f = \epsilon_{mach}$. 58
3.2 L_∞ errors associated with numerical solutions of advection equation (1D) versus number of grid points for a fixed Courant number, $C = 0.5$. 59
3.3 Advection equation (1D). Comparison of profiles of u (at $t = 2$) obtained from the exact solution, and the numerical solutions is shown in the left figure. Spatial distributions of percentage errors are shown in the right figure. Parameter settings: $\tau = 0.01,\ h = 0.2,$ and $\alpha = 1$. 60
3.4 Advection equation (2D). Spatial distributions of numerical errors obtained from the upwind scheme (left) and the proposed invariant scheme (right). Parameter settings: $\tau = 0.05,\ h = k = 0.2,\ \alpha = \beta = 0.5$ where $\varepsilon = u_a - u_n$. 62
3.5 L_∞ errors associated with numerical solutions of two-dimensional advection equation as a function of number of grid points. Parameter settings: $h = k,\ \alpha = \beta = 0.5$, and $\tau/h = 0.25$. 62
3.6 Inviscid Burgers' equation. Comparison of profiles of u (at $t = 0.5,\ 1.5$) obtained from the exact and numerical solutions is shown in the left figures. Spatial distribution of percentage errors is shown in the right figures. Parameter settings: $\tau = 0.05,$ and $h = 0.05$. 64
3.7 L_∞ errors of numerical solutions of inviscid Burgers' equation versus number of grid points for fixed $\tau/h = 0.5$. 65
3.8 Inviscid Burgers' equation. Comparison of shock profiles of u (at $t = 0.5$) obtained from the exact solution, first order upwind scheme, Lax-Wendroff scheme, modified upwind scheme, and proposed (conservative and non-conservative) invariant schemes. Parameter settings: $\tau = 0.01,$ and $h = 0.05$. 66

4.1 Linear advection-diffusion equation (1D). Comparison of profiles of $u(t,x)$, at $t=1$, obtained from the analytical solution (Exact), the classical base scheme (FTCS), the modified scheme (MOD-FTCS), and the proposed invariant scheme (SYM) is shown in the left figure. Spatial distribution of errors obtained from these schemes is displayed in the right figure. Parameter settings: $\tau=0.025,\ h=0.05,\ \alpha=1$, and $\nu=1/60$. 92
4.2 Linear advection-diffusion equation (1D). Comparison of L_∞ errors of numerical schemes as a function of number of grid points. 93
4.3 Inviscid Burgers' equation. Comparison of profiles of $u(t,x)$, at $t=0.5$, obtained from the analytical solution (Exact), the classical base scheme (FTCS), the modified scheme (MOD-FTCS), the proposed invariant scheme SYM-1, and the proposed invariant scheme SYM-2 is shown in the left figure. Spatial distribution of errors is displayed in the right figure. Parameter settings: $\tau=0.1,\ h=0.2$. 95
4.4 Inviscid Burgers' equation. Comparison of L_∞ errors of numerical schemes as a function of number of grid points for a constant ratio of discrete step variables, $\tau/h=0.5$. 96
4.5 Inviscid Burgers' equation. Comparison of L_∞ errors of numerical schemes as a function of number of grid points for a constant ratio of discrete step variables, $\tau/h=0.01$. 97
4.6 Viscous Burgers' equation. Comparison of shock formation profiles, at $t=0.25$, obtained from the analytical solution (Exact), the classical base scheme (FTCS), the modified scheme (MOD-FTCS), and the proposed invariant scheme (SYM) is shown in the left figure. Spatial distribution of errors is displayed in the right figure. Parameter settings: $h=0.05$, $\tau=0.005,\ \nu=1/12$. 99
4.7 Viscous Burgers' equation. Comparison of L_∞ errors of numerical schemes as a function of number of grid points. 100
4.8 Linear advection-diffusion equation (2D). Spatial distributions of numerical errors, at $t=0.5$, obtained from the classical base scheme (left) and the proposed invariant scheme (right). Parameter settings: $h=0.05,\ \tau=0.005,\ \alpha=0.5,\ \beta=0.5,\ \nu=1/60$. 101
4.9 Linear advection-diffusion equation (2D). Comparison of L_∞ errors of numerical schemes as a function of number of grid points. 102

5.1 Inviscid Burgers' equation. Comparison of velocity profiles, at $t=0.5$, obtained from the analytical solution (Exact), the classical forward in time central in space (FTCS) scheme, the standard compact scheme (COMP), and the proposed invariant compact scheme (SYM) is shown in the left plot. Spatial distribution of errors for these numerical schemes is shown in the right figure. Parameter settings: $h=0.2$, $\tau=0.001$, and $\sigma=0.5$ 122

5.2 Inviscid Burgers' equation. Comparison of L_∞ errors of numerical schemes versus number of grid points. 122
5.3 Advection-diffusion equation (1D). Snapshots of velocity profiles, at $t = 1.0$, obtained from the analytical solution (Exact), the classical forward in time central in space (FTCS) scheme, the standard compact scheme (COMP), and the proposed invariant compact scheme (SYM) are displayed in the left figure. Spatial distribution of errors is displayed in the right figure. Parameter settings: $h = 0.2$, $\tau = 0.001$, $\nu = 1/60$. 124
5.4 Advection-diffusion equation (1D). Comparison of L_∞ errors of numerical schemes versus number of grid points. 125
5.5 Viscous Burgers' equation. **Left**: snapshots of shock formation profiles, at $t = 0.25$, obtained from the analytical solution, the classical FTCS scheme, the standard compact scheme (COMP), and the proposed invariant compact scheme (SYM). **Right**: spatial distribution of errors for these numerical schemes (right). Parameter settings: $h = 0.063$, $\tau = 0.0001$, $\nu = 1/12$. 126
5.6 Viscous Burgers' equation. Comparison of L_∞ errors of numerical schemes versus number of grid points. 126
5.7 Viscous Burgers' equation. Snapshots of numerical solutions, obtained from the analytical solution (Exact), classical forward in time central in space (FTCS) scheme, standard compact scheme (COMP), and proposed invariant compact scheme (SYM), evolving from various initial profiles for different values of the Galilean parameter c. **Left:** $h = 0.1$, $\tau = 0.0001$, $\nu = 0.05$, **Right:** $h = 0.02$, $\tau = 0.0005$, $\nu = 0.01$. 127
5.8 Linear advection-diffusion equation (2D). Spatial distributions of numerical errors, at $t = 0.1$, obtained from the classical base scheme (left) and the proposed invariant scheme (right). Parameter settings: $h = 0.16$, $\tau = 0.0001$, $\alpha = 1.0$, $\beta = 1.0$, $\nu = 1/60$. 129
5.9 Advection-diffusion equation in 2D. Comparison of L_∞ errors of numerical schemes versus number of grid points. 130

6.1 Representation of a shock-tube in 1D (top) and 2D (bottom) at $t = 0$. 147
6.2 Euler equations in 1D (*case* 1). Snapshots of exact solution (solid line) and numerical solution based on Lax-Friedrichs scheme (+) at $t = 0.1$. Parameter settings: $h = 0.0025$, $CFL = 0.4$. 147
6.3 Euler equations in 1D (*case* 1). Snapshots of exact solution (solid line) and numerical solution based on invariant Lax-Friedrichs scheme (+), SYM-1, at $t = 0.1$. Parameter settings: $h = 0.0025$, $CFL = 0.4$. . 148
6.4 Euler equations in 1D (*case* 1). Snapshots of exact solution (solid line) and numerical solution based on invariant Lax-Friedrichs scheme (+), SYM-2, at $t = 0.1$. Parameter settings: $h = 0.0025$, $CFL = 0.4$. . 148

6.5 Euler equations in 1D (*case* 1). Snapshots of exact solution (solid line) and numerical solution based on van Leer flux vector splitting scheme (+), at $t = 0.1$. Parameter settings: $h = 0.0025$, $CFL = 0.4$. . 149
6.6 Euler equations in 1D (*case* 1). Snapshots of exact solution (solid line) and numerical solution based on invariant van Leer flux vector splitting scheme (+), SYM-2, at $t = 0.1$. Parameter settings: $h = 0.0025$, $CFL = 0.4$. 149
6.7 Euler equations in 1D (*case* 2). Snapshots of exact solution (solid line) and numerical solution based on Lax-Friedrichs scheme (+), at $t = 0.05$. Parameter settings: $h = 0.0025$, $CFL = 0.4$. 150
6.8 Euler equations in 1D (*case* 2). Snapshots of exact solution (solid line) and numerical solution based on invariant Lax-Friedrichs scheme (+), SYM-2, at $t = 0.05$. Parameter settings: $h = 0.0025$, $CFL = 0.4$. 150
6.9 Euler equations in 1D (*case* 2). Snapshots of exact solution (solid line) and numerical solution based on van Leer flux vector splitting scheme (+), at $t = 0.05$. Parameter settings: $h = 0.0025$, $CFL = 0.4$. . 151
6.10 Euler equations in 1D (*case* 2). Snapshots of exact solution (solid line) and numerical solution based on invariant van Leer flux vector splitting scheme (+), at $t = 0.05$. Parameter settings: $h = 0.0025$, $CFL = 0.4$. 151
6.11 Euler equations in 1D (*case* 3). Snapshots of exact solution (solid line) and numerical solution based on Lax-Friedrichs scheme (+), at $t = 0.02$. Parameter settings: $h = 0.0025$, $CFL = 0.4$. 152
6.12 Euler equations in 1D (*case* 3). Snapshots of exact solution (solid line) and numerical solution based on invariant Lax-Friedrichs scheme (+), SYM-2, at $t = 0.02$. Parameter settings: $h = 0.0025$, $CFL = 0.4$. 152
6.13 Euler equations in 1D (*case* 3). Snapshots of exact solution (solid line) and numerical solution based on van Leer flux vector splitting scheme (+), at $t = 0.02$. Parameter settings: $h = 0.0025$, $CFL = 0.4$. . 152
6.14 Euler equations in 1D (*case* 3). Snapshots of exact solution (solid line) and numerical solution based on invariant van Leer flux vector splitting scheme (+), at $t = 0.02$. Parameter settings: $h = 0.0025$, $CFL = 0.4$. 152
6.15 Euler equations in 2D (*case* 1). Snapshots of numerical solutions, at $t = 0.2$, obtained from a high resolution reference scheme (left), standard Lax-Friedrichs scheme (middle), and invariant Lax-Friedrichs scheme (right). Parameter settings: $h = 0.00125$, $CFL = 0.475$. 153
6.16 Euler equations in 2D (*case* 2). Snapshots of numerical solutions, at $t = 0.2$, obtained from a high resolution reference scheme (left), standard Lax-Friedrichs scheme (middle), and invariant Lax-Friedrichs scheme (right). Parameter settings: $h = 0.00125$, $CFL = 0.475$. 154

6.17 Euler equations in 2D (*case* 3). Snapshots of numerical solutions, at $t = 0.15$, obtained from a high resolution reference scheme (left), standard Lax-Friedrichs scheme (middle), and invariant Lax-Friedrichs scheme (right). Parameter settings: $h = 0.0025$, $CFL = 0.475$. 155
6.18 Euler equations in 2D (*case* 4). Snapshots of numerical solutions, at $t = 0.2$, obtained from a high resolution reference scheme (left), standard Lax-Friedrichs scheme (middle), and invariant Lax-Friedrichs scheme (right). Parameter settings: $h = 0.00125$, $CFL = 0.475$. 156

A.1 Euler equations in 1D (*case* 1). Snapshots of exact solution (solid line) and numerical solution based on the invariant MUSCL scheme with minmod limiter (+). Parameter settings: $h = 0.002$, $CFL = 0.25$, $t = 0.05$. 183
A.2 Euler equations in 1D (*case* 2). Snapshots of exact solution (solid line) and numerical solution based on the invariant MUSCL scheme with minmod limiter (+). Parameter settings: $h = 0.002$, $CFL = 0.25$, $t = 0.02$. 183

Abstract

Lie symmetries are fundamental properties of differential equations that are often not actively considered in construction of numerical schemes relevant to computational fluid dynamics (CFD). While many of these numerical schemes in CFD are constructed based on consideration of a desired order of accuracy and have shown promising results, these schemes usually do not accurately represent fundamental symmetry (or invariance) properties of underlying governing equations. The overall objective of this dissertation is to address this limitation via development of numerical schemes that not only preserve Lie symmetries of underlying differential equations but also ensure a desired order of accuracy.

In this regard, novel methodologies for construction of high order accurate invariant numerical schemes, based on the method of equivariant moving frames, are introduced. Formulation of high order accurate invariant schemes presented in this work involves consideration of (a) modified equations (via perturbation or defect correction) and/or (b) compact schemes. Modified forms of equations are used not only to achieve a desired order of accuracy in associated invariant schemes but also to systematically select convenient moving frames. Further, in the construction of invariant compact schemes, extended symmetry groups of differential equations are considered where point transformations based on these extended groups are used to transform existing base schemes to their invariant forms. Construction and performance of symmetry preserving numerical schemes are discussed for a variety of linear and nonlinear canonical problems (such as linear advection-diffusion equation in 1D/2D, inviscid Burgers' equation, viscous Burgers' equation along with application to Euler equations in 1D/2D). The overall quality of results obtained

from constructed invariant numerical schemes is often found to be notably better than that of standard, non-invariant base numerical schemes. Such improvements in results are particularly more significant when error measures based on symmetry properties of underlying differential equations are considered.

CHAPTER 1

Introduction

1.1 Motivation

In traditional computational fluid dynamics (CFD), fundamental symmetry properties of differential equations are not often considered in development of numerical schemes as the focus is mostly on obtaining a desired order of accuracy in resulting schemes. It is reasonable to expect that preservation of underlying symmetries in numerical schemes could lead to better performance, in the context of accuracy and computational efficiency. Recent developments in the study of geometric integrators are good examples of how preservation of selected geometric properties of equations (such as energy and symplecticity properties or Hamiltonian and Poisson structures of equations) could enhance the quality of results obtained from numerical solutions [1–13]. While Lie symmetries also represent important fundamental geometric properties of differential equations, their inclusion in numerical schemes relevant to CFD has been limited despite the expected benefits.

The primary objective of this dissertation is to address this limitation and to contribute to the current state of knowledge in this regard via presentation of a detailed framework for construction of high order accurate numerical schemes that retain Lie symmetry properties of underlying differential equations relevant to problems in CFD. The main motivation for this objective is that, by preserving symmetries of differential equations (which are fundamental geometric properties) in associated numerical schemes, accuracy and efficiency of these finite difference schemes can be significantly enhanced, and hence these schemes would perform notably better than

those that do not preserve symmetries. The secondary objective of this dissertation involves demonstration of the procedure for an effective use of Lie symmetry analysis to obtain group invariant solutions for a variety of problems ranging from boundary layer flows to hypersonic flows.

For the remainder of this dissertation, we shall attempt to demonstrate how these objectives are achieved starting from a brief description of Lie symmetry groups.

1.2 Historical Preface of Group Theory

In 19^{th} century, the theory of equations was one of the main research topics in mathematics. The French mathematician Evariste Galois (1811 - 1832) proposed the first detailed classification of equations in the form of $a_0\,x^n + a_1\,x^{n-1} + a_2\,x^{n-2} + \cdots + a_n\,x^0 = 0$. He explored general solutions of such equations by involving lower order equations with roots that are functions of these equations [14, 15]. To this end, Galois introduced the notion of "degree of symmetry" of algebraic equations that is described by a set of special permutations of relations between the roots of these equations. Such a set of permutations (that transform all the algebraic relations between the roots of equations to other relations between the same roots) was assumed to have certain properties such as containing an identity permutation, an inverse permutation, and the permutation that is obtained from the product of any two permutations contained in the set. Galois is accepted to be the first mathematician to call such a special set a "group" which is the basic element of the group theory in mathematics.

Marius Sophus Lie (1842 - 1899), a Norwegian mathematician, started his study by investigating continuous groups of transformations (which are usually referred to as Lie groups) that leave differential equations invariant. Lie was the first to use the theory of continuous groups systematically for finding solutions and describing symmetry properties of differential equations. At his time, Lie's approach for solving

differential equations was very highly valued by many mathematicians. However, owing to the rise of computers around 1950s, the general approach for solving the problem of differential equations was systematically transferred to computers, and hence the notion of solvability of differential equations lost its previous importance along with the Lie theory of differential equations. But in the beginning of 1970s, the Lie group theory started to draw attention again when physicists realized that Lie's theory is not only about solving differential equations but also a tool that can be used to systematically identify symmetry properties of differential equations and physicists started to actively use Lie group theory in elementary particle physics [15].

Today, Lie group theory (or Lie symmetry analysis) is used in many different areas of research due to its practical applications and the insight that it brings to describe physical systems. In this regard, one of the main advantages of symmetry analysis is that symmetry properties of equations can be exploited to achieve simplifications in definitions of these equations. In the case of differential equations, these simplifications could be in the forms of order and/or dimension reduction. Symmetries also represent fundamental information regarding conservation laws that describe a physical phenomenon and hence provide a systematic means for an enriched understanding of the phenomenon and the associated conservation laws. Note that, in this regard, Noether's theorem states that every differentiable symmetry has a corresponding conservation law [16]. As a result, knowledge of symmetry properties of equations often opens alternative pathways to approach problems when searching for solutions. Therefore, it is usually a good practice to analyze symmetry properties of equations before a solution strategy (whether it is analytic or numeric) is decided.

In the following section, a more detailed description of the Lie symmetry groups along with its usage in fluid dynamics is presented.

1.3 Lie Symmetry Groups

In mathematics and related fields, an expression is said to possess a symmetry property if one can transform every variable in the expression according to some transformations such that the resulting expression reads exactly the same as the original form of the expression. In this context, a group is an algebraic structure that consists of a set of elements that are equipped with a binary operation that satisfies the following group axioms:

i. existence of inverse element,

ii. existence of identity element,

iii. associativity property,

iv. and closure.

In particular, a Lie symmetry group is a group that is also a smooth manifold as it consists of a set of continuous symmetries that correspond to smooth transformations that, when implemented, map a system to itself in the transformed space. If these symmetries are coordinate transformations, then such groups are called Lie point symmetry groups.

Lie symmetry properties of equations (which are fundamental geometric properties) are frequently considered in many disciplines. In particular, in areas such as finance, differential geometry, high energy physics, and fluid dynamics, Lie symmetry analysis is a fundamental tool and has a wide range of applications [14,15,17–22]. For instance, Lie symmetry groups are often used to obtain group invariant solutions and conservation laws for differential equations relevant to fluid dynamics [23–32]. These symmetry groups are also used for reduction purposes where high order differential equations are usually simplified to lower orders with smaller number of variables. Well-known examples in this area could be those relevant to boundary

layer flows where self-similar solutions are obtained from similarity variables that are determined through Lie symmetry analysis [33–36]. In this regard, Cantwell [33] presented a study where symmetry properties of the two-dimensional stream-function equation were used to determine similarity transformations that lead to self-similar solutions for the underlying PDE. The author also extended this work to the case where kinematic viscosity in the stream-function equation is zero ($\nu = 0$) corresponding to the Euler equations. Additionally, a detailed discussion on other symmetry groups associated with these equations was also included in this work.

In another work, Boutros *et al.* [34] investigated non-linear equations of motion describing laminar, incompressible flow in a rectangular domain with porous walls in the case of successive expansions and contractions with Lie symmetry analysis. Symmetry properties of the relevant differential equations were used to obtain simpler reduced forms for these equations which involve the use of similarity variables determined from these symmetry groups. In a similar work, Avramenko *et al.* [35] used Lie symmetry groups to investigate the differential equations relevant to the process of heat, momentum, and concentration transport in a boundary layer of a nanofluid near a flat wall. Self-similar solutions were identified for these differential equations, and later these solutions were used to evaluate the effects of concentration of nanoparticles on the velocity and temperature profiles as well as on the skin-friction coefficients and relative Nusselt numbers. Further, in a more recent study, Jalil and Asghar [36] presented a detailed work on boundary layer flow of a power-law fluid over a permeable stretching surface. The authors used Lie symmetry analysis to identify possible similarity transformations that lead to self-similar solutions for the associated differential equations. They then evaluated the performance of these self-similar solutions under various flow configurations. In addition to the above examples, many other works exist in various fields where the benefits of Lie symmetry analysis are realized.

1.4 Symmetry Preservation in Numerical Schemes

In the area of numerical analysis, a great deal of effort has been devoted to construction of high order accurate and efficient numerical solutions for partial differential equations as analytical solutions are rarely present [37–39]. Many different methodologies (i.e., finite-volume [39, 40], finite-element [41], and finite difference [42, 43] methods) have been proposed in the literature to approximate solutions for such differential equations. In fluid dynamics and related fields, high order accuracy and efficiency are usually desired in numerical solutions, especially in numerical prediction of complex flows. There exist different approaches to construct such high order accurate and efficient numerical schemes. One approach to achieving high order accuracy is through the method of modified equations, where numerical accuracy of low order schemes is commonly enhanced by introduction of additional terms obtained from truncation error analysis of these low order base schemes, which is also known as defect correction [44–53]. A well-known study by Warming and Hyett [44] is among the first examples of the method of modified equations. In this work, the authors demonstrated the improvement in accuracy of finite difference schemes for some linear and nonlinear PDEs by considering their modified forms. Here the modified forms of difference equations were obtained by first expanding every term of the equation in a Taylor series and then eliminating the time derivatives higher than first order through algebraic manipulations. In another work, Chu [47] presented a method to improve accuracy of low order schemes by introducing special discrete time steps along with non-iterative defect correction procedures. The author successfully constructed high order schemes for some common linear and nonlinear problems. In a more recent work, Razi *et al.* [49] proposed an approach for construction of high order schemes that is based on modified equations and adaptive grids. In this study, the leading error terms of difference equations are removed from

schemes by non-iterative defect corrections, and the singular perturbations of modified equations are regularized by using adaptive grids. The authors demonstrate the application of the method by developing high order accurate schemes for some linear and nonlinear hyperbolic PDEs. Similarly, in a related work, Wasserman *et al.* [51] proposed a robust multigrid method for simulation of chemically-reacting turbulent flows where defect correction procedures are used to improve the coarse-grid-correction in localized regions of high chemical activity. The defect correction procedures considered in this work are based on use of alternative, stable discretization of convection and diffusion operators on coarse levels where the desired order of accuracy on fine-grids are still retained. Despite the common use of modified equations for the purpose of achieving high order accuracy, this technique is not always preferred in construction of high order schemes due to possible increase in the computational cost and cumbersome numerical representations.

Compact finite differencing based on Padé approximants is another commonly used method for construction of high order numerical schemes that is well-documented in the literature. An important objective of this method is to achieve high order accuracy with a relatively small number of stencil points by relating a weighted sum of functions (or dependent variables) to a weighted sum of derivatives evaluated at grid points [54–63]. Hence, numerical solutions based on compact schemes are found to have good spectral-like resolutions (solutions that exponentially converge with increasing resolution) especially in the case of short waves [54]. In this regard, Hirsh [54] presented a detailed application of compact finite differencing which included development and application of fourth order accurate compact schemes to three test problems namely viscous Burgers' equation, Howarth's retarded boundary layer flow, and the incompressible driven cavity problem. The author also provided a brief discussion on how to treat boundary conditions when developing compact finite difference schemes which could be problematic in some cases. The results ob-

tained from the application of the fourth order scheme to the selected test problems were found to be significantly more accurate than standard second order schemes. In another well-known work, Lele [55] extended the earlier works on compact finite differencing by presenting finite difference schemes that provide a better representation of shorter length scales for use on problems with a range of spatial scales. In addition, the author provided a detailed discussion on how to obtain compact finite difference schemes of different orders (up to tenth order) and treat the relevant boundary conditions. In a more recent study, Shukla *et al.* [60] presented a family of high order compact finite-difference schemes that are built on non-uniform grids with spatial orders of accuracy ranging from 4th to 20th. These compact schemes are constructed such that they maintain high order accuracy not only in the interior of a domain but also at its boundaries. The authors demonstrated the application of these compact schemes to the linear wave equation and two-dimensional incompressible Navier-Stokes equations and verified the achievement of high order accuracy for these problems. They further showed (via comparisons with benchmark solutions for the two-dimensional driven cavity flow, thermal convection in a square box, and flow past an impulsively started cylinder) that these high order compact schemes are stable and produce highly accurate results on stretched grids with more points clustered at boundaries.

Although the method of modified equations and compact finite difference schemes can be used to construct high order accurate numerical schemes, in these methods, the geometric properties of underlying differential equations are usually disregarded as the focus is usually on the accuracy of resulting numerical schemes. Numerical schemes that preserve certain geometric properties (i.e., energy, momentum, symplecticity, Hamiltonian and Poisson structures) of equations are categorized under geometric integrators. It is shown in many cases that the overall quality of results obtained from such geometric integrators could be significantly better than those ob-

tained from classical numerical schemes [1–13, 64–67]. In an early work in the area, Channell and Scovel [2] presented algorithms to numerically integrate trajectories of Hamiltonian dynamical systems along with a detailed discussion of earlier works. The algorithms presented in this work exactly preserve the symplectic 2-form (such as all Poincaré invariants) and have been tested on a variety of examples. Results obtained from these algorithms were found to possess long-time stability property and preserve global geometrical structures in phase space. In a more recent work, Gong *et al.* [10] introduced a systematic approach for discretizing general multi-simplectic formulations of Hamiltonian PDEs, including a local energy preserving algorithm, a class of global energy preserving methods and a local momentum preserving algorithm. The implementation of the methods in this work is illustrated by the nonlinear Schrödinger equation and Korteweg-de Vries equation where the numerical experiments clearly verified the conservative properties of the proposed methods. In a similar work, Li and Wu [13] proposed and analyzed some energy preserving functionally fitted methods, in particular, trigonometrically fitted methods of an arbitrary high order for solving oscillatory nonlinear Hamiltonian systems with a fixed frequency. Numerical experiments on oscillatory Hamiltonian systems such as the FPU problem and the nonlinear Schrödinger equation were conducted to evaluate the performance of these methods and results obtained from these solutions were found to be highly accurate.

Lie symmetry groups of differential equations are also geometric properties that could be preserved in numerical schemes. Various researchers have proposed methods for preserving symmetry groups of equations in associated numerical schemes [68–92]. Most of the works in this subject could be categorized into two major groups. In the first group [68–76], an approach based on Lie symmetry analysis is used to determine finite difference invariants of difference equations. Next a set of these invariants which converges to the original equation in the continuous limit is

used to construct an invariant scheme. The latter could be difficult to achieve in the case of multidimensional problems. In this regard, Dorodnitsyn [68] proposed a method to construct finite difference equations together with difference grids that admit the symmetry groups that are isomorphic to the symmetry groups of the original differential model. Eventually, this leads to existence of exact invariant finite difference schemes and conservation laws for invariant variation problem. The implementation of the method is demonstrated through examples such as heat equation and wave equation.

In a related work, Bakirova *et al.* [69] presented three characteristic examples of the construction of finite difference equations and meshes where Lie groups of the original differential equation are preserved in these discrete models. A detailed discussion on the application of the method is also provided in Bakirova *et al.* [69], which uses heat equation with a source as an example. In a more recent work, Xiang-Peng *et al.* [73] presented a procedure for constructing discrete models for multidimensional nonlinear evolution equations that preserve all the Lie symmetry groups of underlying differential equations. The main difference between this work and earlier works is that in this work, the authors construct discrete models for potential equations instead of original differential equations. As an example, the authors consider the $(2+1)$-dimensional Burgers' equation and constructed invariant discrete models that preserve all continuous symmetries of this equation.

In the second group [83–94], invariant finite difference equations are constructed via equivariant moving frames. The invariantization procedure involves determination of point transformations based on Lie symmetry groups and implementation of these transformations in selected non-invariant base finite difference schemes to find their invariant forms [83–86]. In this method, unknown symmetry parameters that appear in the point transformations are usually determined via method of moving frames [83, 95]. In this regard, the first work was published by Fels and

Olver [83, 84] who introduced the theoretical aspects of general theory of moving frames. The authors formulated a practical and easy implementation of explicit methods to compute moving frames, invariant differential forms, differential invariants and operators and hence solve for finite dimensional Lie group actions. A detailed discussion on application of these methods ranging from differential equations to differential geometry were presented in this work as well. Almost a decade later, Kim [85–87] introduced an invariantization method for difference equations where the general theory of moving frames are used to determine unknown symmetry parameters in point transformations that are obtained from Lie groups of relevant differential equations. The author also provided a detailed discussion on practical application of the method where symmetry preserving numerical schemes were constructed for heat equation and Viscous Burgers' equation. The methods (for construction of invariant numerical schemes) proposed in this dissertation are also based on the method of equivariant moving frames. In this context, we extend the earlier works by proposing different methods for construction of high order accurate invariant finite difference schemes (including compact schemes) with a desired order of accuracy. We show the implementation of the proposed methodologies in a variety of problems, including the implementation in one- and two-dimensional Euler equations.

1.5 Scope of the Dissertation

In the context of the previously mentioned objectives, the remainder of the dissertation is organized in the following manner. A comprehensive discussion on Lie symmetry analysis that lays out the steps involved in the determination of Lie symmetry groups of differential equations is presented in Chapter 2. Further, to demonstrate the implementation of Lie symmetry analysis, various test problems relevant to incompressible boundary layer flows over different wall configurations and analy-

sis of stagnation point state of an inviscid, compressible flow past a blunt-body are also considered in this chapter, where similarity transformations determined from Lie symmetry groups of underlying differential equations are used to obtain group invariant solutions for these problems. Here it is important to note that, in most cases, Lie symmetry analysis makes it possible to systematically identify similarity transformations, for the purpose of finding self-similar solutions for differential equations, as opposed to predicting these similarity transformations based on intuition and other more difficult approaches.

In Chapter 3, we propose a method to construct invariant finite difference schemes for solution of partial differential equations (PDEs) via consideration of modified forms of the underlying PDEs. The invariant schemes, which preserve Lie symmetries, are obtained based on the method of equivariant moving frames. While it is often difficult to construct invariant numerical schemes for PDEs owing to complicated symmetry groups associated with cumbersome discrete variable transformations, we note that symmetries associated with more convenient transformations can often be obtained by appropriately modifying the original PDEs. In some cases, modifications to the original PDEs are also found to be useful in order to avoid trivial solutions that might arise from particular selections of moving frames. In our proposed method, modified forms of PDEs can be obtained either by addition of perturbation terms to the original PDEs or through defect correction procedures. These additional terms, whose primary purpose is to enable symmetries with more convenient transformations, are then removed from the system by considering moving frames for which these specific terms go to zero. Further, we explore selection of appropriate moving frames that result in improvement in accuracy of invariant numerical schemes based on modified PDEs. The proposed method is tested using the linear advection equation (in 1D and 2D) and the inviscid Burgers' equation. Results obtained for these tests cases indicate that numerical schemes developed

through the proposed method perform significantly better than existing schemes not only by virtue of improvement in numerical accuracy but also due to preservation of qualitative properties or symmetries of the underlying differential equations.

In Chapter 4, we present a novel mathematical approach that is based on modified equations and the method of equivariant moving frames for construction of high order accurate invariant finite difference schemes that preserve Lie symmetry groups of underlying partial differential equations (PDEs). In the proposed approach, invariant (or symmetry preserving) numerical schemes with a desired (or fixed) order of accuracy are constructed from some non-invariant (base) numerical schemes. Modified forms of PDEs are used to improve order of accuracy of existing schemes where modified forms are obtained through addition of defect correction terms to the original forms of PDEs. These defect correction terms of modified PDEs that are noted from truncation error analysis are either completely removed from schemes or their representation is significantly simplified by considering convenient moving frames. This feature of the proposed method can especially be useful to avoid cumbersome numerical representations when high order schemes are developed from low order ones via the method of modified equations. The proposed method is demonstrated via construction of invariant numerical schemes with fixed (and higher) order of accuracy for some common linear and nonlinear problems (including the linear advection-diffusion equation in 1D and 2D, inviscid Burgers' equation, and viscous Burgers' equation) and the performance of these invariant numerical schemes is further evaluated. Results suggest that such invariant numerical schemes obtained from existing base numerical schemes have the potential to significantly improve the quality of results not only in terms of desired higher order accuracy but also in the context of preservation of appropriate symmetry properties of underlying PDEs.

In Chapter 5, we propose another novel method for development of high order

accurate invariant compact finite difference schemes that retain Lie symmetry properties of underlying partial differential equations. In this method, variable transformations that are obtained from the extended symmetry groups of underlying PDEs are used to transform independent and dependent variables and derivative terms of compact finite difference schemes (constructed for these PDEs) such that the resulting compact numerical schemes are invariant under the chosen symmetry groups. The unknown symmetry parameters that arise from the application of these transformations are determined through selection of convenient moving frames. In some cases, due to selection of convenient moving frames, numerical representations of the invariant (or symmetry preserving) compact numerical schemes that are developed through the proposed method are found to be notably simpler than those of the standard compact numerical schemes. Further, the order of accuracy of these invariant compact schemes can be arbitrarily set to a desired order by considering suitable compact finite difference algorithms. The application of the proposed method is demonstrated through construction of invariant compact finite difference schemes for some common linear and nonlinear PDEs (including the linear advection-diffusion equation in 1D/2D, the inviscid equation in 1D, and the viscous Burgers' equation in 1D). Results obtained from these simulations indicate that the invariant compact schemes not only inherit selected symmetry properties of underlying PDEs but are also comparably more accurate than the standard non-invariant schemes.

In Chapter 6, one- and two-dimensional Euler equations of gas dynamics are considered and symmetry preserving finite difference schemes are constructed for these equations. Two different discretization methods, namely Lax-Friedrichs and Van-Leer flux splitting schemes, are used to solve the Euler equations for various initial conditions. Results obtained from these invariant schemes suggest that the invariant schemes not only store important geometric properties of Euler equations

but also yield accurate numerical results. The proposed schemes can be used as a basis to further enhance the state of knowledge regarding the numerical solution of the Euler equations by harvesting certain advantages that become available with symmetry preservation.

The final chapter, Chapter 7, and appendices (Appendix B and Appendix C) of this dissertation include a summary of the main results obtained from various chapters of this dissertation along with a detailed discussion on possible issues and ideas for future work. In the appendices, a discussion on preliminary results regarding construction of invariant finite difference schemes for the solution of the three-dimensional Euler equations and multidimensional incompressible Navier-Stokes equations is presented. Further, the full Lie symmetry groups of these equations and the steps involved in determination of relevant point transformations are also included in these appendices.

CHAPTER 2

Lie Symmetry Analysis of Differential Equations

2.1 Scope of the Chapter

In this chapter, the standard procedure to determine Lie symmetry groups of differential equations is presented in detail. A discussion on the available computational tools for determination of Lie symmetry groups of differential equations is also included. Further, the use of Lie symmetry analysis to obtain group invariant solutions and/or self-similar solutions for differential equations is demonstrated through three examples. In the first test problem, Lie symmetry analysis is used to obtain self-similar solutions for a chemically reactive, incompressible boundary layer flow over a stretching flat surface. Similarly, in the second test problem, self-similar solutions are found for incompressible boundary layer flow over a wedge with slip boundaries. And finally, in the last test problem, group invariant solutions are obtained to describe the state of the stagnation point conditions in an inviscid, compressible flow past a blunt-body. Results obtained from these solutions are also discussed in this chapter.

2.2 Introduction to Lie symmetry Analysis

Recall that in mathematics, an expression is said to possess a symmetry property if one can transform every variable (i.e., independent and dependent) in that expression according to a transformation such that the final form of the resulting output reads exactly the same as the original form of the expression. This expression is

also said to be invariant under the action of that particular transformation. In this context, let the following be a one-parameter Lie symmetry group

$$\begin{aligned} \tilde{x}^j &= \tilde{x}^j(\mathbf{x}, \mathbf{u}, s) \\ \tilde{u}^i &= \tilde{u}^i(\mathbf{x}, \mathbf{u}, s) \end{aligned} \tag{2.1}$$

where s is the symmetry parameter that defines a one-to-one invertible map from a source space $S : (\mathbf{x}, \mathbf{u})$ to a target space $\tilde{T} : (\tilde{\mathbf{x}}, \tilde{\mathbf{u}})$ as shown in figure 2.1. The functions $\tilde{x}^j(\mathbf{x}, \mathbf{u}, s)$ and $\tilde{u}^i(\mathbf{x}, \mathbf{u}, s)$ are continuous analytic functions of the symmetry parameter s that are expandable in Taylor series about any value of s. Here, it is important to note that, although both the source function $E(x, u, s)$ and target function $\epsilon(\tilde{x}, \tilde{u})$ are shown on different coordinate systems in figure 2.1, these functions are expanded about the source point for only small values of s, hence the target points are only infinitesimal distance away [14]. Therefore, the source and target functions are considered to be on the same coordinate system. The one-parameter Lie group given in Eq. (2.1) has infinitely many members corresponding to a possible value of the group parameter s. This property ensures that the transformation functions $\tilde{x}^j(\mathbf{x}, \mathbf{u}, s)$ and $\tilde{u}^i(\mathbf{x}, \mathbf{u}, s)$ are always differentiable and therefore, can be expanded in Taylor series about any value of s. Further, the outcome curve formed on the target space, $\epsilon(\tilde{x}, \tilde{u})$, is strictly dependent on the symmetry parameter s. Different values of s will lead to different curves. A particularly interesting case occurs when the resulting function $E(x, u, s)$ reads exactly the same as the target function $\epsilon(\tilde{x}, \tilde{u})$ with the symmetry parameter s vanishing from the expression:

$$\epsilon(\tilde{x}, \tilde{u}) = E(x, u, s) = \epsilon(x, u) \ .$$

For this particular case, all points on the curve ϵ are mapped to other point on the same curve. In other words, the curve ϵ is mapped to itself, and therefore, said to

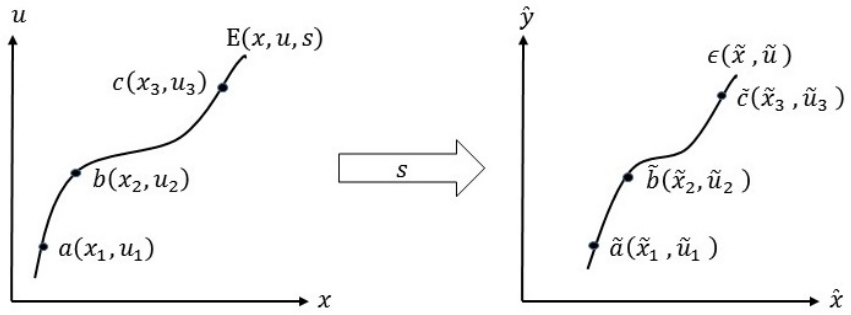

Fig. 2.1. Mapping of points on a curve from a source space to a target space.

be invariant under the action of the Lie group given in Eq. (2.1). Note that this invariance condition does not only apply to independent and dependent variables but also to every derivative term of the curve ϵ as shown below

$$\epsilon(\tilde{x}, \tilde{u}, \frac{d\tilde{u}}{d\tilde{x}}, \cdots) = \epsilon(x, u, \frac{du}{dx}, \cdots) \ .$$

So far, we only demonstrated invariance of differential equations under a one-parameter Lie group. Determination of such Lie groups that leave differential equations unchanged under the action of such groups is another aspect of Lie symmetry analysis that is well-documented in the literature [15, 20–22, 33].

Let us briefly illustrate the procedure to determine Lie symmetry groups of differential equations. In this regard, let the surface $\epsilon(\mathbf{x}, \mathbf{u}, \mathbf{u}_1, \mathbf{u}_2, \cdots, \mathbf{u}_p)$ be a pth-order differential equation associated with a Lie group G, where the vectors $\mathbf{x} = (x^1, x^2, \cdots, x^n)$ and $\mathbf{u} = (u^1, u^2, \cdots, u^n)$ represent the independent and dependent variables, respectively, and $\mathbf{u}_p$ indicates the vector of all possible pth-order derivatives. We seek the Lie group G that will leave the surface ϵ invariant as follows:

$$\epsilon(\tilde{\mathbf{x}}, \tilde{\mathbf{u}}, \tilde{\mathbf{u}}_1, \tilde{\mathbf{u}}_2, \cdots, \tilde{\mathbf{u}}_p) = \epsilon(\mathbf{x}, \mathbf{u}, \mathbf{u}_1, \mathbf{u}_2, \cdots, \mathbf{u}_p) \tag{2.2}$$

In order for the relation in Eq. (2.2) to hold true, the following invariance condition

must be satisfied

$$\mathbf{X}_{[p]}\,\epsilon(\mathbf{x},\,\mathbf{u},\,\mathbf{u}_1,\cdots,\mathbf{u}_p)=0\ , \qquad (\mathrm{mod}\,\epsilon=0) \tag{2.3}$$

where, $\mathbf{X}_{[p]}$ is the pth order extended (or prolonged) group operator that is given by

$$\mathbf{X}_{[p]}=\xi^j\frac{\partial}{\partial x^j}+\eta^i\frac{\partial}{\partial u^i}+\cdots+\eta^i_{[j_1\cdots j_p]}\frac{\partial}{\partial u^i_{j_1j_2\cdots j_p}}\ . \tag{2.4}$$

The group operator is usually extended such that it accounts for all the derivatives in the surface ϵ. In the above equation, ξ^j and η^i are the coordinate functions (or group infinitesimals) that determine how the coordinate variables (i.e., independent and dependent variables) transform under the action of the group, and $\eta^i_{[j_1\cdots j_p]}$ is pth extended coordinate function that determines how the pth derivative is transformed under the action of the applied group and is given by the following:

$$\eta^i_{[j_1\cdots j_p]}=D_{j_p}\eta^i_{[j_1\cdots j_{p-1}]}-u^i_{j_1\cdots j_{p-1}k}D_{j_p}\xi^k \tag{2.5}$$

where D_{j_p} represents total derivative operator [14]. Once these coordinate functions are determined, the associated Lie groups can be inferred from these functions. Let us illustrate this procedure through an example. Consider the one-dimensional inviscid Burgers' equations whose form is given by the following:

$$\Omega(t,x,u,u_t,u_x)\,=\,u_t+u\,u_x\,=\,0\ . \tag{2.6}$$

We seek for the Lie group G that will satisfy the invariance condition $\Omega(\tilde{t},\tilde{x},\tilde{u},\tilde{u}_{\tilde{t}},\tilde{u}_{\tilde{x}})=\Omega(t,x,u,u_t,u_x)$. Applying a once extended group operator of the form

$$\mathbf{X}_{[1]}=\zeta\frac{\partial}{\partial t}+\xi\frac{\partial}{\partial x}+\eta\frac{\partial}{\partial u}+\eta_{[t]}\frac{\partial}{\partial u_t}+\eta_{[x]}\frac{\partial}{\partial u_x} \tag{2.7}$$

to the inviscid Burgers' equation given in Eq. (2.6)

$$\mathbf{X}_{[1]}\,\Omega = 0, \qquad (\mathrm{mod}\;\Omega = 0)$$

yields the following relation:

$$\eta_{[t]} + u_x\,\eta + u\,\eta_{[x]} = 0 \tag{2.8}$$

where $\eta_{[t]}$ and $\eta_{[x]}$ are the once extended coordinate functions that determine how the first derivatives of u (with respect to t and x) transform under the action of the group and can be found from the following relations:

$$\begin{aligned} \eta_{[t]} &= \eta_t + u_t\,\eta_u - u_x\,(\xi_t + u_t\,\xi_u) - u_t\,(\zeta_t + u_t\,\zeta_u) \\ \eta_{[x]} &= \eta_x + u_x\,\eta_u - u_x\,(\xi_x + u_x\,\xi_u) - u_t\,(\zeta_x + u_x\,\zeta_u)\ . \end{aligned} \tag{2.9}$$

By substituting Eq. (2.9) into Eq. (2.8), and replacing u_t with $-u\,u_x$ (which is inferred from the invariance condition as it holds on Eq. (2.6)), the following relation is obtained

$$\eta_{[t]} + u_x\eta + u\eta_{[x]} = (u^2\zeta_x + u\zeta_t - u\xi_x - \xi_t + \eta)u_x + (\eta_t + u\eta_x) = 0\ . \tag{2.10}$$

In the above equation, x, t, and u are completely independent in the context of infinitesimals and the coordinate functions (ζ, ξ, and η) are only functions of these independent variables. As there is no restriction on the derivatives of u, the latter equation can be considered as an identity in the powers of the derivatives u_t and u_x, and therefore, setting the coefficients of these terms to zero results in the following overdetermined set of linear PDEs that are commonly referred to as the determining

equations:

$$\begin{aligned} u^2\zeta_x + u\zeta_t - u\xi_x - \xi_t + \eta = 0 \\ \eta_t + u\eta_x = 0 \ . \end{aligned} \tag{2.11}$$

The determining equations can be solved either analytically or through ansatz made on the form of the coordinate functions, and the solution of these equations gives the coordinate functions (ζ, ξ, and η) of the group G (that leaves the inviscid Burgers' equation invariant). One approach to solve this set of linear PDEs is to assume the coordinate functions of the group G are polynomials and therefore, a power series solution is applicable (through the substitution of these coordinate functions into the determining equations) [14]. Software modules capable of symbolic computations are also available on various platforms (i.e., Mathematica, Maple, Macsyma) for obtaining solutions for such systems and for finding Lie symmetry groups of differential equations [14,96,97]. For the inviscid Burgers' equation, the related coordinate functions (obtained from the solution of the associated determining equations) are found to be

$$\zeta = s_1\, t^2 + s_2\, t\, x + 2 s_3\, t + s_5\, x + s_6 \tag{2.12}$$

$$\xi = s_1\, t\, x + s_2\, x^2 + s_3\, x + s_4\, t + s_7 \tag{2.13}$$

$$\eta = s_1\, (x - t\, u) + s_2\, u\, (x - t\, u) - s_3\, u + s_4 - s_5\, u^2 \tag{2.14}$$

where each symmetry parameter $s_{i=1,\cdots,6}$ represents a subgroup of the group G and can be associated to a specific group operator $X_{i=1,\cdots,6}$. For this particular solution of the coordinate functions, it can be seen that Eq. (2.10) is indeed satisfied as

shown in the relation below:

$$\begin{aligned}\eta_{[t]} + u_x\eta + u\eta_{[x]} =&(u^2(s_2t+s_5)+u(2s_1t+s_2x+2s_3)-u(s_1t+2s_2x+s_3)\\ &-(s_1x+s_4)+(s_1x-s_1tu+s_2xu-s_2tu^2-s_3u \\ &+s_4-s_5u^2))u_x+((-s_1u-s_2u^2)+u(s_1+s_2u))=0\ .\end{aligned} \tag{2.15}$$

In the coordinate functions (or group infinitesimals) given in Eqs. (2.12)–(2.14), both s_1 and s_2 represent projection groups,

$$X_1 = t^2\,\frac{\partial}{\partial t} + x\,t\,\frac{\partial}{\partial x} + (x - t\,u)\,\frac{\partial}{\partial u} \tag{2.16}$$

$$X_2 = t\,x\,\frac{\partial}{\partial t} + x^2\,\frac{\partial}{\partial x} + u\,(x - t\,u)\,\frac{\partial}{\partial u} \tag{2.17}$$

s_3 represents a scaling group,

$$X_3 = 2\,t\,\frac{\partial}{\partial t} + x\,\frac{\partial}{\partial x} - u\,\frac{\partial}{\partial u} \tag{2.18}$$

s_4 represents a Galilean group,

$$X_4 = t\,\frac{\partial}{\partial x} + \frac{\partial}{\partial u} \tag{2.19}$$

s_6 and s_7 represent translations in time and space,

$$X_6 = \frac{\partial}{\partial t} \tag{2.20}$$

$$X_7 = \frac{\partial}{\partial x} \tag{2.21}$$

and finally, s_5 represents some special form of transformation,

$$X_5 = x\,\frac{\partial}{\partial t} - u^2\,\frac{\partial}{\partial u}\ . \tag{2.22}$$

The point transformation, $\tilde{z} = (\tilde{t}, \tilde{x}, \tilde{u})$, associated with each subgroup is determined through the application of the Lie series expansion to the group operator as follows

$$\tilde{z}_i = e^{(s_j X_j)}\, z_i = z_i + s_j\,(X_j\, z_i) + \frac{s_j^2}{2!}\, X_j(X_j\, z_i) + \frac{s_j^3}{3!}\, X_j(X_j(X_j\, z_i)) + \cdots \qquad (2.23)$$

where $z = (t, x, u)$. For instance, the transformation of x-variable through the subgroup X_1 can be found as

$$\tilde{x} = x + s_1\,(x\,t) + \frac{s_1^2}{2!}\,(2\,x\,t^2) + \frac{s_1^3}{3!}\,(6\,x\,t^3) + \cdots = \frac{x}{1 - s_1\,t}\ , \quad \text{for} \quad |s_1\,t| < 1\ .$$

This latter step is repeated for all the variables and the selected subgroups to obtain the global transformations associated with the differential equation under consideration. More extensive information on the procedure to find Lie point symmetries of equations can also be found in the literature [14, 20, 21].

2.3 Applications and Discussion

Let us illustrate the use of Lie symmetry analysis to obtain group invariant and/or self-similar solutions for some common problems relevant to fluid dynamics.

2.3.1 Chemically Reactive Boundary Layer flow

In the first example, we consider a chemically reactive boundary layer flow over an exponentially stretching porous flat surface (with partial slip) that was first described in reference [98]. Boundary layer flow over stretching surfaces is important as such flows are commonly encountered in engineering and related areas (i.e., electrochemistry, polymer processing). Obtaining self-similar solutions for such problems has been a topic of many research efforts [98–102]. As opposed to the solution procedure presented in reference [98], we investigate this problem via a more sys-

tematic approach based on Lie symmetry analysis, where similarity transformations are obtained from symmetries of the underlying differential equations.

In this regard, consider an incompressible, viscous fluid flow past a flat surface in the half-plane $y > 0$ with two equal and opposite forces acting on the x-axis such that the flat surface is stretched, and the origin is kept fixed. The governing equations (such as continuity, momentum, and concentration equations) for this problem can be written as

$$\begin{aligned} \frac{\partial u}{\partial x} + \frac{\partial v}{\partial y} &= 0 \\ u\frac{\partial u}{\partial x} + v\frac{\partial u}{\partial y} &= \nu\frac{\partial^2 u}{\partial y^2} \\ u\frac{\partial C}{\partial x} + v\frac{\partial C}{\partial y} &= D\frac{\partial^2 C}{\partial y^2} - k(C - C_\infty) \end{aligned} \tag{2.24}$$

where u and v are velocity components in x and y directions, respectively, ν is the kinematic viscosity, C is the concentration of the chemically reactive species, D is the molecular diffusivity, and the parameter k is the rate of chemical conversion of the irreversible reaction that is defined by $k = (1/2)k_0 e^{x/L}$. The boundary conditions for this problem are

$$\begin{aligned} u = U + N\nu\frac{\partial u}{\partial y}, \qquad v = -V(x), \qquad C = C_w, \qquad &\text{at } y = 0 \\ u \to 0, \qquad C \to C_\infty, \qquad &\text{as } y \to \infty \end{aligned} \tag{2.25}$$

where $C_w = C_\infty + C_0 e^{x/2L}$ is the concentration on the wall, $U = U_0 e^{x/L}$ is the stretching velocity, C_0 and U_0 are reference concentration and velocity, respectively, $N = N_0 e^{-x/2L}$ is the velocity slip factor where N_0 is its initial value, and $V(x)$ is the velocity on the wall which is in the form of either suction $V(x) > 0$ or blowing $V(x) < 0$. Also, V_0 is the initial strength of suction/blowing, and k_0 is a constant that has the same dimensions as k.

For simplicity reasons, let us rewrite the governing equations given in Eq. (2.24) in the stream function notation as shown below:

$$\begin{aligned} \frac{\partial\psi}{\partial y}\frac{\partial^2\psi}{\partial x\partial y} - \frac{\partial\psi}{\partial x}\frac{\partial^2\psi}{\partial y^2} &= \nu\frac{\partial^2\psi}{\partial y^3} \\ \frac{\partial\psi}{\partial y}\frac{\partial C}{\partial x} - \frac{\partial\psi}{\partial x}\frac{\partial C}{\partial y} &= D\frac{\partial^2 C}{\partial y^2} - k(C - C_\infty) \end{aligned} \tag{2.26}$$

where $u = \frac{\partial\psi}{\partial y}$ and $v = -\frac{\partial\psi}{\partial x}$. A similar notation is also considered for the boundary conditions. The above system of equations admits the following seven-parameter Lie group:

$$\begin{aligned} \xi^x &= -2Ls_1 \\ \xi^y &= s_2 + s_1 y + s_4 x + s_5 x^2 + s_6 x^3 \\ \eta^\psi &= s_3 - s_1\psi \\ \eta^C &= s_7\frac{C_\infty - C}{C_\infty} \end{aligned}$$

which corresponds to the following subgroups:

$$\begin{aligned} X_1 &= -2L\frac{\partial}{\partial x} + y\frac{\partial}{\partial y} - \psi\frac{\partial}{\partial\psi} \\ X_2 &= \frac{\partial}{\partial y} \\ X_3 &= \frac{\partial}{\partial\psi} \\ X_4 &= x\frac{\partial}{\partial y} \\ X_5 &= x^2\frac{\partial}{\partial y} \\ X_6 &= x^3\frac{\partial}{\partial y} \\ X_7 &= \frac{C_\infty - C}{C_\infty}\frac{\partial}{\partial C}\ . \end{aligned}$$

The symmetry parameters $s_{i=1,\cdots,7}$ are arbitrary, and can be chosen freely. Consid-

ering a linear combination of subgroups X_1 and X_7 which correspond to setting s_2, s_3, s_4, s_5, and s_6 to zero, the coordinate functions can be simplified to the following.

$$\begin{aligned} \xi^x &= -2Ls_1 \\ \xi^y &= s_1 y \\ \eta^\psi &= -s_1 \psi \\ \eta^C &= s_7 \frac{C_\infty - C}{C_\infty} \ . \end{aligned} \tag{2.27}$$

At this point, the method of characteristics can be used to determine the similarity variables associated to this particular system of equations for the selected subgroups as shown below

$$\frac{dx}{-2Ls_1} = \frac{dy}{s_1 y} = \frac{d\psi}{-s_1 \psi} = \frac{dC}{s_7 (C_\infty - C)/C_\infty} \ . \tag{2.28}$$

The first similarity variable can be obtained from the integration of the first two terms on the left side of Eq. (2.28)

$$\frac{dx}{-2Ls_1} = \frac{dy}{s_1 y}$$

which eventually leads to the following similarity variable

$$\alpha^* = y e^{x/2L} \ .$$

Here we note that the variable α^* is simply the integration constant of the above operation and can be non-dimensionalized as follows:

$$\alpha = y e^{x/2L} \sqrt{\frac{U_0}{2\nu L}} \ . \tag{2.29}$$

Similarly, from the first and third terms of Eq. (2.28)

$$\frac{dx}{-2Ls_1} = \frac{d\psi}{-s_1\psi}$$

the following similarity variable can be obtained

$$F(\alpha)^* = \psi e^{-x/2L}$$

which can also be non-dimensionalized as

$$F(\alpha) = \psi e^{-x/2L} \frac{1}{\sqrt{2\nu U_0 L}} \ . \tag{2.30}$$

And finally, the last similarly variable can be found from the first and last terms of Eq. (2.28) as

$$G(\alpha) = s_7(C - C_\infty)\ e^{-\frac{s_7 x}{2LC_\infty s_1}}. \tag{2.31}$$

The unknown symmetry parameters s_1 and s_7 which appear in the last similarity variable can be determined through the wall boundary condition ($y = 0$):

$$\alpha = 0: \quad C = C_w = C_\infty + C_0 e^{x/2L}, \quad G(0) = 1, \quad s_7 = 1/C_0, \quad s_1 = \frac{1}{C_0 C_\infty} \ . \tag{2.32}$$

The velocity components u and v can be re-expressed based on these similarity variables as follows:

$$\begin{aligned} u &= \frac{\partial \psi}{\partial y} = U_0 e^{x/L} F' \\ v &= -\frac{\partial \psi}{\partial x} = -\sqrt{\frac{\nu}{2L}}\ e^{x/2L}\ (F + \alpha F') \ . \end{aligned} \tag{2.33}$$

By substituting Eq. (2.33) along with the similarity variables given in Eqs. (2.29)–(2.31) into the governing equations given in Eq. (2.24), we reduce these equations

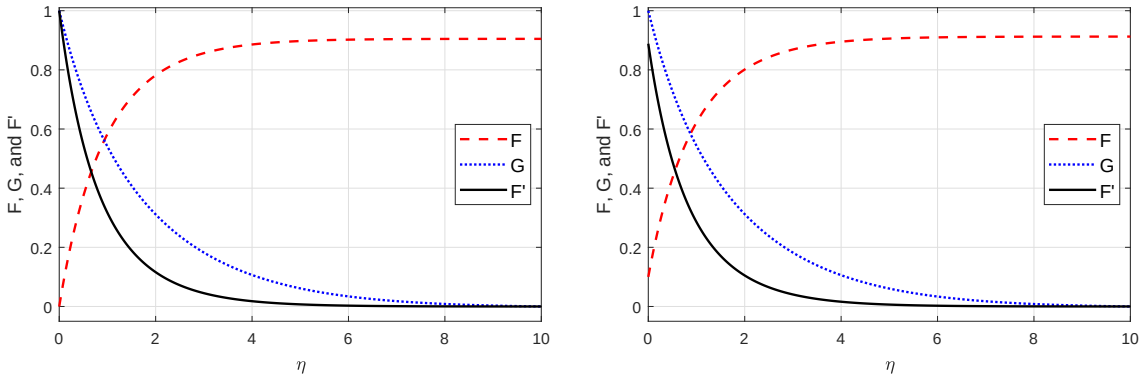

Fig. 2.2. Stream function (F), velocity (F'), and concentration (G) versus the distance from the surface (α). Parameter settings: $left: S=0,\ \gamma=0,\ \ \beta=0.1,\ Sc=0.7,\ right: S=0.1,\ \ \gamma=0.1,\ \ \beta=0.1,\ \ Sc=0.7$.

to the following self-similar form

$$\begin{aligned} F''' + FF'' - 2F'^2 &= 0 \\ G'' + Sc(FG' - F'G - \beta G) &= 0 \end{aligned} \tag{2.34}$$

where $Sc=\nu/D$ is the Schmidt number, and $\beta=k_0L/U_0$ is the reaction rate parameter. Similarly, the boundary conditions given in Eq. (2.25) can also be rewritten in terms of the new similarity variables

$$\begin{aligned} F' = 1+\gamma F''\ , \qquad F=S, \qquad G=1, \qquad \text{at } \alpha=0 \\ F'\to 0, \qquad G\to 0, \qquad \text{as } \alpha\to\infty \end{aligned} \tag{2.35}$$

where $\gamma = N_0\sqrt{U_0\nu/(2L)}$ is the velocity slip constant, and $S=\sqrt{\frac{2LV_0^2}{\nu U_0}}$ represents the suction/blowing parameter.

The above equations, Eq. (2.34), and relevant boundary conditions, Eq. (2.35), can be numerically solved by first converting this problem into an initial value problem. Then a fourth order Runge-Kutta method with a step size $\Delta\alpha=0.01$ is considered. Variations of the stream function F, horizontal velocity F', and concentration of the chemically reactive species G with respect to the distance from

the flat surface is demonstrated in figure 2.2 for cases: i) no suction/blowing or partial slip ($left$), ii) with suction and partial slip ($right$) at the boundaries.

2.3.2 Boundary Layer flow over a Wedge with Slip

Similarly, in the second example, we consider an incompressible boundary layer flow over a wedge, figure 2.3, with slip boundary conditions that was first described in reference [103]. In contrast to reference [103], we consider a systematic approach that is based on Lie symmetry analysis to investigate this problem. The governing equations for this particular problem can be written as

$$\begin{aligned} \frac{\partial u}{\partial x}+\frac{\partial v}{\partial y}&=0 && (continuity)\\ u\frac{\partial u}{\partial x}+v\frac{\partial u}{\partial y}&=-\frac{1}{\rho}\frac{dP(x)}{dx}+\nu\frac{\partial^2 u}{\partial y^2} && (x-momentum)\\ u\frac{\partial T}{\partial x}+v\frac{\partial T}{\partial y}&=\alpha\frac{\partial^2 T}{\partial y^2} && (energy) \end{aligned} \tag{2.36}$$

where P is the pressure, T is the temperature, and u and v denote velocity components in x- and y-coordinates, respectively. The pressure gradient $\frac{\partial P}{\partial x}$ can be expressed in terms of the external flow velocity $U(x)$ as follows

$$\frac{\partial P}{\partial x}=-\rho U(x)\frac{dU(x)}{dx}=-m\rho b^2 x^{2m-1}\ .$$

Note that in this work, we have considered an external velocity profile of the form $U(x)=bx^m$, where ρ is the density, b is a function of the wedge geometry, and the exponent $m=\beta/(2-\beta)$ is a function of the angle β (see figure 2.3). The governing equations given in Eq. (2.36) can also be written in the stream function notation as follows:

$$\frac{\partial\psi}{\partial y}\frac{\partial^2\psi}{\partial x\partial y}-\frac{\partial\psi}{\partial x}\frac{\partial^2\psi}{\partial y^2}=U\frac{dU}{dx}+\nu\frac{\partial^3\psi}{\partial y^3} \qquad (x-momentum) \tag{2.37}$$

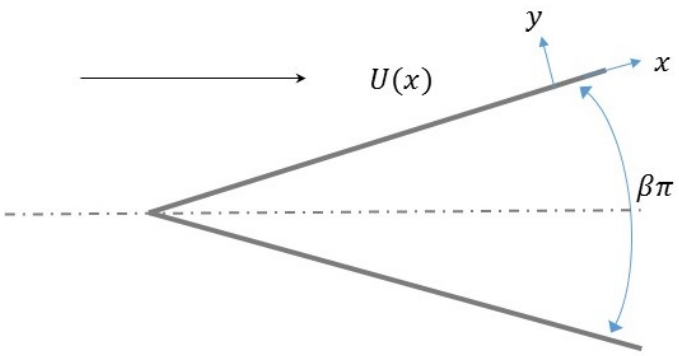

Fig. 2.3. Boundary layer flow over a Wedge.

$$\frac{\partial \psi}{\partial y}\frac{\partial T}{\partial x} - \frac{\partial \psi}{\partial x}\frac{\partial T}{\partial y} = \alpha \frac{\partial^2 T}{\partial y^2} \ . \qquad (energy) \tag{2.38}$$

The coordinate functions for the Lie symmetry group associated with the above governing equations are found as

$$\begin{aligned}
\xi^x &= s_1 + s_2 x \\
\xi^y &= s_3 + s_4 y + s_5 x + s_6 x^2 + s_7 x^3 \\
\eta^\psi &= s_8 + (s_2 - s_4)\psi \\
\eta^U &= (s_2 - 2s_4)U \\
\eta^T &= s_9 + s_{10} T \ .
\end{aligned}$$

Setting s_1, s_3, s_5, s_6, s_7, s_9, and s_{10} to zero, the coordinate functions can be simplified and used in the characteristics equations as follows:

$$\frac{dx}{s_2 x} = \frac{dy}{s_4 y} = \frac{d\psi}{(s_2 - s_4)\psi} = \frac{dU}{(s_2 - 2s_4)U} = \frac{dT}{0} \ . \tag{2.39}$$

Alternatively, Eq. (2.39) can be written as

$$\frac{dx}{x} = \frac{dy}{\tau y} = \frac{d\psi}{\varepsilon \psi} = \frac{dU}{MU} = \frac{dT}{0} \tag{2.40}$$

where

$$M = \frac{s_2 - 2s_4}{s_2} \ , \qquad \tau = \frac{1-M}{2} \ , \qquad \text{and} \qquad \varepsilon = \frac{1+M}{2} \ .$$

From the first and fourth terms of the above equation

$$\frac{dx}{x} = \frac{dU}{MU} \ , \tag{2.41}$$

we can determine that $U = \zeta x^M$ where ζ is the integration constant. As the external flow velocity is known to be only a function x and given by $U(x) = bx^m$, we can infer that $\zeta = b$ and $M = m$. From the first and second terms of Eq. (2.40), we can identify the first similarity variable as $\eta^* = yx^{-\tau}$ which can be non-dimensionalized as follows:

$$\eta = yx^{-\tau}\sqrt{b\frac{\varepsilon}{\nu}} \ . \tag{2.42}$$

Similarly, the non-dimensionalized version of the second similarity variable can be determined from the integration of the first and third terms of Eq. (2.40) as shown in the following:

$$\psi = x^{\varepsilon}\sqrt{b\frac{\nu}{\varepsilon}}F(\eta,\kappa) \ . \tag{2.43}$$

Here, a nonlinear parameter κ is included in the definition of the similarity variable $F(\eta,\kappa)$ to account for the velocity slips at boundaries which occur at sufficiently large Knudsen numbers and, for an isothermal wall, is given by following non-dimensionalized form [103]

$$\kappa = \frac{2-\sigma_M}{\sigma_M}\sqrt{b\frac{\varepsilon}{\nu}}\,\lambda\, x^{-\tau}$$

where, σ_M is the tangential momentum accommodation coefficient, and λ is the mean-free path of the gas. Here we note that, for this particular boundary layer flow configuration, the classical no-slip boundary condition is replaced with the

following slip condition [103]:

$$\eta = 0, \qquad \frac{\partial F}{\partial \eta} = \kappa \frac{\partial^2 F}{\partial \eta^2} \tag{2.44}$$

which also indicates that as κ approaches to zero, the no-slip boundary condition will be recovered. Also, for large values of κ, free molecular flow will occur which corresponds to following boundary conditions

$$\kappa \to \infty, \qquad F(\eta, \kappa \to \infty) = \eta \ , \qquad \frac{\partial F}{\partial \eta} = 1 \ . \tag{2.45}$$

Further, the last similarity variable can be found from the first and last terms of Eq. (2.40) as follows:

$$\frac{T - T_w}{T_0 - T_w} = \Theta(\eta, \kappa) \tag{2.46}$$

where the wall temperature T_w and the freestream temperature T_0 is used to non-dimensionalize T. The relevant boundary conditions can also be written in terms of new similarity variables as shown below:

$$\text{at} \quad \eta = 0 \ : \qquad \Theta(0, \kappa) = \frac{2\gamma}{Pr(1+\gamma)} \kappa \left. \frac{\partial \Theta}{\partial \eta} \right|_{wall} \tag{2.47}$$

$$\text{as} \quad \eta \to \infty \quad \text{or} \quad \kappa \to \infty \ : \qquad \Theta(\infty, \kappa) = \Theta(\eta, \infty) = 1 \ . \tag{2.48}$$

And finally, the governing equations given in Eq. (2.37) and Eq. (2.38) can be reduced to the following differential system by using the above similarity variables

$$F_{\eta\eta\eta} + F F_{\eta\eta} + \beta(1 - F_\eta^2) + K(1-\beta)(F_\eta F_{\eta\kappa} - F_\kappa F_{\eta\eta}) = 0 \tag{2.49}$$

$$\Theta_{\eta\eta} + Pr\, F\, \Theta_\eta + \kappa\, Pr(1-\beta)(F_\eta \Theta_\kappa - F_\kappa \Theta_\eta) = 0 \tag{2.50}$$

where Pr is the Prandtl number and γ is the ratio of the specific heats.

2.3.3 Analysis of Stagnation Point Conditions in an Inviscid, Compressible Blunt-Body Flow

As our last example, we investigate the stagnation point conditions of an inviscid, compressible blunt-body flow that were extensively studied in an early work by Vinokur [104]. In equilibrium flows, the state of stagnation point is usually well-defined and is known to solely depend on the free-stream conditions. However, this is not the case for non-equilibrium flows [104]. It is known that in non-equilibrium inviscid blunt-body flows, the gases at the stagnation points are usually in thermodynamic equilibrium for finite relaxation times and the stagnation point enthalpy is equal to the total free-stream enthalpy. Although stagnation point enthalpy of blunt-body flows does not appear to be affected by the non-equilibrium processes and the body shape, Vinokur [104] raised the question whether this was also true for other state variables and proposed a resolution to this question. In this work, we propose an alternative solution approach that is based on Lie symmetry analysis to study this problem and provide some preliminary results.

In this context, let us consider a blunt-body flow in the Cartesian co-ordinate system with origin at the stagnation point (as shown in figure 2.4) and let the shock nose radius R_s, free-stream density ρ_∞, and free-stream velocity U_∞ be reference quantities. The general conservation equations associated with an inviscid blunt-body flow can be written as

$$(\rho u)_x + (\rho v)_y = 0 \qquad (continuity) \tag{2.51}$$

$$u u_x + v u_y + p_x/\rho = 0 \qquad (x\text{–}momentum) \tag{2.52}$$

$$u v_x + v v_y + p_y/\rho = 0 \qquad (y\text{–}momentum) \tag{2.53}$$

$$h + \frac{1}{2}(u^2 + v^2) = h_\infty + \frac{1}{2}U_\infty^2 \qquad (energy) \tag{2.54}$$

where, u and v are velocity components in x and y directions, respectively, p is

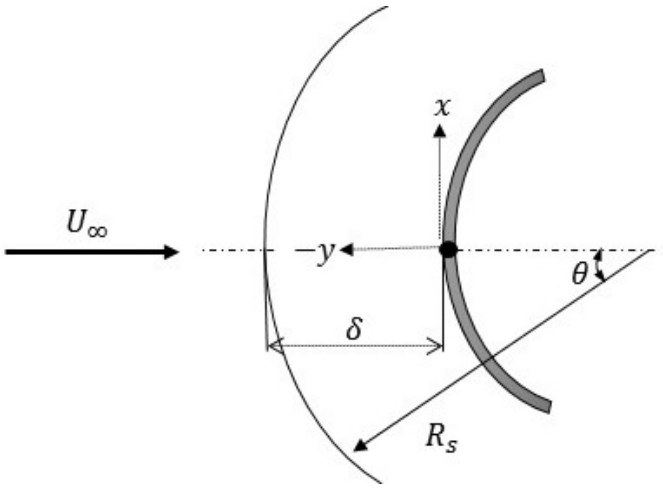

Fig. 2.4. Representation of stagnation point in a blunt-body flow.

the pressure, ρ is the density, and h refers to the enthalpy. Here we note that, in non-equilibrium flows, the state variables such as the density ρ, specific entropy S, temperature T, and frozen sound speed a_f are all functions of the independent variables p, h, and $\mathbf{q} = (q_1, q_2, \cdots, q_n)$ where $\mathbf{q}$ represents n general non-equilibrium variables (i.e., specific energy of vibrational, rotational, or electronic state of species and concentration of species). The state variables are not independent but are related through laws of thermodynamics [104] as

$$\left.\frac{\partial S}{\partial h}\right|_{p,q_i} = \frac{1}{T}, \quad \left.\frac{\partial S}{\partial p}\right|_{h,q_i} = -\frac{1}{\rho T}, \quad \left.\frac{\partial \rho}{\partial p}\right|_{S,q_i} \equiv \frac{1}{\rho}\left.\frac{\partial \rho}{\partial h}\right|_{p,q_i} + \left.\frac{\partial \rho}{\partial p}\right|_{h,q_i} = \frac{1}{a_f^2} \tag{2.55}$$

and the non-equilibrium processes are governed by m coupled reactions (i.e., $\mathbf{R} = (r_1, r_2, \cdots, r_m)$). The rate of change of non-equilibrium variables due to a particular reaction r_j is given by

$$\left.\frac{Dq_i}{Dt}\right|_{r_j} = \left.\left(u\frac{\partial q_i}{\partial x} + v\frac{\partial q_i}{\partial y}\right)\right|_{r_j} = \omega_{i,j}(p, h, \mathbf{q}) = \frac{\chi_{i,j}(p, h, \mathbf{q})}{\tau_{i,j}(p, h, \mathbf{q})} \tag{2.56}$$

where $\tau_{i,j}$ refers to the local relaxation time. Similarly, the rate of change of a particular non-equilibrium variable q_i due to all reactions is simply equal to

$\sum_{j=1}^{m} \omega_{i,j}$. As in equilibrium flows, the thermodynamic state of a gas is only a function of density and enthalpy, the variables $q_i = q_i^e(p,h)$ are also function of these independent variables. Hence the state variables at the equilibrium can be redefined as $\rho^e(p,h) = \rho(p,h,\mathbf{q^e})$, $S^e(p,h) = S(p,h,\mathbf{q^e})$, $T^e(p,h) = T(p,h,\mathbf{q^e})$, and $a_f^e(p,h) = a_f(p,h,\mathbf{q^e})$ where $\mathbf{q^e} = (q_1^e, q_2^e, \cdots, q_n^e)$. The latter indicates that $\omega_{i,j} = 0$ for all the variables and reactions at equilibrium and hence function $\chi_{i,j}$ must satisfy $\chi_{i,j}(p,h,\mathbf{q}^e) = 0$.

At this point, let us consider the special two-dimensional flow near the axis of symmetry (i.e., near the stagnation point streamline in figure 2.4). It is assumed that in the vicinity of the axis of symmetry [104]

$$u \approx x u_x, \qquad p_x \approx x p_{xx}, \qquad v \approx v(y), \qquad \rho \approx \rho(y)$$

which also indicates that the first derivative of the function u with respect to x is only a function of the independent variable y. Based on these assumptions, the governing equations given in Eqs. (2.51)–(2.54) can be rewritten as

$$\rho u_x + \frac{d(\rho v)}{dy} = 0 \qquad (continuity) \tag{2.57}$$

$$u_x^2 + v\frac{du_x}{dy} = -\frac{1}{\rho}p_{xx} \qquad (x\text{–}momentum) \tag{2.58}$$

$$v\frac{dv}{dy} = -\frac{1}{\rho}\frac{dp}{dy} \qquad (y\text{–}momentum) \tag{2.59}$$

$$h + \frac{1}{2}v^2 = h_\infty + \frac{1}{2}U_\infty^2 \ . \qquad (energy) \tag{2.60}$$

The above equations admit the following 10 parameters Lie group

$$\xi^x = s_2 + s_1 x$$

$$\xi^y = s_3 + s_1 y$$

$$\eta^u = s_6 + s_4 u + s_7 y + s_8 y^2 + s_9 y^3$$

$$\eta^v = s_4 v$$

$$\eta^p = s_{10} + s_5 p + s_{11} x$$

$$\eta^\rho = (s_5 - 2s_4)\rho \ .$$

Considering the symmetry groups corresponding to s_1, s_2, s_3, s_4, s_5, s_6, and s_{10}, the characteristics equations for this problem can be written as

$$\frac{dx}{s_1 x + s_2} = \frac{dy}{s_1 y + s_3} = \frac{du}{s_4 x + s_6} = \frac{dv}{s_4 v} = \frac{dp}{s_5 p + s_{10}} = \frac{d\rho}{(s_5 - 2s_4)\rho} \tag{2.61}$$

which can also be simplified to

$$\frac{dx}{x + x_o} = \frac{dy}{y + y_o} = \frac{du}{\beta u + u_o} = \frac{dv}{\beta v} = \frac{dp}{\epsilon p + p_o} = \frac{d\rho}{(\epsilon - 2\beta)\rho} \tag{2.62}$$

where $x_o = s_2/s_1$, $y_o = s_3/s_1$, $\beta = s_4/s_1$, $u_o = s_6/s_1$, $\epsilon = s_5/s_1$, and $p_o = s_{10}/s_1$.

At this point, similarity variables can be obtained using the characteristics equations given in Eq. (2.62). Considering that the velocity component v and density ρ are only functions of y, one can determine the relevant similarity transformations as follows:

$$\frac{dy}{y + y_o} = \frac{dv}{\beta v} \qquad \Longleftrightarrow \qquad v = C_2 (y + y_o)^\beta \tag{2.63}$$

$$\frac{dy}{y + y_o} = \frac{d\rho}{(\epsilon - 2\beta)\rho} \qquad \Longleftrightarrow \qquad \rho = C_4 (y + y_o)^{(\epsilon - 2\beta)} \tag{2.64}$$

where C_2 and C_4 are the integration constants. The parameter y_o can be determined from the boundary conditions, as on the stagnation point ($x = 0$, $y = 0$) the velocity component v is equal to zero. Similarly, other similarity variables can be found

through Eq. (2.62) as shown in the following

$$\frac{dx}{x+x_o} = \frac{dy}{y} \qquad \Longleftrightarrow \qquad \alpha = \frac{y}{x+x_o} \tag{2.65}$$

$$\frac{dx}{x+x_o} = \frac{du}{\beta u + u_o} \qquad \Longleftrightarrow \qquad u = f_1[\alpha]\,\frac{(x+x_o)^\beta}{\beta} - \frac{u_o}{\beta} \tag{2.66}$$

$$\frac{dx}{x+x_o} = \frac{dp}{\epsilon p + p_o} \qquad \Longleftrightarrow \qquad p = f_3[\alpha]\,\frac{(x+x_o)^\epsilon}{\epsilon} - \frac{p_o}{\epsilon}\ . \tag{2.67}$$

On the stagnation point ($x = 0$, $y = 0$) the derivative of the velocity component v with respect to y is assumed to be finite as shown below [104]

$$\frac{\partial v}{\partial y} = -C$$

where C is a constant. From this relation, the parameters β and C_2 can be found as 1 and $-C$, respectively. Further, the functions f_1 and f_3 can be found through the implementation of the above similarity transformations to the governing equations given in Eqs. (2.57)–(2.60). The function f_1 can be found from the continuity equation, Eq. (2.57), as follows

$$f_1[\alpha] = C_1\,\alpha + C\,(\epsilon - 1) \quad \Leftrightarrow \quad u = C_1\,y + C(\epsilon-1)(x+x_o) - u_o \tag{2.68}$$

where C_1 is a constant. We assumed that near the stagnation point $u = xu_x$, and in order for this to hold true, the following must also be true

$$C_1 = 0, \qquad x_o = 0, \qquad u_0 = 0\ .$$

Similarly, from x-momentum, Eq. (2.58), we can find f_3 as

$$f_3[\alpha] = C_3\,\alpha^\epsilon + C_{31}\,\alpha^{\epsilon-1} - \frac{CC_4(\epsilon-1)}{\epsilon}$$

and hence the pressure is

$$p = \frac{1}{\epsilon}\left[C_3\, y^{\epsilon} + C_{31}\, x\, y^{\epsilon-1} - \frac{CC_4(\epsilon-1)}{\epsilon}x^{\epsilon} - p_o\right] .$$

Recall that we assumed that near the stagnation point $p_x = xp_{xx}$. For this to hold true, the constants C_{31} and ϵ must be equal to 0 and 2, respectively. Also from the boundary condition (on stagnation point)

$$\text{at} \quad x = 0, \quad y = 0 \ , \quad \Longrightarrow \qquad p = p_b \ , \qquad \rho = \rho_b \ ,$$

we find that $p_o = -2p_b$ and $C_4 = \rho_b$. Further, from y-momentum, Eq. (2.59), we can determine that

$$C_3 = -C^2\, C_4 \ .$$

At this point, the transformed variables are as follows:

$$u = Cx, \quad v = -Cy, \quad \rho = C_4, \quad p = p_b - \frac{1}{2}C^2\, C_4\, y^2 - \frac{1}{4}CC_4\, x^2 \ . \tag{2.69}$$

At the stagnation point, the derivative of the velocity component v with respect to y is known to be finite which is satisfied by the above definition of v. The constant C_2 is usually positive and must be determined from a global solution. Furthermore, at the stagnation point, h is equal to h_b and can be found through the energy equation, Eq. (2.60), as

$$h_b = h_\infty + \frac{1}{2}\, U_\infty^2 \ .$$

Hence, on the axial streamline ($x = 0$) where $\rho = \rho_b$, the final form of the system variables simplifies to the following:

$$u = 0, \quad v = -Cy, \quad \rho = \rho_b, \quad p = p_b - \frac{1}{2}C^2\, \rho_b\, y^2, \quad h = h_b - \frac{1}{2}C^2\, y^2 \ . \tag{2.70}$$

To conclude, we have demonstrated a systematic approach based on Lie symmetry analysis to investigate the stagnation point state of an inviscid, compressible blunt-body flow. Further details on the subject can be found in reference [104].

CHAPTER 3

Numerical Solution of Modified Differential Equations based on Symmetry Preservation

3.1 Scope of the Chapter

In this chapter, we present a methodology that is based on the method of equivariant moving frames to construct invariant numerical schemes for solution of PDEs via consideration of their modified forms. Modified forms of equations are considered due to several important practical advantages (including treatment of transformations obtained from symmetries and possible improvements in accuracy of invariant numerical schemes) and are obtained either through addition of perturbation terms to the original PDEs or by defect correction procedures (or leading error analysis of truncation error). The new terms that are added to the original PDEs to obtain the modified forms are later (either completely or partially) removed from the discrete equation in the transformed space by considering equivariant moving frames for which the numerical representation of these terms go to zero. This procedure that is based on the method of equivariant moving frames is used to construct invariant schemes for such modified forms of PDEs. To demonstrate the proposed method, we consider some test cases (including linear advection equation in 1D and 2D and inviscid Burgers' equation) and construct invariant (Lie symmetry preserving) schemes considering modified forms of equations. Performance of these invariant numerical schemes is evaluated in this dissertation and our studies suggest that preservation of symmetries in numerical schemes has the potential to significantly improve accu-

racy of some existing schemes besides embedding information about the geometric structure of underlying PDEs.

Note that construction of invariant schemes as numerical solutions of PDEs through the method of equivariant moving frames involves the mapping of every discrete variable in related difference equations according to some transformations that are obtained from symmetries of these PDEs. However, symmetry groups underlying such PDEs often lead to discrete variable transformations that are difficult to implement in many existing base schemes. In this work, we found that the use of modified forms of equations in some cases result in symmetries that are associated with more convenient transformations that are easy to apply on existing schemes. In addition, we also found that the use of modified equations could be very practical for identification of moving frames (among vast number of possibilities) that lead to significant improvements on the accuracy of the resulting (invariant) schemes. Further, for some problems, the selection of certain moving frames that are needed to ensure improvements in accuracy of invariant schemes might result in trivial solutions that can also be avoided by considering the modified forms of these PDEs.

3.2 Mathematical Formulation and Moving Frames

The method of equivariant moving frames presented by Fels and Olver [83, 84] can be used to construct invariant numerical schemes [85, 87]. In this method, a (right) moving frame ρ is defined on a manifold M such that it is a topological map $\rho : M \to G$ that satisfies the following relation:

$$\rho(g \cdot \mathbf{z}) = \rho(\mathbf{z})\, g^{-1} \qquad \forall g \in G \tag{3.1}$$

where G is the symmetry group acting on the manifold M, and g represents the action of a particular element of the group G on the local variables. Let $L(\mathbf{z}, \mathbf{p}) = 0$ be a

general form of a partial differential equation where $\mathbf{z} = (\mathbf{x}, \mathbf{u})$. Here, $\mathbf{x} = (x_1, \cdots, x_n)$ and $\mathbf{u} = (u_1, \cdots, u_m)$ denote the independent and dependent variables, respectively, and $\mathbf{p} = (\mathbf{u}_{[\mathbf{x}]}, \mathbf{u}_{[\mathbf{x},\mathbf{x}]}, \cdots, \mathbf{u}_{[\mathbf{x},\mathbf{x},\cdots,\mathbf{x}]})$ represents the derivatives of the dependent variables with respect to the independent variables. A numerical scheme, $\tilde{N}(\mathbf{z}) = 0$, and stencil equation, $\tilde{\phi}(\mathbf{z}) = 0$, constructed as an approximation for a surface $L(\mathbf{z}, \mathbf{p}) = 0$ are said to be invariant under the group G if the following is true:

$$\begin{aligned} \tilde{N}(\rho(\mathbf{z}) \cdot \mathbf{z}) = 0 \quad &\Leftrightarrow \quad \tilde{N}(\mathbf{z}) = 0 \\ \tilde{\phi}(\rho(\mathbf{z}) \cdot \mathbf{z}) = 0 \quad &\Leftrightarrow \quad \tilde{\phi}(\mathbf{z}) = 0 \ . \end{aligned} \tag{3.2}$$

There is a large family of moving frames that satisfy the invariance condition given in Eq. (3.2), and not all of them will result in a more accurate numerical scheme. Therefore, a careful selection of cross-sections (or normalization conditions) is necessary [85,87]. For any given (non-invariant) numerical scheme $N(\mathbf{z}) = 0$ associated with $L(\mathbf{z}, \mathbf{p}) = 0$, a corresponding invariant scheme can be obtained as $\tilde{N}(\mathbf{z}) \equiv N(\rho(\mathbf{z}) \cdot \mathbf{z}) = 0$ [85,87,88]. Note that in some cases, the equation system under consideration has cumbersome symmetry structures which make it very difficult to preserve them in a numerical algorithm due to coupling between the independent and dependent variables in the transformation relations. The proposed work seeks to address such limitations through the use modified equations and appropriate selections of cross-sections.

In this context, consider a differential equation $L_0(\mathbf{z}, \mathbf{p}) = 0$ that is associated with an r-dimensional symmetry group G_0. And let $N_0(\mathbf{z}) = 0$ be a numerical approximation for $L_0(\mathbf{z}, \mathbf{p})$. In some cases, it is difficult to determine the action of the group element $g_0 \in G_0$ on the local variables of the differential equation $L_0(\mathbf{z}, \mathbf{p}) = 0$ which is required to form the related point transformations as $g_0 \cdot \mathbf{z} = \tilde{\mathbf{z}}(s_1, \ldots, s_r; \mathbf{z})$, where $\tilde{\mathbf{z}}$ represents the transformation relation and $s_1, \ldots, s_r$ are the related symmetry parameters. In contrast to previous works in the literature, in this

dissertation, we propose to address such limitations through the use of a modified equation $L_m(\mathbf{z}, \mathbf{p}) = 0$, which (in some cases) is associated with more convenient point transformations (in comparison to the original PDE, $L_0(\mathbf{z}, \mathbf{p}) = 0$), and given by

$$L_m(\mathbf{z}, \mathbf{p}) \equiv L_0(\mathbf{z}, \mathbf{p}) + \kappa(\mathbf{z}, \mathbf{p}) = 0 \ . \tag{3.3}$$

Here, $\kappa(\mathbf{z}, \mathbf{p})$ is a (sufficiently small) regularization term introduced to the system (either through truncation error analysis or via convenient perturbations) for various practical advantages. And let G_m be the point symmetry group associated with the modified equation $L_m(\mathbf{z}, \mathbf{p})$. Corresponding to the latter equation, we then construct an invariant numerical scheme as $\tilde{N}_m(\mathbf{z}) = N_m(g_m \cdot \mathbf{z})$, $\forall g_m \in G_m$, where $N_m(\mathbf{z}) = N_0(\mathbf{z}) + N_\kappa(\mathbf{z}) = 0$. Here, we note that the action of the group element g_m on the local variables $\mathbf{z}$ can be chosen (through convenient selection of moving frames) such that $N_\kappa(g_m \cdot \mathbf{z}) = 0$, and therefore, $N_m(g_m \cdot \mathbf{z}) = N_0(g_m \cdot \mathbf{z})$. In some cases, the invariant scheme constructed for the modified equation, $N_m(g_m \cdot \mathbf{z})$, is found to be more accurate than the base (non-invariant) numerical scheme $N_0(\mathbf{z})$.

Further, recall that there is a large family of moving frames that satisfy Eq. (3.2). However, an improvement in accuracy of the constructed invariant numerical scheme could be observed, if one chooses moving frames that are more likely to reduce the truncation error associated with any given numerical scheme $N_0(\mathbf{z})$. In some cases, the use of such moving frames (required to ensure an improvement in the accuracy) could result in trivial solutions and could pose challenges for construction of invariant schemes (with improved accuracy). Such trivial solutions could also be avoided if modified forms of underlying equations are considered for discretization. In this context, let us consider $N_h(\mathbf{z}) \equiv N_0(\mathbf{z}) + N_\kappa(\mathbf{z})$ to be a higher order numerical scheme (in comparison to $N_0(\mathbf{z})$) where the form of the term $N_\kappa(\mathbf{z})$ is prescribed through the truncation error analysis. Note that $N_h(\mathbf{z})$ can be associated with a corresponding modified equation (similar to $L_m(\mathbf{z}, \mathbf{p}) = 0$). An invariant form of this

scheme can be constructed as $\tilde{N}_h(\mathbf{z}) = N_h(g_0 \cdot \mathbf{z})$ which could be significantly more accurate than the base scheme $N_0(\mathbf{z})$. Such a construction of an invariant scheme is especially preferred when the action of a group element g_0 on $\mathbf{z}$ (corresponding to a particular moving frame) results in an invariant scheme $N_0(g_0 \cdot \mathbf{z}) = 0$ with a trivial solution. Here, we also note that, in the transformed space, the form of the additional term $N_\kappa(g_0 \cdot \mathbf{z})$, and in some cases the form of the base scheme $N_0(g_0 \cdot \mathbf{z})$ as well, are more convenient for programming as the moving frames associated with g_0 are chosen such that it reduces the truncation error via setting the numerical representation of certain terms in the truncation error to zero.

More details on the application of the proposed method for construction of invariant numerical schemes are given in the following sections where symmetry preserving schemes are constructed for some linear and nonlinear problems.

3.3 Method of Modified Equations

In this section, procedures to modify equations either through addition of perturbation terms or through defect correction are presented in detail. In particular, modified forms for the linear advection equation and the inviscid Burgers' equation are presented.

3.3.1 Linear Advection Equation

We consider the following form of the linear advection equation or first order wave equation:

$$\frac{\partial u(t,x)}{\partial t} + \alpha \frac{\partial u(t,x)}{\partial x} = 0 \tag{3.4}$$

which describes transport of a property (or quantity) $u(t,x)$ with a constant characteristic speed α. Generalizations of this form of advection equation are commonly

found in many disciplines relevant to transport phenomena (including fluid dynamics). One approach to solve Eq. (3.4) is through approximation of the temporal and spatial derivatives using finite difference approximations with a certain order of accuracy. In this work, we consider a (first order accurate) forward in time and upwind in space finite difference scheme as our base scheme, as shown below, from which higher order invariant numerical schemes are constructed:

$$\frac{u(t+\tau,x)-u(t,x)}{\tau}+\alpha\,\frac{u(t,x)-u(t,x-h)}{h}=0\;+\;O(\tau,h)\;. \tag{3.5}$$

Here, the symbols τ and h are the discrete time and space variables, respectively, and $O(\tau,h)$ denotes the order of the truncation error. The objective is to construct a numerical scheme that preserves the symmetries of Eq. (3.4) in addition to increasing numerical accuracy. However, the present form of Eq. (3.4) results in symmetries with transformations that are difficult to apply to the discrete algorithm given in Eq. (3.5). More convenient transformations can be obtained if an artificial diffusion is introduced to the system as a perturbation term as given in the following

$$\frac{\partial\,u(t,x)}{\partial t}+\alpha\,\frac{\partial\,u(t,x)}{\partial x}=f\,\frac{\partial^2\,u(t,x)}{\partial\,x^2}\;. \tag{3.6}$$

We observe that Eq. (3.6) has symmetries that result in more convenient transformations, and further details on this can be found in the next section where the symmetry methods are discussed. The RHS of Eq. (3.6) represents a perturbation term that can be removed from the system by choosing a moving frame for which the numerical approximation of that term goes to zero in the transformed space. Although the perturbation term is removed from the system, the artificial diffusion coefficient f still appears in the discrete variable transformations obtained from the symmetries of Eq. (3.6). The main reason for the addition of the perturbation term to the system is to obtain more convenient transformations. Therefore, the coeffi-

cient f can be considered to have a sufficiently small and arbitrary value which in this work is chosen to be of the order of machine precision, as $\epsilon_{mach} = 2.22 \times 10^{-16}$. A discrete form of the modified equation, Eq. (3.6), with this choice for the artificial diffusion coefficient f is used to construct an invariant numerical scheme (referred to as SYM-1), which will be discussed further in the subsequent sections.

Another approach to prescribe the value of the diffusion coefficient f is through the analysis of the truncation error of the discrete equation constructed from the original PDE. It can be shown (using Taylor series expansion) that the accuracy of the first order accurate upwind scheme given by Eq. (3.5) can be improved by considering a modified form of the advection equation that includes a defect correction term as shown in Eq. (3.6). In this case, the defect correction term (on RHS) includes the artificial diffusion coefficient $f \equiv f(\tau, h)$, that depends on τ and h. Note that the use of an upwind scheme for the LHS and a second order (or more) accurate discretization for the defect term on the RHS would make the overall numerical scheme more accurate. In particular, we obtain a scheme (referred to as MOD-1) with $O(\tau^2, h)$ accuracy when $f = \frac{1}{2}\tau\alpha^2$. A discrete form of the modified equation with this particular selection of f is used to construct an invariant numerical scheme (referred to as SYM-2). As the modified form of equation is used only to obtain symmetries that are associated with more convenient transformations, this particular selection of f is deemed to be sufficient for obtaining an accurate solution. As discussed in the results section, this selection of f can result in an invariant numerical scheme that has improved accuracy $O(\tau^2, h^2)$, in comparison to MOD-1 scheme that is non-invariant and is only $O(\tau^2, h)$ accurate. A non-invariant numerical scheme (referred to as MOD-2) based on Eq. (3.6), where, $f = \frac{1}{2}\alpha\,(\tau\alpha - h)$ is also considered for the sake of comparison with our invariant numerical scheme (SYM-2), as both schemes are second order accurate ($O(\tau^2, h^2)$).

3.3.2 Inviscid Burgers' Equation

The inviscid Burgers' equation (IBE) is another commonly used PDE that models nonlinear wave propagation and takes the following (non-conservative) form

$$\frac{\partial u}{\partial t} + u\,\frac{\partial u}{\partial x} = 0\ , \qquad u(0,x) = u_0 \tag{3.7}$$

that can also be written in the conservative form as

$$\frac{\partial u}{\partial t} + \frac{\partial f}{\partial x} = 0 \tag{3.8}$$

where $f = \frac{1}{2}\,u^2$. In this nonlinear PDE, in contrast to the linear advection equation, the characteristic wave speed is dependent on the solution $u(t,x)$. Exact analytical solutions for the inviscid Burgers' equation, Eq. (3.7), are rare and those available solutions are usually obtained through the method of characteristics. Hence, numerical methods are often used for the solution of the inviscid Burgers' equation. In our computations, we consider a forward in time and backward in space (or upwind) finite difference scheme

$$\frac{u(t+\tau,x) - u(t,x)}{\tau} + u(t,x)\,\frac{u(t,x) - u(t,x-h)}{h} = 0\ +\ O(\tau,h) \tag{3.9}$$

as our base scheme from which invariant numerical schemes associated with modified forms of the equation are derived. Employing a similar procedure as before, the modified form of the inviscid Burgers' equation on the continuous domain can be approximated through a defect correction procedure as following

$$\frac{\partial u}{\partial t} + u\,\frac{\partial u}{\partial x} = \tau\,u\left(\frac{\partial u}{\partial x}\right)^2 - \frac{1}{2}(h - \tau\,u)\,u\,\frac{\partial^2 u}{\partial x^2} + O(\tau^2, h^2)\ . \tag{3.10}$$

Similarly, the modified equation for the conservative form of the inviscid Burgers' equation, Eq. (3.8), is found to be

$$\frac{\partial u}{\partial t}+\frac{\partial f}{\partial x}=\frac{\tau}{2\,u}\left(\frac{\partial f}{\partial x}\right)^2-\frac{1}{2}\,(h-\tau\,u)\,\frac{\partial^2 f}{\partial x^2}+O(\tau^2,h^2)\;. \tag{3.11}$$

3.4 Construction of Invariant Modified Schemes

In this section, we briefly outline the method to construct invariant numerical schemes, using (modified forms of) the linear advection equation (in 1D and 2D) and the inviscid Burgers' equation as examples.

3.4.1 Linear Advection Equation in 1D

The modified advection equation given in Eq. (3.6) admits the following six parameter Lie group:

$$\begin{aligned}
X_1 &= 2\,t^2\,\frac{\partial}{\partial t}+2\,x\,t\,\frac{\partial}{\partial x}-u\,(t+\frac{(x-\alpha\,t)^2}{2\,f})\,\frac{\partial}{\partial u}\\
X_2 &= 4\,t\,\frac{\partial}{\partial t}+2(x+\alpha\,t)\,\frac{\partial}{\partial x}\\
X_3 &= t\,\frac{\partial}{\partial x}-u\,\frac{(x-\alpha\,t)}{2\,f}\,\frac{\partial}{\partial u}\\
X_4 &= u\,\frac{\partial}{\partial u}\\
X_5 &= \frac{\partial}{\partial x}\\
X_6 &= \frac{\partial}{\partial t}\;.
\end{aligned} \tag{3.12}$$

Next, we use the following Lie series approximation for each group to determine the related point transformations $\tilde{z}^j=(\tilde{z}^1,\tilde{z}^2,\tilde{z}^3)=(\tilde{t},\tilde{x},\tilde{u})$:

$$\tilde{z}^j\;=z^j+s_i\,(X_i\,z^j)+\frac{s_i^2}{2!}\,X_i(X_i\,z^j)+\frac{s_i^3}{3!}\,X_i(X_i(X_i\,z^j))+\cdots \tag{3.13}$$

where $s_{i=1,\cdots,6}$ and $X_{i=1,\cdots,6}$ are the specific group parameters and operators, respectively. Here the unknown group parameters (related to each subgroup) in the transformations are determined through the method of equivariant moving frames by selection of convenient moving frames.

For the sake of simplicity, the scaling groups X_2 and X_4 are ignored and not considered in the determination of the point transformations. For all the other symmetries of Eq. (3.12), the Lie series approximation, Eq. (3.13), is used to find the transformation relations for each system variable. Once these transformations are known, we can combine them in an arbitrary order to obtain a general transformation relation that includes all the desired symmetries as given in the following:

$$\tilde{t} = \frac{t + s_6}{1 - 2\,s_1\,(t + s_6)} \tag{3.14}$$

$$\tilde{x} = \frac{x + s_5}{1 - 2\,s_1\,(t + s_6)} \tag{3.15}$$

$$\tilde{u} = u\,\sqrt{1 - 2\,s_1\,(t + s_6)}\,\exp\left[-\frac{s_1\,((x + s_5) - \alpha\,(t + s_6))^2}{2\,f\,(1 - 2\,s_1\,(t + s_6))}\right]. \tag{3.16}$$

Using a forward in time backward in space (or upwind) finite difference scheme, Eq. (3.6) can be discretized as shown in the following

$$\frac{u_i^{n+1} - u_i^n}{\tau} + \alpha\,\frac{u_i^n - u_{i-1}^n}{h} - f\,\frac{u_{i+1}^n - 2\,u_i^n + u_{i-1}^n}{h^2} = 0 \tag{3.17}$$

where u^{n+1} and $u_{i\pm1}$ represent $u(t+\tau, x)$ and $u(t, x \pm h)$, respectively. And the discrete step variables are defined as $\tau = t^{n+1} - t^n$ and $h = x_i - x_{i-1}$. The invariantization procedure starts with transforming each variable in Eq. (3.17) according to the point transformations given in Eqs. (3.14)–(3.16) as

$$\frac{\tilde{u}^{n+1} - \tilde{u}^n}{\tilde{\tau}} + \alpha\,\frac{\tilde{u}_i - \tilde{u}_{i-1}}{\tilde{h}} - \tilde{f}\,\frac{\tilde{u}_{i+1} - 2\,\tilde{u}_i + \tilde{u}_{i-1}}{\tilde{h}^2} = 0 \tag{3.18}$$

where $\tilde{\tau} = \tilde{t}^{n+1} - \tilde{t}^{n}$ and $\tilde{h} = \tilde{x}_i - \tilde{x}_{i-1}$. These transformations have three undefined components: the symmetry parameters s_1, s_5, and s_6. The unknown symmetry parameters can be determined using Cartan's method of normalization. There is a large family of cross-sections (or normalization conditions) that can be used to define the symmetry parameters. Not all choices will result in a more accurate numerical scheme. Therefore, the normalization condition must be chosen carefully. We first choose the normalization conditions for the independent variables that result in simple stencils in the transformed space. Then we seek for conditions that will remove the leading error terms in the truncation error of the numerical scheme. If complete removal of the leading order term in the truncation error is unachievable, then we can choose a cross-section that would lead to a reduction in the truncation error (by removing as many terms as possible). For this specific problem, we choose the following cross-sections:

$$
\begin{aligned}
&\tilde{t}^{n} = 0 \quad \Rightarrow \quad s_6 = -t^n \\
&\tilde{x}_i = 0 \quad \Rightarrow \quad s_5 = -x_i \\
&\partial_{\tilde{x}\tilde{x}}\, \tilde{u} = 0 \quad \Rightarrow \quad \frac{\tilde{u}_{i+1} - 2\,\tilde{u}_i + \tilde{u}_{i-1}}{\tilde{h}^2} = 0 \quad \Rightarrow \quad s_1 = -\frac{2f}{h^2} \ln\left[\frac{2u_i^n}{u_{i+1}^n + u_{i-1}^n}\right]
\end{aligned}
\tag{3.19}
$$

where $\partial_{\tilde{x}\tilde{x}}$ in this case represents the numerical discretization for the second order derivative in the transformed space. Next, we use these specific moving frames to re-express each term in Eq. (3.18):

$$
\begin{aligned}
\tilde{u}_i^{n+1} &= u_i^{n+1}\, \lambda^{0.5} \left(\frac{2\,u_i^n}{u_{i+1}^n + u_{i-1}^n}\right)^{R^2/\lambda} \\
\tilde{u}_{i\pm1}^{n} &= u_{i\pm1}^{n} \left(\frac{2\,u_i^n}{u_{i+1}^n + u_{i-1}^n}\right) \\
\tilde{u}_i^{n} &= u_i^n \\
\tilde{h} &= \tilde{x}_i - \tilde{x}_{i-1} = h
\end{aligned}
$$

$$\tilde{\tau} = \tilde{t}^{n+1} - \tilde{t}^{n} = \frac{\tau}{\lambda}$$
$$\lambda = 1 - 2\, s_1\, \tau$$
$$R = \alpha\, \frac{\tau}{h}\ . \tag{3.20}$$

And finally, we obtain the invariant numerical scheme for the modified advection equation by substituting Eq. (3.20) into Eq. (3.18) which simplifies to

$$u^{n+1} = u_i^n\, \lambda^{-1.5} \left(\frac{u_{i+1}^n + u_{i-1}^n}{2\, u_i^n} \right)^{R^2/\lambda} \left[\lambda - R \left(\frac{u_{i+1}^n - u_{i-1}^n}{u_{i+1}^n + u_{i-1}^n} \right) \right]\ . \tag{3.21}$$

The invariance condition is checked by transforming Eq. (3.18) one more time according to the transformations defined in Eq. (3.14)–Eq. (3.16)

$$\frac{\tilde{\tilde{u}}^{n+1} - \tilde{\tilde{u}}^{n}}{\tilde{\tilde{\tau}}} + \alpha\, \frac{\tilde{\tilde{u}}_i - \tilde{\tilde{u}}_{i-1}}{\tilde{\tilde{h}}} - \tilde{\tilde{f}}\, \frac{\tilde{\tilde{u}}_{i+1} - 2\, \tilde{\tilde{u}}_i + \tilde{\tilde{u}}_{i-1}}{\tilde{\tilde{h}}^2} = 0\ . \tag{3.22}$$

If Eq. (3.18) is invariant under the considered symmetries then transforming this equation according to transformations given in Eq. (3.14) – Eq. (3.16) will result in the same equation. This can be verified by applying these transformations to every member of Eq. (3.22) and simplifying the results according to the definitions given in Eq. (3.20) as

$$\begin{aligned}
\tilde{s}_1 &= -\frac{2\tilde{f}}{\tilde{h}^2} \ln\left[\frac{2\tilde{u}_i^n}{\tilde{u}_{i+1}^n + \tilde{u}_{i-1}^n} \right] = 0 \\
\tilde{\lambda} &= 1 - 2\, \tilde{s}_1\, \tilde{\tau} = 1 \\
\tilde{\tilde{h}} &= \tilde{h} \\
\tilde{\tilde{\tau}} &= \frac{\tilde{\tau}}{\tilde{\lambda}} = \tilde{\tau} \\
\tilde{\tilde{u}}_i^{n+1} &= \tilde{u}_i^{n+1}\, \tilde{\lambda}^{0.5} \left(\frac{2\, \tilde{u}_i^n}{\tilde{u}_{i+1}^n + \tilde{u}_{i-1}^n} \right)^{\tilde{R}^2/\tilde{\lambda}} = \tilde{u}_i^{n+1} \\
\tilde{\tilde{u}}_{i\pm1}^{n} &= \tilde{u}_{i\pm1}^{n} \left(\frac{2\, \tilde{u}_i^n}{\tilde{u}_{i+1}^n + \tilde{u}_{i-1}^n} \right) = \tilde{u}_{i\pm1}^{n}
\end{aligned} \tag{3.23}$$

$$\tilde{\tilde{u}}_i^n = \tilde{u}_i^n \ .$$

Considering the relations in Eq. (3.23), it can be seen that Eq. (3.22) reads exactly the same as Eq. (3.18) verifying invariance under the considered symmetry groups.

3.4.2 Linear Advection Equation in 2D

In the case of two-dimensional linear advection equation, the symmetries of the system also have complicated structures which make them cumbersome to use in numerical algorithms. Instead we propose a slightly different approach to preserve the symmetries and invariantize the existing numerical scheme. It is known that the advection equation in 2-D with initial condition u_0

$$\frac{\partial u}{\partial t} + \alpha \frac{\partial u}{\partial x} + \beta \frac{\partial u}{\partial y} = 0 \tag{3.24}$$

can be split into two equations,

$$\frac{\partial u}{\partial t} + \alpha \frac{\partial u}{\partial x} = 0 \tag{3.25}$$

$$\frac{\partial u}{\partial t} + \beta \frac{\partial u}{\partial y} = 0 \tag{3.26}$$

by using dimensional splitting techniques, without introducing any splitting error to the system [105–107]. However, we still have the numerical error due to the truncation error of the discretization. Both split equations can be treated separately for the invariantization procedure. We have already obtained an invariant numerical scheme for the modified version of Eq. (3.25). Similarly, we can modify Eq. (3.26) by introducing an artificial diffusion to the RHS of the equation as a single perturbation

term

$$\frac{\partial u}{\partial t} + \beta \frac{\partial u}{\partial y} = g \frac{\partial^2 u}{\partial y^2} \ . \tag{3.27}$$

Here, the artificial diffusion coefficient g is also considered to be equal to machine precision ϵ_{mach}. The symmetry structures and transformation formulas of both Eq. (3.27) and Eq. (3.6) are identical except that they are defined in different spatial dimensions as given in the following

$$\tilde{t} = \frac{t + p_6}{1 - 2\,p_1\,(t + p_6)} \tag{3.28}$$

$$\tilde{y} = \frac{y + p_5}{1 - 2\,p_1\,(t + p_6)} \tag{3.29}$$

$$\tilde{u} = u\sqrt{1 - 2\,p_1\,(t + p_6)}\,\exp\left[-\frac{p_1\,((y + p_5) - \beta\,(t + p_6))^2}{2\,g\,(1 - 2\,p_1\,(t + p_6))}\right] . \tag{3.30}$$

The symmetry parameters (p_1, p_5 and p_6) are obtained by considering the same normalization conditions as before but this time using (t, y) coordinates instead of (t, x) as

$$\begin{aligned} \tilde{t}^n = 0 \quad &\Rightarrow \quad p_6 = -t^n \\ \tilde{y}_j = 0 \quad &\Rightarrow \quad p_5 = -y_j \\ \partial_{\tilde{y}\tilde{y}}\,\tilde{u} = 0 \quad &\Rightarrow \quad p_1 = -\frac{2g}{k^2}\,\ln\left[\frac{2u_j^n}{u_{j+1}^n + u_{j-1}^n}\right] . \end{aligned} \tag{3.31}$$

And finally, we can construct an invariant upwind numerical scheme for Eq. (3.27) as

$$u_j^{n+1} = u_j^n\,\Lambda^{-1.5}\left(\frac{u_{j+1}^n + u_{j-1}^n}{2\,u_j^n}\right)^{C^2/\Lambda}\left[\Lambda - C\left(\frac{u_{j+1}^n - u_{j-1}^n}{u_{j+1}^n + u_{j-1}^n}\right)\right] \tag{3.32}$$

where, $\Lambda = 1 - 2p_1\tau$, and $C = \beta\tau/k$ is the CFL number. After constructing invariant numerical schemes for both Eq. (3.25) and Eq. (3.26), we use a Strang splitting algorithm [106] to combine both equations.

3.4.3 Inviscid Burgers' Equation

Similarly, the inviscid Burgers' equations is associated with the following Lie group:

$$\begin{aligned}
X_1 &= t^2\frac{\partial}{\partial t} + xt\frac{\partial}{\partial x} + (x - tu)\frac{\partial}{\partial u} \\
X_2 &= tx\frac{\partial}{\partial t} + x^2\frac{\partial}{\partial x} + u(x - tu)\frac{\partial}{\partial u} \\
X_3 &= 2t\frac{\partial}{\partial t} + x\frac{\partial}{\partial x} - u\frac{\partial}{\partial u} \\
X_4 &= x\frac{\partial}{\partial t} - u^2\frac{\partial}{\partial u} \\
X_5 &= t\frac{\partial}{\partial x} + \frac{\partial}{\partial u} \\
X_6 &= \frac{\partial}{\partial t} \\
X_7 &= \frac{\partial}{\partial x}\ .
\end{aligned} \tag{3.33}$$

Based on the above Lie group, we first construct an invariant numerical scheme for the non-conservative form of the inviscid Burgers' equation (Eq. (3.7)) that preserves certain symmetries of the equation. Note that for this particular problem, determination of the discrete variable transformations that are associated with all the symmetries of the inviscid Burgers' equation, Eq. (3.33), may not be achievable as the forms of these transformations are strongly affected by these symmetries and become complex if more symmetries are considered. Therefore, we ignore some of the symmetries and only consider the symmetry groups X_1, X_6, and X_7 in this work. For these specific groups, the application of Eq. (3.13) to each group in an

arbitrary order results in the following variable transformations

$$\begin{aligned}\tilde{t} &= \frac{t+p_6}{1-p_1\,(t+p_6)} \\ \tilde{x} &= \frac{x+p_7}{1-p_1\,(t+p_6)} \\ \tilde{u} &= u\,[1-p_1(t+p_6)]+p_1(x+p_7)\ .\end{aligned} \tag{3.34}$$

The symmetry parameters p_1, p_6, and p_7 are defined by choosing the following normalization conditions:

$$\begin{aligned}\tilde{t}^n &= 0 \quad \Rightarrow \quad p_6 = -t^n \\ \tilde{x}_i &= 0 \quad \Rightarrow \quad p_7 = -x_i\end{aligned} \tag{3.35}$$

and

$$\tilde{u}_{\tilde{x}} = 0 \quad \Rightarrow \quad \frac{\tilde{u}_i-\tilde{u}_{i-1}}{\tilde{x}_i-\tilde{x}_{i-1}} = 0 \quad \Rightarrow \quad \tilde{p}_1 = -u_x = -\frac{u_i-u_{i-1}}{h}\ . \tag{3.36}$$

The above normalization condition ($\tilde{u}_{\tilde{x}} = 0$) is chosen because it simplifies the non-conservative form of the modified IBE, Eq. (3.10), in the transformed space by removing all the terms that include $\tilde{u}_{\tilde{x}}$. In other words, the numerical approximation of the first spatial derivative goes to zero for this specific selection of the moving frame, simplifying Eq. (3.10) such that it reads as

$$\frac{\partial\,\tilde{u}}{\partial\tilde{t}} = \frac{1}{2}(\tilde{\tau}\,\tilde{u}-\tilde{h})\,\tilde{u}\,\frac{\partial^2\,\tilde{u}}{\partial\,\tilde{x}^2} + O(\tilde{\tau}^2,\tilde{h}^2)\ . \tag{3.37}$$

And finally, the finite difference scheme constructed for the modified IBE, Eq. (3.10), that is invariant under the symmetry groups X_1, X_6 and X_7 is given as

$$\frac{\tilde{u}_i^{n+1}-\tilde{u}_i^n}{\tilde{\tau}} = \frac{1}{2}(\tilde{\tau}\,\tilde{u}_i^n-\tilde{h})\,\tilde{u}_i^n\,\frac{\tilde{u}_{i+1}^n-2\tilde{u}_i^n+\tilde{u}_{i-1}^n}{\tilde{h}^2} \tag{3.38}$$

where

$$
\begin{aligned}
&\tilde{h} = \tilde{x}_i - \tilde{x}_{i-1} = 0 - (-h) = h \\
&\tilde{\tau} = \tilde{t}^{n+1} - \tilde{t}^{n} = \frac{\tau}{1-\tau\, p_1} - 0 = \frac{\tau}{1-\tau\, p_1} \\
&\tilde{u}_{i\pm1} = u_{i\pm1} \pm h\, p_1 \\
&\tilde{u}_i^n = u_i^n \\
&\tilde{u}_i^{n+1} = u_i^{n+1}[1-\tau\, p_1] + p_1\,(x^{n+1} - x^n)\ .
\end{aligned}
\tag{3.39}
$$

The quantity $x^{n+1} - x^n$ is zero when a solution grid that is regular in time and space is used in computations.

As for the conservative form of the inviscid Burgers' equation, Eq. (3.8), the procedure to construct an invariant scheme is similar to that of the previous (non-conservative) case. The moving frames defined in Eq. (3.35) and Eq. (3.36) are applicable to this problem as well. Note that the latter moving frame which was used to set the numerical representation of the spatial first derivative to zero ($\tilde{u}_{\tilde{x}} = 0$) also indicates that the numerical approximation of the spatial first derivative of f is zero ($\tilde{f}_{\tilde{x}} = 0$). Hence, the final form of the invariant scheme constructed through the modified form of the (conservative) IBE, Eq. (3.11), in the transformed space is found as

$$
\frac{\partial\, \tilde{u}}{\partial \tilde{t}} = \frac{1}{2}(\tilde{\tau}\, \tilde{u} - \tilde{h})\, \frac{\partial^2 \tilde{f}}{\partial\, \tilde{x}^2} + O(\tilde{\tau}^2, \tilde{h}^2)
\tag{3.40}
$$

where $\tilde{f} = \frac{1}{2}\, \tilde{u}^2$.

In order to check if Eq. (3.38) and Eq. (3.40) are invariant under the considered symmetry groups, each member of both equations is transformed again per variable transformations given in Eq. (3.34). If these equations are invariant under these symmetry groups, the resulting equations must read exactly the same as Eq. (3.38)

and Eq. (3.40) as shown in the following

$$
\begin{aligned}
&\tilde{p}_1 = -\tilde{u}_{\tilde{x}} = 0 \\
&\tilde{\tilde{h}} = \tilde{h} = h \\
&\tilde{\tilde{\tau}} = \frac{\tilde{\tau}}{1 - \tilde{\tau}\tilde{p}_1} = \tilde{\tau} \\
&\tilde{\tilde{u}}_i^{n+1} = \tilde{u}_i^{n+1}[1 - \tilde{\tau}\,\tilde{p}_1] + \tilde{p}_1\,(\tilde{x}^{n+1} - \tilde{x}^n) = \tilde{u}_i^{n+1} \\
&\tilde{\tilde{u}}_{i\pm1}^{n} = \tilde{u}_{i\pm1}^{n} \pm \tilde{p}_1\,(\tilde{x}^{n+1} - \tilde{x}^n) = \tilde{u}_{i\pm1}^{n} \\
&\tilde{\tilde{u}}_i^{n} = \tilde{u}_i^{n} \\
&\tilde{\tilde{f}}_i^{n} = \tilde{f}_i^{n} \\
&\tilde{\tilde{f}}_{i\pm1}^{n} = \frac{1}{2}(\tilde{u}_{i\pm1}^{n})^2 \pm \tilde{p}_1\,\tilde{h}\,\tilde{u}_{i\pm1}^{n} + (\tilde{p}_1\tilde{h})^2 = \tilde{f}_{i\pm1}^{n}\ .
\end{aligned}
\tag{3.41}
$$

3.5 Numerical Experiments

In this section, we discuss the performance of the proposed invariant numerical schemes constructed for the linear advection (in 1D and 2D) and the inviscid Burgers' equations. Comparisons are also made with the analytical solutions. In all the test problems considered here, the proposed invariant numerical schemes were found to be more accurate than the corresponding (base) classical numerical schemes.

3.5.1 Linear Advection Equation in 1D

We first evaluate the performance of the proposed invariant numerical scheme constructed for the modified advection equation in one-dimension, Eq. (3.21), over the domain $\Gamma = [-4, 8]$. The exact analytical solution for this problem is given by

$$
u_{exact} = c_o + \frac{1}{\sigma\sqrt{2\,\pi}} \exp\left[\frac{-(x - \alpha\,t)^2}{2\,\sigma^2}\right] \tag{3.42}
$$

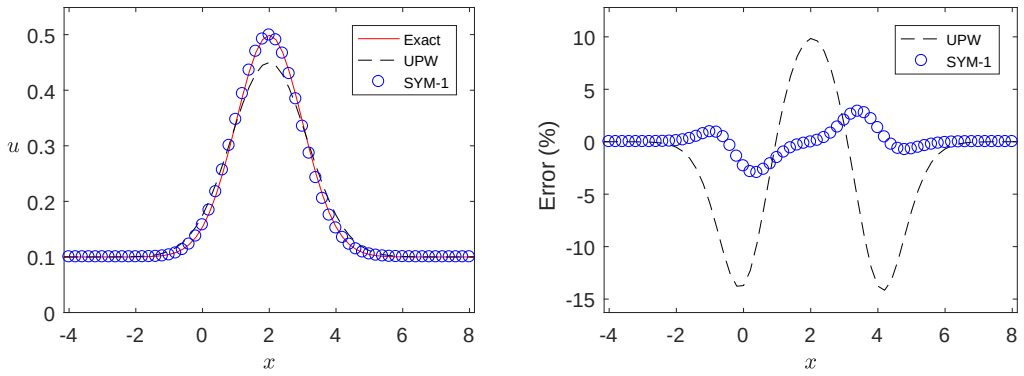

Fig. 3.1. Advection equation (1D). Comparison of profiles of u (at $t = 2$) obtained from the exact solution, first order upwind scheme, and proposed invariant scheme is shown in the left figure. Spatial distributions of percentage errors are shown in the right figure. Parameter settings: $\tau = 0.05,\ h = 0.2,\ \alpha = 1,$ and $f = \epsilon_{mach}$.

where, σ represents the characteristic width of the kernel (analogous to standard deviation), α represents the characteristic (constant) wave speed and the parameter c_o represents a simple shift (or translation). For all our test cases, we assume $\sigma = 1$, $\alpha = 1$ and $c_o = 0.1$. The initial and boundary conditions can be inferred from the above exact solution.

In figure 3.1 (left), snapshots of the propagating wave u, at $t = 2$, obtained using the exact analytical solution (Eq. (3.42)), first order upwind scheme (Eq. (3.5)), and proposed invariant scheme (Eq. (3.21)) are shown. The artificial diffusion coefficient f needed for the invariant solution (SYM-1) is assumed to be equal to the machine precision ϵ_{mach}. Although a coarse mesh with 61 spatial grid nodes is used for this specific run, the invariant (or symmetric) scheme (SYM-1) predicts the evolution of u with a high degree of accuracy in contrast to the upwind scheme which is not as accurate, and the latter especially fails to reliably capture the behavior near the wave crest. The spatial distribution of percentage error of both numerical schemes, $100 \times (u_a - u_n)/u_a$, along x axis is presented in figure 3.1 (right), where u_a and u_n denote the analytical and numerical solutions respectively. In this figure, we note that the invariant scheme has enhanced accuracy by virtue of preservation of

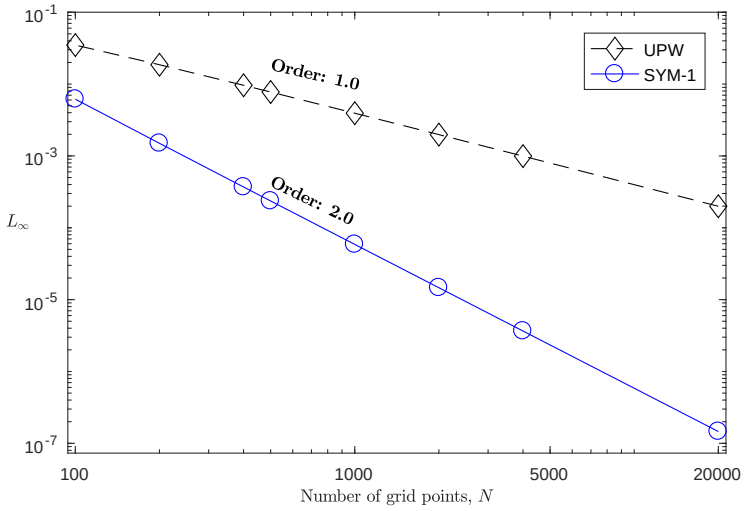

Fig. 3.2. L_∞ errors associated with numerical solutions of advection equation (1D) versus number of grid points for a fixed Courant number, $C = 0.5$.

symmetries in the discrete formulas. The L_∞ errors, estimated as $max(|u_a - u_n|)$, of both the upwind and invariant solutions in this case are found to be 0.049 and 0.007, respectively. Similarly, the root mean square errors, estimated as $RMSE = \sqrt{\sum (u_a - u_n)^2 / N}$, corresponding to both methods are noted to be 0.013 (UPW) and 0.002 (SYM-1). Based on the error comparisons presented here (along with figure 3.1), it appears that the proposed invariant scheme performs better than the classical first order upwind scheme.

Figure 3.2 shows the variations of the L_∞ errors of both numerical schemes with respect to number of spatial grid nodes for a constant Courant number ($C = 0.5$). From this figure, it appears that the proposed invariant scheme (SYM-1) is at least one order more accurate than the classical first order upwind scheme (UPW). Such improvement in accuracy due to symmetry preservation, is also useful for extension to development of high order accurate schemes for multidimensional problems.

Recall that the artificial diffusion term is only added to the linear advection equation to obtain symmetries associated with more convenient discrete variable transformations, Eq. (3.14) – Eq. (3.16). The behavior of various discrete schemes

Table 3.1
Root mean square error (RMSE) and L_∞ error in numerical solutions of advection equation obtained from various numerical schemes for $\tau = 0.01,\ h = 0.2,$ and $\alpha = 1$.

Error	UPW	MOD-1	MOD-2	SYM-1	SYM-2
RMSE	1.58×10^{-2}	1.65×10^{-2}	2.20×10^{-3}	2.30×10^{-3}	2.40×10^{-3}
L_∞	5.92×10^{-2}	6.16×10^{-2}	7.00×10^{-3}	8.00×10^{-3}	6.00×10^{-3}

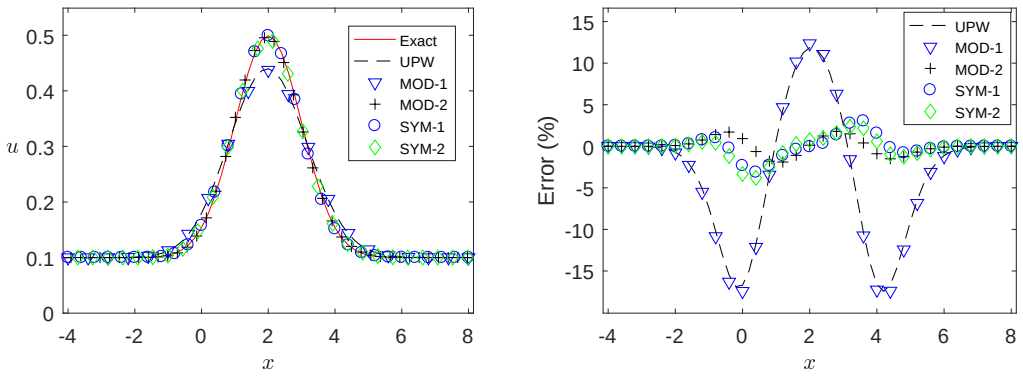

Fig. 3.3. Advection equation (1D). Comparison of profiles of u (at $t = 2$) obtained from the exact solution, and the numerical solutions is shown in the left figure. Spatial distributions of percentage errors are shown in the right figure. Parameter settings: $\tau = 0.01,\ h = 0.2,$ and $\alpha = 1$.

for different values of the artificial diffusion coefficient f is shown in figure 3.3. The cases considered here include numerical solutions obtained from the upwind scheme, modified upwind-1 (MOD-1, $f = 0.5\,\alpha^2\,\tau$) scheme, modified upwind-2 (MOD-2, $f = 0.5\,\alpha^2\,[\tau - h/\alpha]$) scheme, proposed invariant-1 (SYM-1, $f = \epsilon_{mach}$) scheme and proposed invariant-2 (SYM-2, $f = 0.5\,\alpha^2\,\tau$) scheme. Note that the modified upwind-2 scheme, with this particular selection of the artificial diffusion coefficient f, is a second order accurate scheme in space and time. Snapshots of numerical solutions obtained from these numerical schemes are shown in figure 3.3 (left). It appears that both invariant schemes (SYM-1 and SYM-2) perform comparably better than the upwind scheme and modified upwind-1 scheme in terms of numerical accuracy. The proposed invariant schemes also predict the evolution of the quantity u at least as accurate as the modified upwind-2 scheme which is known to be second order accurate in time and space. On the right plot in figure 3.3, the spatial distribution

of percentage errors for all these numerical schemes are plotted against the x-axis. The invariant solutions have significantly less numerical error compared to the classical upwind and modified solutions and captures the wave propagation significantly better (with less error), particularly around the wave crest. The root mean square errors and L_∞ errors of these numerical schemes for this specific test run are given in Table 3.1. The table of errors shows that both (proposed) invariant schemes are one order of magnitude more accurate than the classical upwind and modified upwind-1 solutions whereas they are at the same order of magnitude as the modified upwind-2 solution.

3.5.2 Linear Advection Equation in 2D

Further, we evaluate the performance of the proposed invariant scheme constructed for the two-dimensional advection equation over the domain $\Gamma = [-4, 6]$ (in both x- and y-coordinates). The analytical solution for this problem is given by

$$u_{exact} = \frac{1}{\sigma\sqrt{2\,\pi}} \exp\left[-\frac{(x-\alpha\,t)^2 + (y-\beta\,t)^2}{2\,\sigma^2}\right] \tag{3.43}$$

where, α and β represent characteristic wave speeds and σ represents the characteristic width of the kernel. For simplicity reasons only, we assume $\alpha = \beta = 0.5$, $\sigma = 1$, and used a mesh that is regular in space ($h = k$) in all numerical tests.

The spatial distribution of numerical errors, $\varepsilon = u_a - u_n$, obtained from both the upwind scheme (left) and proposed invariant scheme (right) constructed for the advection equation (in 2D) are depicted in figure 3.4. As it was the case for the one-dimensional advection equation, the proposed invariant scheme developed for this particular problem also performs significantly better than the classical first order upwind solution in terms of numerical accuracy. For this specific test case, the root mean square errors of both the upwind and invariant schemes are found

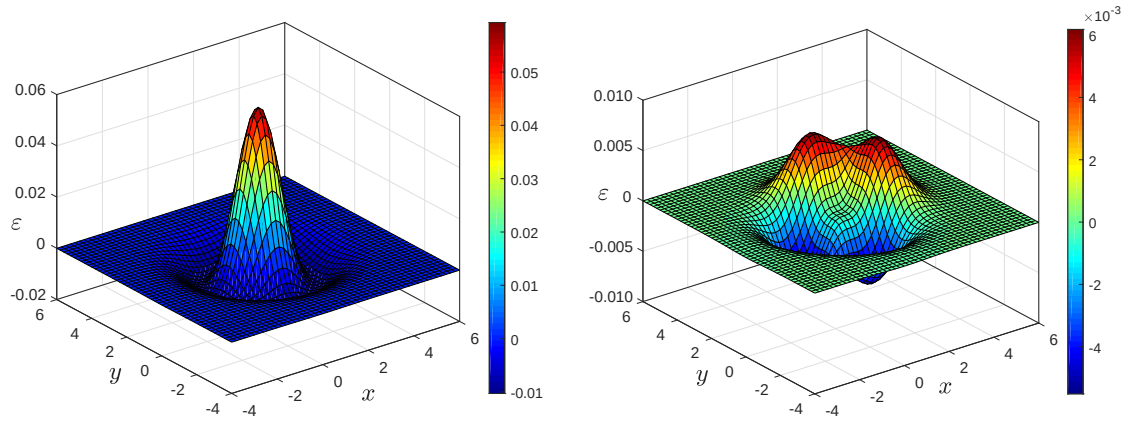

Fig. 3.4. Advection equation (2D). Spatial distributions of numerical errors obtained from the upwind scheme (left) and the proposed invariant scheme (right). Parameter settings: $\tau = 0.05,\ h = k = 0.2,\ \ \alpha = \beta = 0.5$ where $\varepsilon = u_a - u_n$.

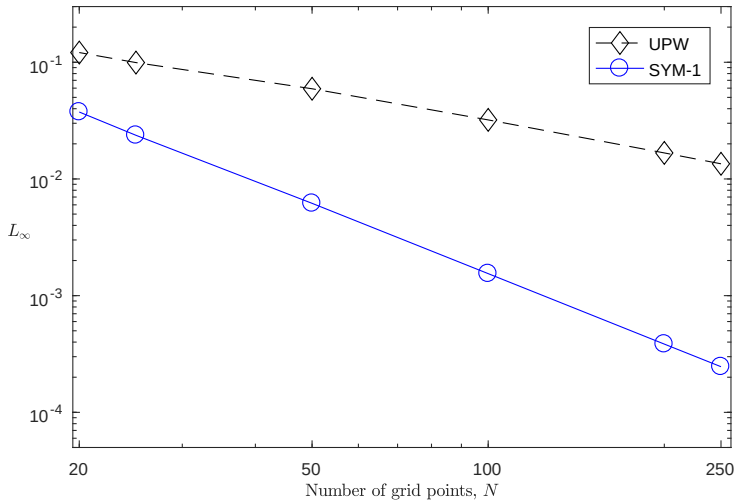

Fig. 3.5. L_∞ errors associated with numerical solutions of two-dimensional advection equation as a function of number of grid points. Parameter settings: $h = k$, $\alpha = \beta = 0.5$, and $\tau/h = 0.25$.

to be 0.008 and 0.001, respectively. Similarly, the L_∞ error of solutions are noted as 0.061 (upwind) and 0.006 (invariant). As it is obvious from the error analysis, the invariant scheme has significantly less error compared to the classical upwind scheme in this case as well.

Furthermore, the comparisons of L_∞ errors of both the classical upwind and proposed invariant schemes (developed for two-dimensional advection equation) with

Table 3.2
Root mean square error (RMSE) and L_∞ error in numerical solutions of inviscid Burgers' equation obtained from various schemes, with $\tau = 0.01,$ and $h = 0.05$.

t	Error	UPW	Lax-W	MOD	SYM-NC
0.5	RMSE	1.85×10^{-3}	1.20×10^{-4}	1.10×10^{-4}	8.01×10^{-5}
0.5	L_∞	5.56×10^{-3}	4.70×10^{-4}	4.30×10^{-4}	2.90×10^{-4}
1.5	RMSE	8.90×10^{-3}	1.46×10^{-3}	1.40×10^{-3}	1.18×10^{-3}
1.5	L_∞	5.12×10^{-2}	1.12×10^{-2}	1.17×10^{-2}	1.02×10^{-2}

respect to the number of grid points are displayed in figure 3.5. The order of accuracy of numerical schemes obtained from the slopes of these plots indicate that the proposed invariant scheme is at least one order more accurate than the classical first order upwind scheme. This implies that the computation time required to successfully simulate multidimensional problems with high numerical accuracy can be significantly shortened when a standard scheme is modified to preserve Lie symmetries of the associated continuous differential equation.

3.5.3 Inviscid Burgers' Equation

Finally, the performance of the classical upwind scheme, Eq. (3.9), modified upwind scheme, Eq. (3.10), Lax-Wendroff scheme, and proposed invariant schemes, Eq. (3.38) and Eq. (3.40), constructed for the inviscid Burgers' equation are evaluated. Two different kinds of initial conditions are considered including (a) a continuous (Gaussian) profile and (b) a discontinuous profile. In the former case, the initial and boundary conditions can be noted from the following analytical solution:

$$u = \frac{1}{\sigma \sqrt{2\,\pi}} \exp\left[\frac{-(x - t\,u)^2}{2\,\sigma^2}\right] . \tag{3.44}$$

Snapshots of the profile u (at $t = 0.5, 1.5$) obtained from the analytical solution, classical upwind solution, modified upwind solution, Lax-Wendroff solution, and proposed (non-conservative) invariant solution are displayed in figure 3.6 (left

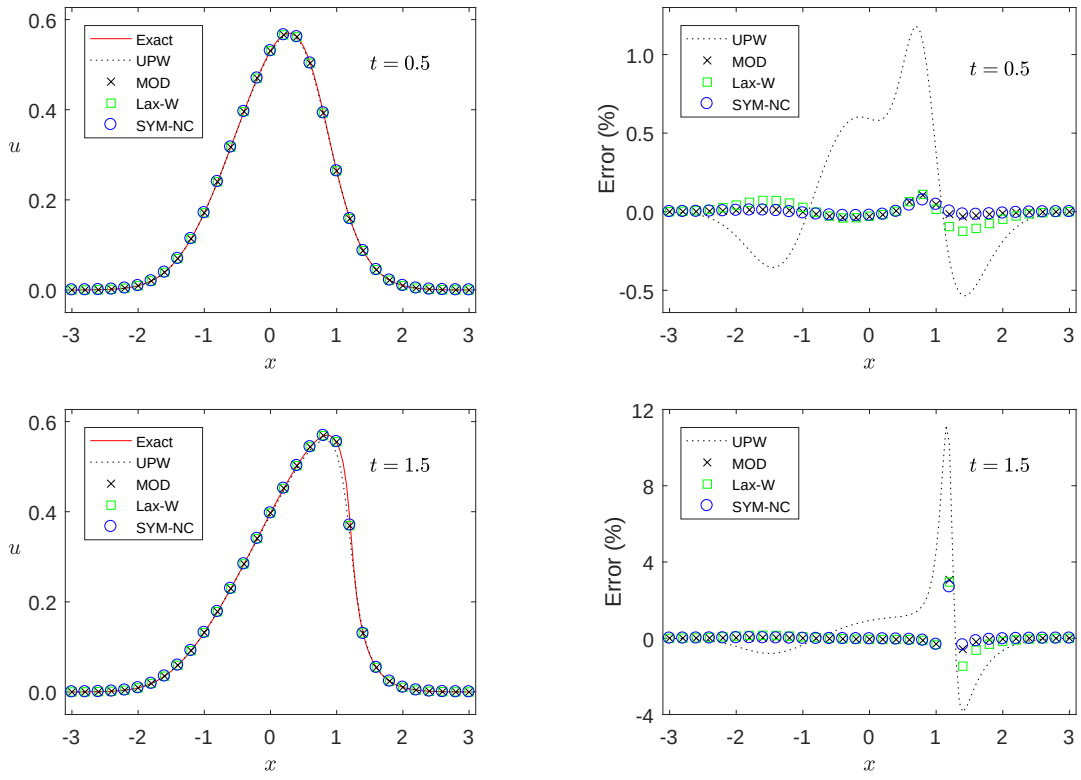

Fig. 3.6. Inviscid Burgers' equation. Comparison of profiles of u (at $t = 0.5,\ 1.5$) obtained from the exact and numerical solutions is shown in the left figures. Spatial distribution of percentage errors is shown in the right figures. Parameter settings: $\tau = 0.05$, and $h = 0.05$.

plots). The spatial distribution of percentage errors for these particular numerical solutions are also displayed in figure 3.6 (right plots). It appears that the invariant scheme performs significantly better than the upwind, and slightly better the modified upwind and the Lax-Wendroff (which are known to be second order accurate) schemes. This improvement in numerical accuracy is particularly visible around the crest of the nonlinear wave where the behavior of the proposed invariant scheme is comparably better than the other classical schemes. The error analysis of these schemes given in table 3.2 also verify that the invariant scheme performs with less error in comparison to the other schemes. Although, the proposed invariant scheme and the other classical schemes appear to capture the wave propagation at a later time (closer to a breaking time), $t = 1.5$, it appears that these methods fail to ob-

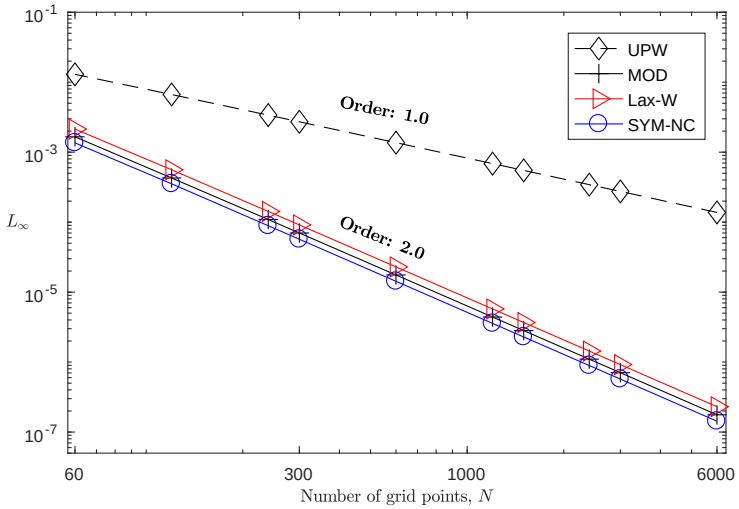

Fig. 3.7. L_∞ errors of numerical solutions of inviscid Burgers' equation versus number of grid points for fixed $\tau/h = 0.5$.

tain a numerical solution (for this particular initial profile) past a breaking time. We attribute the inability of the proposed invariant scheme (relevant to obtaining a solution past a breaking time) to the limitations inherited from the (considered) base numerical scheme. This limitation of the proposed invariant scheme could perhaps be mitigated by choosing base numerical schemes that are better equipped to capture the evolution of such initial (Gaussian) profiles (e.g., WENO schemes [108]).

To further investigate the performance of the numerical schemes constructed for the inviscid Burgers' equation with the Gaussian initial profile, the L_∞ errors of these schemes (at $t = 0.5$) are plotted against the number of spatial grid points (figure 3.7). Similar to the cases relevant to the advection equation (in 1D and 2D), it appears that, in this case as well, the proposed invariant scheme performs much better than the classical first order upwind scheme as the accuracy is increased from the first to second order. The invariant scheme also generates slightly better results than the second order modified upwind and Lax-Wendroff schemes.

Further, the performance of the selected numerical schemes is evaluated in the case of a shock problem where the initial discontinuity is given by the following

Table 3.3
Root mean square error (RMSE) and L_∞ error in numerical solutions of inviscid Burgers' equation (in the case of a Riemann problem) obtained from various schemes for $\tau = 0.01,$ and $h = 0.05$.

Error	UPW	Lax-W	MOD	SYM-NC	SYM-C
RMSE	3.07×10^{-2}	3.05×10^{-2}	2.22×10^{-2}	2.28×10^{-2}	2.20×10^{-2}
L_∞	2.08×10^{-1}	2.02×10^{-1}	1.51×10^{-1}	1.61×10^{-1}	1.24×10^{-1}

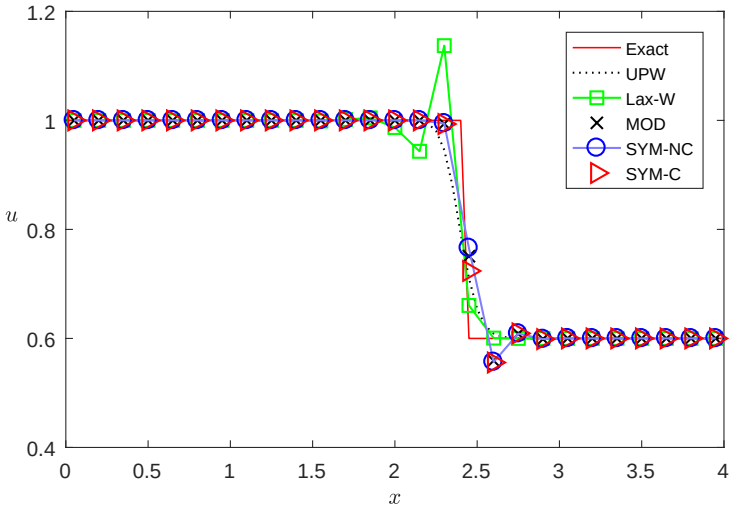

Fig. 3.8. Inviscid Burgers' equation. Comparison of shock profiles of u (at $t = 0.5$) obtained from the exact solution, first order upwind scheme, Lax-Wendroff scheme, modified upwind scheme, and proposed (conservative and non-conservative) invariant schemes. Parameter settings: $\tau = 0.01,$ and $h = 0.05.$

profile

$$u(0,x) = \begin{cases} 1.0 & \text{if} \quad x \leq 2.0 \ , \\ 0.6 & \text{if} \quad x > 2.0 \ . \end{cases} \tag{3.45}$$

Snapshots of the propagating shocks (at $t = 0.5$) obtained from the exact, upwind (UPW), Lax-Wendroff (Lax-W), modified (MOD), proposed non-conservative invariant (SYM-NC), and proposed conservative invariant (SYM-C) solutions are given in figure 3.8. In addition, the root mean square errors and L_∞ errors of these schemes are presented in table 3.3. Although all the numerical schemes successfully generate a solution for this particular problem, the Lax-Wendroff, modified upwind,

and both proposed invariant schemes develop oscillations near the discontinuity (which is commonly referred to as Gibbs phenomenon). However, error analysis of these numerical solutions shows that the proposed invariant schemes have less errors compared to the other schemes. Note that, as mentioned earlier, when dealing with problems where shocks exist/develop, it is important to choose base numerical schemes (for construction of invariant schemes) that are more convenient for capturing such discontinuities as certain limitations of these base schemes might be inherited by the constructed invariant schemes. The improvement in numerical accuracy encountered in the solution of this nonlinear problem also verifies that symmetry preservation can improve the quality of results obtained from existing (base) schemes for both linear and nonlinear problems in addition to retaining qualitative properties of associated continuous differential equations.

3.6 Chapter Summary

In this chapter, we presented a method to develop invariant (or Lie symmetry preserving) finite difference schemes for solution of PDEs based on modified forms of these PDEs and the method of equivariant moving frames. Our focus was not only to construct invariant schemes but also to improve the accuracy of numerical schemes using modified forms of PDEs. These modified forms that are obtained either through addition of perturbation terms to the original PDEs or through defect correction procedures can lead symmetry groups that are associated with transformations that are more convenient to handle. The additional terms that appear in the modified forms of PDEs are either completely or partially removed from the system via selection of appropriate moving frames. The performance of these invariant schemes was found to be considerably better than the existing base schemes, based on tests conducted for the linear advection equation (in 1D and 2D) and the nonlinear advection equation.

We first applied the proposed method to construct an invariant numerical scheme for the one-dimensional linear advection equation. In this case, the modification procedure involves addition of an artificial diffusion term ($f\,\partial_{xx}u$) to the partial differential equation. Each variable of the equation is transformed according to symmetries of the modified equation. The artificial diffusion term is removed from the system by choosing a convenient normalization condition for which the discrete representation of this diffusion term goes to zero (i.e., $\partial_{\tilde{x}\tilde{x}}\tilde{u} = 0$). Although the resulting discrete form of the modified equation in terms of new variables (i.e., the proposed invariant form) is identical to the discrete form of original advection equation (e.g. the classical first order upwind scheme), a significant improvement in accuracy (from first to second order) was achieved through the use of the proposed invariant scheme. Further, we constructed an invariant numerical scheme for the two-dimensional linear advection equation and found similar improvement in accuracy.

Moreover, to test the proposed method for a nonlinear problem, invariant numerical schemes were constructed for the non-conservative and conservative forms of the inviscid Burgers' equation as well. For this nonlinear problem, although the particular normalization condition $\tilde{u}_{\tilde{x}} = 0$ that removes terms from the leading order truncation error (by setting the discrete representation of the first derivative to be zero) appears to have the potential to increase accuracy, this condition results in a trivial solution when applied to the original form of the PDE. This obstacle is easily avoided by considering a modified form of the PDE that includes additional terms obtained via defect correction (or analysis of leading order truncation error). By consideration of symmetry preservation in numerical schemes, it was found that invariant numerical schemes with improved accuracy can be constructed based on modification of classical schemes. In particular, we constructed second order accurate invariant numerical schemes for the inviscid Burgers' equation by modifying the first order accurate (non-conservative and conservative) base schemes. The perfor-

mance of these numerical schemes was found to be better than the other schemes in terms of numerical accuracy. We also note that for cases where initial profiles have discontinuities (or where discontinuous solutions emerge past a certain time), the performance of the invariant schemes (constructed through our proposed method) appears to depend on the chosen base (non-invariant) numerical schemes as certain limitations of these base schemes are inherited by the invariant schemes.

We conclude that construction of invariant numerical schemes with the proposed method which is based on method of moving frames has the potential to offer significant improvements (in accuracy and qualitative properties or symmetries) over classical finite difference schemes. The proposed approach for construction of invariant numerical schemes using defect correction techniques can also be extended to generation of high order accurate invariant numerical schemes with a desired order of accuracy.

CHAPTER 4

High Order Accurate Finite Difference Schemes based on Symmetry Preservation

4.1 Scope of the Chapter

In this chapter, we introduce a mathematical approach that is based on the method of equivariant moving frames for development of high order accurate invariant numerical schemes (for solution of PDEs) with desired order of accuracy. We propose the use of modified forms of PDEs for construction of invariant schemes not only to improve the quality of numerical solutions (by virtue of invariance) but also to fix the accuracy of the invariant numerical scheme to any desired order. The latter feature is a novel aspect of the work presented in this chapter, unlike previous works on invariant schemes [68, 77, 88]. Further, the modified forms of equations are found be very useful for identifying moving frames (among infinite possibilities) that lead to invariant schemes with enhanced accuracy. Note that modified forms of PDEs are obtained by addition of defect correction terms (obtained from truncation error analysis) to the original forms of PDEs, and these additional terms are then either completely removed from schemes or significantly simplified by considering appropriate moving frames. In some cases, appropriate choice of moving frames also removes selected terms of the discrete form of the PDE (besides defect correction terms). This is an attractive feature of the proposed method that simplifies the representation of defect correction terms and their implementation in simulation codes for attaining higher order accuracy (besides symmetry preservation). In contrast,

traditional high order methods developed from some lower order (non-invariant) base schemes through the method of modified equations can be cumbersome to implement due to the presence of multiple defect correction terms. To demonstrate the application of the proposed method, we consider some linear and nonlinear problems and construct high order accurate invariant numerical schemes for these problems. In all the test cases, the proposed invariant schemes appear to be performing significantly better in terms of numerical accuracy than the considered non-invariant base schemes, thereby verifying the potential advantages of symmetry preservation in numerical schemes.

As our first test case, we consider the linear advection-diffusion equation in 1D and construct a fourth order accurate invariant numerical scheme that is obtained (via the proposed method) from a classical second order (non-invariant) base scheme. The modified form of the linear advection-diffusion equation contains multiple defect correction terms that include first, second, third, and fourth order spatial derivatives in various configurations. By considering convenient moving frames, along with a special time step, all the defect terms of the modified equation are completely removed from the scheme in the transformed space. Moreover, with this particular selection of moving frames, the diffusion term of the original linear advection-diffusion equation is also removed from the scheme. The final form of the fourth order accurate invariant scheme is found to be of the form of a linear advection equation in the transformed space. This indicates that a fourth order accurate invariant scheme is constructed only on a three-point stencil which can be considered as a major simplification in the numerical representation of the scheme. We further test the proposed method by constructing several different invariant numerical schemes for the inviscid Burgers' equation. Two second order accurate invariant schemes that preserve different symmetry groups of the inviscid Burgers' equation are constructed and some important measures of their performance are compared.

The objective is to evaluate the effect of the choice of preserved symmetries on the accuracy of the resulting invariant schemes. Results indicate that both invariant schemes (although one of them preserves more symmetries and has a much more complex numerical representation) perform similar and the differences are minor. Another fourth order accurate invariant numerical scheme was constructed for the inviscid Burgers' equation by considering only selected symmetries. As our next problem, we consider the viscous Burgers' equation, another commonly used equation, and construct a fourth order invariant numerical scheme. Similar to the linear advection-diffusion case, the modified form of the equation includes spatial derivative terms of various orders. Therefore, applying a similar procedure as before, all the defect terms except one are removed from the scheme in the transformed space. Additionally, the nonlinear transport term in the original form of the viscous Burgers' equation is also eliminated from the scheme. The final form of the fourth order invariant scheme constructed for the viscous Burgers' equation is found to be of the form of a nonlinear diffusion equation. We conclude our tests by constructing two fourth order accurate invariant numerical schemes for the two-dimensional linear advection-diffusion equation. Each invariant scheme is constructed by considering different set of moving frames for the purpose of evaluating the effect of the selected moving frames on the accuracy of invariant schemes. It is seen that both schemes are fourth order accurate and the effect of choice of selected moving frames on the accuracy of the schemes appears to be minor.

4.2 Construction of High Order Invariant Schemes

In this section, we present a method that is based on modified equations and equivariant moving frames to construct fourth order accurate invariant numerical schemes for the linear advection-diffusion equation in 1D and 2D, the inviscid Burgers' equation, and the viscous Burgers' equation. Note that the order of accuracy of these

invariant schemes can be arbitrarily fixed by considering modified forms of underlying equations which are also covered in this section.

4.2.1 Linear Advection-Diffusion Equation in 1D

As our first test case, we consider the one-dimensional linear advection-diffusion equation of the form

$$u_t + \alpha\, u_x = \nu\, u_{xx} \tag{4.1}$$

which describes the evolution of a quantity $u(t,x)$ due to linear advection and diffusion processes. Here, the symbols α and ν represent the constant characteristic speed and the diffusion coefficient, respectively. To test our proposed method for construction of invariant numerical schemes, we consider a forward in time and central in space (FTCS) finite difference scheme (that is first order accurate in time and second order in space) given by

$$\frac{u_i^{n+1} - u_i^n}{\tau} + \alpha \frac{u_{i+1}^n - u_{i-1}^n}{2h} = \nu \frac{u_{i+1}^n - 2u_i^n + u_{i-1}^n}{h^2} + O(\tau, h^2) \tag{4.2}$$

as our non-invariant base scheme. Here, the symbols τ and h represent the discrete time step and spatial step, respectively. The objective is to construct an invariant scheme with a desired order of accuracy, therefore, we first modify the equation such that its accuracy improves to second order in time and fourth order in space. For this particular problem, we add the following defect correction terms recovered from the truncation error analysis of Eq. (4.2),

$$d_c = \frac{1}{2}\tau\alpha^2\, u_{xx} + \frac{1}{12}(6\nu\tau - h^2)\,[\nu u_{xxxx} - 2\alpha u_{xxx}] + O(\tau^2, h^4) \tag{4.3}$$

to the original discrete equation, Eq. (4.2), to obtain the following discrete form of the modified equation

$$\frac{u_i^{n+1}-u_i^n}{\tau}+\alpha\frac{u_{i+1}^n-u_{i-1}^n}{2h}=\nu\frac{u_{i+1}^n-2u_i^n+u_{i-1}^n}{h^2}+d_c\ . \tag{4.4}$$

Note that any improvement in order of accuracy of finite difference schemes can be arbitrarily set by consideration of appropriate defect correction terms based on truncation error analysis. Once the modified forms of PDEs are obtained, one then determines the symmetries of the linear advection-diffusion equation through Lie symmetry analysis as discussed in the previous section. The application of this procedure to the one-dimensional linear advection-diffusion equation yields the following symmetry groups

$$\begin{aligned}
X_1 &= 2\,t^2\,\frac{\partial}{\partial\,t}+2\,x\,t\,\frac{\partial}{\partial\,x}-u\,(t+\frac{(x-\alpha\,t)^2}{2\,\nu})\,\frac{\partial}{\partial\,u}\\
X_2 &= 4\,t\,\frac{\partial}{\partial\,t}+2(x+\alpha\,t)\,\frac{\partial}{\partial\,x}\\
X_3 &= t\,\frac{\partial}{\partial\,x}-u\,\frac{(x-\alpha\,t)}{2\,\nu}\,\frac{\partial}{\partial\,u}\\
X_4 &= u\,\frac{\partial}{\partial\,u}\\
X_5 &= \frac{\partial}{\partial\,x}\\
X_6 &= \frac{\partial}{\partial\,t}
\end{aligned} \tag{4.5}$$

where each group operator, $X_{i=1,\cdots,6}$, represents different subgroups. The next step is to preserve these symmetries in the associated numerical algorithms. Transformations obtained from the symmetries of equations are used to transform every discrete variable of the considered base scheme such that the resulting scheme is invariant under those symmetries. However, in some cases, it might not possible or practical to preserve all the symmetries of equations in the related numerical algorithms as it could result in cumbersome representations without significantly

improving accuracy. This is covered in more detail in the next section. For these particular reasons, we ignore some of these symmetries and construct a scheme that only preserves X_1, X_5, and X_6 (which represent projection, translation in time, and translation in space) subgroups of the linear advection-diffusion equation, Eq. (4.1). The discrete variable transformations related to the selected symmetry groups are obtained by substituting each group operator in the Lie series given by Eq. (2.23). For these particular symmetry groups, the following transformations

$$\begin{aligned}
\tilde{t} &= \frac{t+s_6}{1-2\,s_1\,(t+s_6)} \\
\tilde{x} &= \frac{x+s_5}{1-2\,s_1\,(t+s_6)} \\
\tilde{u} &= u\sqrt{1-2\,s_1\,(t+s_6)}\,\exp\left[-\frac{s_1\,((x+s_5)-\alpha\,(t+s_6))^2}{2\,\nu\,(1-2\,s_1\,(t+s_6))}\right]
\end{aligned} \tag{4.6}$$

are obtained. Here, the unknowns s_1, s_5, and s_6 are arbitrary symmetry parameters that are related to the corresponding group operators. These unknown parameters are determined through Cartan's method of normalization. Recall that there exist infinite number of applicable normalization conditions (or moving frames), and not all of them improve quality of results obtained from numerical schemes. It is convenient to choose normalization conditions that lead to a simple computational stencil. Therefore, the following normalization conditions are found to be very practical for determining s_5 and s_6 as the selections

$$\begin{aligned}
\tilde{t}^n = 0 \quad &\Rightarrow \quad s_6 = -t^n \\
\tilde{x}_i = 0 \quad &\Rightarrow \quad s_5 = -x_i
\end{aligned}$$

lead to a simple computational stencil. Here, the discrete spatial step in the transformed space $\tilde{h}$ is equal to h, and similarly, the time step in the transformed space $\tilde{\tau}$ is equal to $\tau/(1-2\tau s_1)$ for these particular moving frames. Further, the pro-

jection parameter s_1 is determined by considering a normalization condition that corresponds to a moving frame for which the discrete definition of the second order spatial derivative goes to zero as shown below

$$\partial_{\tilde{x}\tilde{x}}\,\tilde{u}=0 \quad \Rightarrow \quad \frac{\tilde{u}^n_{i+1}-2\,\tilde{u}^n_i+\tilde{u}^n_{i-1}}{\tilde{h}^2}=0 \quad \Rightarrow \quad s_1=-\frac{2\nu}{h^2}\,\ln\left[\frac{2u^n_i}{u^n_{i+1}+u^n_{i-1}}\right]. \tag{4.7}$$

By considering this particular normalization condition, all the terms in the following modified equation, Eq. (4.4),

$$\begin{aligned}\frac{u^{n+1}_i-u^n_i}{\tau}+\alpha\frac{u^n_{i+1}-u^n_{i-1}}{2h} =&\nu\frac{u^n_{i+1}-2u^n_i+u^n_{i-1}}{h^2}+\frac{1}{2}\tau\alpha^2u_{xx}\\ &+\frac{1}{12}(6\nu\tau-h^2)\left[\nu u_{xxxx}-2\alpha u_{xxx}\right]+O(\tau^2,h^4)\end{aligned} \tag{4.8}$$

that include the second order spatial derivative of $u(t,x)$ can be removed from the scheme in the transformed space. Besides, Eq. (4.8) can be further simplified by considering a special discrete time step as given in the following relation:

$$(6\,\nu\,\tau-h^2)=0 \quad \Rightarrow \quad \tau_{sp}=\frac{h^2}{6\,\nu}\,. \tag{4.9}$$

The use of such a special discrete time step and the particular moving frame given in Eq. (4.7) allows us to completely remove all the defect terms from the scheme in the transformed space. Additionally, the viscous term of the original one-dimensional linear advection-diffusion equation is also removed from the scheme. The viscosity information is included in the definition of the particular moving frame. The final form of the fourth order accurate discrete modified equation in the transformed space is

$$\frac{\tilde{u}^{n+1}-\tilde{u}^n}{\tilde{\tau}}+\alpha\,\frac{\tilde{u}_{i+1}-\tilde{u}_{i-1}}{2\tilde{h}}=0. \tag{4.10}$$

We can also express Eq. (4.10) in terms of the original discrete variables by applying the transformations given in Eq. (4.6) as

$$u^{n+1} = u_i^n \, \lambda^{-1.5} \left(\frac{u_{i+1}^n + u_{i-1}^n}{2u_i^n} \right)^{4R^2/\lambda} \left[\lambda - 2R \frac{u_{i+1}^n - u_{i-1}^n}{u_{i+1}^n + u_{i-1}^n} \right] \tag{4.11}$$

where

$$R = \frac{\alpha\tau}{2h} \qquad \text{and} \quad \lambda = 1 - 2\,\tau\, s_1 \ .$$

Eq. (4.11) is invariant under the selected symmetries, and this property can be verified by applying the transformations given in Eq. (4.6) to this equation. The resulting scheme will be identical to Eq. (4.11).

4.2.2 Inviscid Burgers' Equation

As our second test case, we consider the inviscid Burgers' equation (IBE) which is a model that describes nonlinear wave propagation as

$$u_t + u\, u_x = 0 \ . \tag{4.12}$$

To numerically solve this equation, we construct several high order accurate invariant numerical schemes (that preserve different symmetries). A forward in time and central in space finite differencing technique

$$\frac{u_i^{n+1} - u_i^n}{\tau} + u_i^n \, \frac{u_{i+1}^n - u_{i-1}^n}{2\,h} = 0 \ + \ O(\tau, h^2) \tag{4.13}$$

is used as the non-invariant base scheme to approximate a numerical solution for the inviscid Burgers' equation, Eq. (4.12). The symmetry groups associated with

this PDE are

$$
\begin{aligned}
X_1 &= t^2 \frac{\partial}{\partial t} + x\,t \frac{\partial}{\partial x} + (x - t\,u) \frac{\partial}{\partial u} \\
X_2 &= t\,x \frac{\partial}{\partial t} + x^2 \frac{\partial}{\partial x} + u\,(x - t\,u) \frac{\partial}{\partial u} \\
X_3 &= 2\,t \frac{\partial}{\partial t} + x \frac{\partial}{\partial x} - u \frac{\partial}{\partial u} \\
X_4 &= x \frac{\partial}{\partial t} - u^2 \frac{\partial}{\partial u} \\
X_5 &= t \frac{\partial}{\partial x} + \frac{\partial}{\partial u} \\
X_6 &= \frac{\partial}{\partial t} \\
X_7 &= \frac{\partial}{\partial x} \ .
\end{aligned}
\tag{4.14}
$$

We first construct a second order accurate invariant numerical scheme (referred to as SYM-1) that preserves the symmetry groups X_1, X_6, and X_7 (corresponding to projection, translation in time, and translation in space, respectively). The discrete variable transformations associated with these particular symmetry groups are found to be

$$
\begin{aligned}
\tilde{t} &= \frac{t + \tilde{s}_6}{1 - \tilde{s}_1\,(t + \tilde{s}_6)} \\
\tilde{x} &= \frac{x + \tilde{s}_7}{1 - \tilde{s}_1\,(t + \tilde{s}_6)} \\
\tilde{u} &= u\,[1 - \tilde{s}_1(t + \tilde{s}_6)] + \tilde{s}_1(x + \tilde{s}_7) \ .
\end{aligned}
\tag{4.15}
$$

We then construct another second order accurate invariant numerical scheme (referred to as SYM-2) that preserves the projection symmetry X_2 in addition to the earlier symmetries (X_1, X_6, and X_7). The transformations related to these particular symmetry groups are noted as

$$
\widehat{t} = \frac{t + \widehat{s}_6}{1 - \widehat{s}_2\,(x + \widehat{s}_7) - \widehat{s}_1\,(t + \widehat{s}_6)}
$$

$$\widehat{x} = \frac{x + \widehat{s}_7}{1 - \widehat{s}_2\,(x + \widehat{s}_7) - \widehat{s}_1\,(t + \widehat{s}_6)}$$
$$\widehat{u} = \frac{u + \widehat{s}_1\,[x + \widehat{s}_7 - (t + \widehat{s}_6)\,u]}{1 - \widehat{s}_2\,[x + \widehat{s}_7 - (t + \widehat{s}_6)\,u]}\ . \tag{4.16}$$

Here, the dimensions of the symmetry parameters $\widehat{s}_1$ and $\widehat{s}_2$ are $[T]^{-1}$ and $[L]^{-1}$, respectively. As the symmetry parameters can be chosen arbitrarily, we set $\widehat{s}_1$ to be equal to $S \cdot a$ and $\widehat{s}_2$ to be $S \cdot b$ where S is a dimensionless parameter, and a and b are equal to unity, with dimensions $[T]^{-1}$ and $[L]^{-1}$, respectively. The objective is to investigate how the preservation of the additional projection symmetry X_2 affects the numerical representation and accuracy of the resulting invariant scheme. All the other symmetries of the IBE are ignored as their inclusion (in addition to already chosen symmetries) would result in a cumbersome numerical scheme that might not always lead to a substantial improvement in accuracy. Similar to the one-dimensional linear advection-diffusion equation case, in order to fix the order of accuracy of both invariant numerical schemes (to second order accuracy in time and space), the following defect correction terms

$$d_c = \frac{\tau}{2}(u^2\,u_{xx} + 2\,u\,u_x^2) \ +\ O(\tau^2, h^2) \tag{4.17}$$

obtained from the truncation error analysis are added to the base numerical scheme, Eq. (4.13), as shown in the following

$$\frac{u_i^{n+1} - u_i^n}{\tau} + u_i^n\,\frac{u_{i+1}^n - u_{i-1}^n}{2\,h} = 0 \ +\ d_c\ . \tag{4.18}$$

The unknown symmetry parameters s_1, s_6, and s_7 in the transformation expressions given in Eq. (4.15) and Eq. (4.16) are determined through the method of equivariant moving frames. For both cases, we first consider normalization conditions that

generate simple solution stencils such as

$$\begin{aligned}
\tilde{t}^n &= 0 \quad \Rightarrow \quad \tilde{s}_6 = -t^n \\
\tilde{x}_i &= 0 \quad \Rightarrow \quad \tilde{s}_7 = -x_i \\
\widehat{t}^n &= 0 \quad \Rightarrow \quad \widehat{s}_6 = -t^n \\
\widehat{x}_i &= 0 \quad \Rightarrow \quad \widehat{s}_7 = -x_i \ .
\end{aligned} \tag{4.19}$$

We then consider moving frames for which numerical representation of modified equations simplifies significantly. For this particular problem, the normalization conditions

$$\begin{aligned}
\tilde{u}_{\tilde{x}} &= 0 \quad \Rightarrow \quad \frac{\tilde{u}_{i+1} - \tilde{u}_{i-1}}{\tilde{x}_{i+1} + \tilde{x}_{i-1}} = 0 \quad \Rightarrow \quad \tilde{s}_1 = -\frac{u_{i+1} - u_{i-1}}{2h} \\
\widehat{u}_{\widehat{x}} &= 0 \quad \Rightarrow \quad \frac{\widehat{u}_{i+1} - \widehat{u}_{i-1}}{\widehat{x}_{i+1} + \widehat{x}_{i-1}} = 0 \quad \Rightarrow \quad S = -\frac{u_{i+1} - u_{i-1}}{b\,h\,(u_{i+1} + u_{i-1}) + 2\,a\,h}
\end{aligned} \tag{4.20}$$

are found to be very effective for simplifying the discrete modified equation given in Eq. (4.18) as the numerical representation of all the terms in the equation that include the first order spatial derivative are removed from the scheme for these particular moving frames. In the case of SYM-1, by considering these particular moving frames, the discrete modified equation can be simplified to the following

$$\frac{\tilde{u}_i^{n+1} - \tilde{u}_i^n}{\tilde{\tau}} = \frac{\tilde{\tau}}{2} \left((\tilde{u}_i^n)^2 \, \frac{\tilde{u}_{i+1}^n - 2\tilde{u}_i^n + \tilde{u}_{i-1}^n}{\tilde{h}^2} \right) + \ O(\tilde{\tau}^2, \tilde{h}^2) \tag{4.21}$$

in the transformed space, where

$$\begin{aligned}
\tilde{u}_i^{n+1} &= \tilde{\eta}\, u_i^{n+1} + \tilde{s}_1\, (x^{n+1} - x^n) \\
\tilde{u}_i^n &= u_i^n \\
\tilde{u}_{i\pm1} &= u_{i\pm1} \pm \tilde{s}_1\, h \\
\tilde{\eta} &= 1 - \tilde{s}_1\, \tilde{\tau}
\end{aligned} \tag{4.22}$$

$$\tilde{\tau} = \tilde{t}^{\,n+1} - \tilde{t}^{\,n} = \tau/_{\tilde{\eta}}$$

$$\tilde{h} = \tilde{x}_{i+1} - \tilde{x}_i = \tilde{x}_i - \tilde{x}_{i-1} = h \ .$$

The final form of the second order accurate numerical scheme SYM-1 (which is invariant under the symmetry groups X_1, X_6, and X_7) in terms of the original discrete variables is obtained (by substituting Eq. (4.22) into Eq. (4.21)) as

$$u_i^{n+1} = \frac{u_i^n}{\tilde{\eta}} \left[1 + \frac{\tau^2}{2h^2\,\tilde{\eta}^2}\, u_i^n \,(u_{i+1}^n - 2u_i^n + u_{i-1}^n) \right] + \ O(\tau^2, h^2) \ . \tag{4.23}$$

Similarly, the discrete modified equation can be simplified to the following

$$\frac{\widehat{u}_i^{n+1} - \widehat{u}_i^n}{\widehat{\tau}} = \frac{\widehat{\tau}}{4} \left((\widehat{u}_i^n)^2 \, \frac{\widehat{u}_{i+1}^n - 2\widehat{u}_i^n + \widehat{u}_{i-1}^n}{\widehat{h}_+^2 + \widehat{h}_-^2} \right) + \ O(\tilde{\tau}^2, \tilde{h}^2) \tag{4.24}$$

when the transformations and moving frames considered for SYM-2 are considered. Every discrete variable in Eq. (4.24) can be expressed in terms of the original discrete variables by using the transformations given in Eq. (4.16) as

$$\begin{aligned} \widehat{u}_i^{n+1} &= \frac{\widehat{\eta}\, u_i^{n+1}}{1 + \widehat{s}_2\, \tau\, u_i^{n+1}} \\ \widehat{u}_i^n &= u_i^n \\ \widehat{u}_{i\pm1}^n &= \frac{u_{i\pm1}^n \pm \widehat{s}_1\, h}{\mu_\pm} \end{aligned} \tag{4.25}$$

where

$$\widehat{\tau} = \widehat{t}^{\,n+1} - \widehat{t}^{\,n} = \tau/_{\widehat{\eta}}$$

$$\widehat{h}_+ = \tilde{x}_{i+1} - \tilde{x}_i = h/_{\mu_+}$$

$$\widehat{h}_- = \tilde{x}_i - \tilde{x}_{i-1} = h/_{\mu_-}$$

and

$$\widehat{\eta} = 1 - \widehat{s}_1 \, \tau$$

$$\mu_+ = 1 - \widehat{s}_2 \, h$$

$$\mu_- = 1 + \widehat{s}_2 \, h \ .$$

Hence, the final form of the second order accurate numerical scheme that is invariant under the symmetry groups considered for SYM-2 in terms of the original variables is found by substituting Eq. (4.25) into Eq. (4.24)

$$u_i^{n+1} = \frac{\kappa}{\widehat{\eta} - \widehat{s}_2 \, \tau \, \kappa} \tag{4.26}$$

where

$$\kappa = u_i^n + \frac{\mu_+ \mu_-}{\mu_+^2 + \mu_-^2} (\frac{\tau u_i^n}{h})^2 \left[(u_{i+1}^n + 1)\mu_- - 2(u_i^n + 1)\mu_+ \mu_- + (u_{i-1}^n + 1)\mu_+ \right] . \tag{4.27}$$

Note that we use a solution grid that is regular in time and space, and therefore, the quantity $x^{n+1} - x^n$ that appears when transforming discrete variables is always assumed to be zero.

For this problem setup, results obtained from both invariant numerical schemes, Eq. (4.23) and Eq. (4.26), suggest that preserving only the symmetry groups X_1, X_6, and X_7 is enough to achieve a desired order of accuracy. More discussion on the performance of these proposed invariant schemes are presented in Section 6.5 where the results are evaluated. To further investigate the influence of the choice of symmetry groups, we construct a third invariant numerical scheme that is fourth order accurate in time and space and preserves only X_1, X_6, and X_7. The following

defect correction terms

$$d_c = \frac{\tau}{2}(u^2 u_{xx} + 2uu_x^2) - \frac{\tau^2}{6}(6uu_x^3 + 9u^2 u_x u_{xx} + u^3 u_{xxx}) + \frac{h^2}{6} uu_{xxx} + \frac{\tau^3}{24}(24uu_x^4 + 72u^2 u_x^2 u_{xx} + 12u^3 u_{xx}^2 + 16u^3 u_x u_{xxx} + u^4 u_{xxxx}) + O(\tau^4, h^4) \tag{4.28}$$

are added to the base numerical scheme to obtain the discrete form of the modified equation,

$$\frac{u_i^{n+1} - u_i^n}{\tau} + u_i^n \frac{u_{i+1}^n - u_{i-1}^n}{2h} = 0 + d_c \, . \tag{4.29}$$

Next, the discrete form of the modified equation (Eq. (4.29)) in the transformed space based on transformations and moving frames considered for the SYM-1 case is obtained as

$$\frac{\tilde{u}_i^{n+1} - \tilde{u}_i^n}{\tilde{\tau}} = \frac{\tilde{\tau}}{2}(\tilde{u}^2 \tilde{u}_{\tilde{x}\tilde{x}}) - \frac{\tilde{\tau}^2}{6}\tilde{u}^3 \tilde{u}_{\tilde{x}\tilde{x}\tilde{x}} + \frac{\tilde{h}^2}{6}\tilde{u}\tilde{u}_{\tilde{x}\tilde{x}\tilde{x}} + \frac{\tilde{\tau}^3}{24}(12\tilde{u}^3 \tilde{u}_{\tilde{x}\tilde{x}}^2 + \tilde{u}^4 \tilde{u}_{\tilde{x}\tilde{x}\tilde{x}\tilde{x}}) + O(\tilde{\tau}^4, \tilde{h}^4) \, .$$

Hence, the final form of the numerical scheme that is fourth order accurate in both time and space and is invariant under the symmetry groups X_1, X_6, and X_7 is obtained as

$$\begin{aligned} u_i^{n+1} = \frac{1}{\tilde{\eta}} \Bigg[& u_i^n + \frac{1}{2}\left(\frac{\tau u_i^n}{h\tilde{\eta}}\right)^2 \left(1 + \frac{\tau^2 u_i^n}{h^2 \tilde{\eta}^2}\right)(u_{i+1}^n - 2u_i^n + u_{i-1}^n) \\ & + \frac{1}{12}\frac{\tau u_i^n}{h\tilde{\eta}}\left(1 - \frac{\tau^2 (u_i^n)^2}{h^2 \tilde{\eta}^2}\right)(u_{i+2}^n - 2u_{i+1}^n + 2u_{i-1}^n - u_{i-2}^n) \\ & + \frac{1}{24}\left(\frac{\tau u_i^n}{h\tilde{\eta}}\right)^4 (u_{i+2}^n - 4u_{i+1}^n + 6u_i^n - 4u_{i-1}^n + u_{i-2}^n) \Bigg] \, . \end{aligned} \tag{4.30}$$

4.2.3 Viscous Burgers' Equation

As our next test case, we consider the viscous Burgers' equation which is of the form

$$u_t + u\,u_x = \nu\,u_{xx} \tag{4.31}$$

and construct a fourth order accurate invariant numerical scheme for the solution of this PDE. Similar to previous test problems, we use a forward in time and central in space finite difference scheme,

$$\frac{u_i^{n+1} - u_i^n}{\tau} + u\frac{u_{i+1}^n - u_{i-1}^n}{2h} = \nu\frac{u_{i+1}^n - 2u_i^n + u_{i-1}^n}{h^2} + O(\tau, h^2) \tag{4.32}$$

as our base scheme for the construction of a fourth order accurate invariant scheme. Next, we add the following defect correction terms obtained from truncation error analysis

$$d_c = \frac{\tau}{2}\left(2uu_x^2 + u^2u_{xx} - 4\nu u_x u_{xx}\right) + \frac{1}{12}(6\nu\tau - h^2)\left[\nu u_{xxxx} - 2uu_{xxx}\right] + O(\tau^2, h^4) \tag{4.33}$$

to the base scheme, Eq. (4.32), to obtain the following discrete form of the modified equation

$$\frac{u_i^{n+1} - u_i^n}{\tau} + \alpha\frac{u_{i+1}^n - u_{i-1}^n}{2h} = \nu\frac{u_{i+1}^n - 2u_i^n + u_{i-1}^n}{h^2} + d_c\ . \tag{4.34}$$

The defect correction terms can be further simplified by considering a special time step (as before) which is obtained from the following relation

$$(6\nu\tau - h^2) = 0 \quad \Rightarrow \quad \tau_{sp} = \frac{h^2}{6\nu}\ . \tag{4.35}$$

Next, we determine the Lie point symmetries of the viscous Burgers' equation via Lie symmetry analysis which results in the following symmetry groups

$$\begin{aligned} X_1 &= t^2 \frac{\partial}{\partial t} + x\, t \frac{\partial}{\partial x} + (x - t\, u) \frac{\partial}{\partial u} \\ X_2 &= t \frac{\partial}{\partial x} + \frac{\partial}{\partial u} \\ X_3 &= 2t \frac{\partial}{\partial t} + x \frac{\partial}{\partial x} - u \frac{\partial}{\partial u} \\ X_4 &= \frac{\partial}{\partial t} \\ X_5 &= \frac{\partial}{\partial x} \ . \end{aligned} \tag{4.36}$$

For simplicity, we only consider the symmetry groups X_1, X_4, and X_5 (which correspond to projection, translation in time, and translation in space symmetries) for preservation in the related numerical algorithm. The transformations associated to these symmetries are found to be

$$\begin{aligned} \tilde{t} &= \frac{t + s_4}{1 - s_1 (t + s_4)} \\ \tilde{x} &= \frac{x + s_5}{1 - s_1 (t + s_4)} \\ \tilde{u} &= u \left[1 - s_1 (t + s_4)\right] + s_1 (x + s_5) \end{aligned} \tag{4.37}$$

where the unknown symmetry parameters are determined by considering the following normalization conditions

$$\begin{aligned} \tilde{t}^n = 0 \quad &\Rightarrow \quad s_4 = -t^n \\ \tilde{x}_i = 0 \quad &\Rightarrow \quad s_5 = -x_i \end{aligned}$$

and

$$\partial_{\tilde{x}}\, \tilde{u} = 0 \quad \Rightarrow \quad \frac{\tilde{u}^n_{i+1} - \tilde{u}^n_{i-1}}{2\, \tilde{h}} = 0 \quad \Rightarrow \quad s_1 = -\frac{u^n_{i+1} - u^n_{i-1}}{2\, h} \ . \tag{4.38}$$

The normalization condition in Eq. (4.38) ensures that all terms in the modified equation, Eq. (4.34), that includes the first order spatial derivative will be removed from the scheme in the transformed space. Therefore, by considering these particular moving frames along with the special time step given in Eq. (4.35), the discrete form of the modified equation in the transformed space can be significantly simplified as its final form is given as

$$\frac{\tilde{u}^{n+1}-\tilde{u}^{n}}{\tilde{\tau}}=\left(\nu+\frac{1}{2}\,\tilde{\tau}\,(u_i^n)^2\right)\frac{\tilde{u}_{i+1}-2\,\tilde{u}_i+\tilde{u}_{i-1}}{\tilde{h}^2}\ . \tag{4.39}$$

And finally, the fourth order accurate invariant scheme (constructed for the viscous Burgers' equation) is obtained in terms of the original discrete variables by transforming every variable in Eq. (4.39) according to the transformations given in Eq. (4.37)

$$u^{n+1}=\frac{1}{\lambda}\left[u_i^n-\left(\frac{R}{\lambda}+2\frac{C^2\,(u_i^n)^2}{\lambda^2}\right)(u_{i+1}^n-2\,u_i^n+u_{i-1}^n)\right] \tag{4.40}$$

where

$$\lambda=1-\tau\,s_1\,,\qquad C=\frac{\tau}{2h}\,,\quad\text{and}\quad R=\frac{\nu\,\tau}{h^2}\ .$$

4.2.4 Linear Advection-Diffusion Equation in 2D

As our last test case, we consider the two-dimensional linear advection-diffusion equation

$$u_t+\alpha\,u_x+\beta\,u_y=\nu\,(u_{xx}+u_{yy}) \tag{4.41}$$

and construct a couple of fourth order accurate invariant numerical schemes that preserve the same symmetry groups but defined on different moving frames. Here,

α and β represent (constant) characteristic wave speeds along x- and y-coordinates, respectively. We use a forward in time and central in space (FTCS) scheme

$$\frac{u_{i,j}^{n+1}-u_{i,j}^{n}}{\tau}+\alpha\frac{u_{i+1,j}^{n}-u_{i-1,j}^{n}}{2h}+\beta\frac{u_{i,j+1}^{n}-u_{i,j-1}^{n}}{2k}= \\ \nu\left(\frac{u_{i+1,j}^{n}-2u_{i,j}^{n}+u_{i-1,j}^{n}}{h^2}+\frac{u_{i,j+1}^{n}-2u_{i,j}^{n}+u_{i,j-1}^{n}}{k^2}\right)+O(\tau,h^2,k^2) \tag{4.42}$$

as our base scheme for this problem as well. To improve the accuracy of the base scheme to fourth order, the following defect correction terms noted from the truncation error analysis

$$\begin{aligned} d_c =&\frac{\tau}{2}[2\nu^2 u_{xxyy}-2\nu(\alpha u_{xyy}+\beta u_{xxy})+\alpha^2 u_{xx}+2\alpha\beta u_{xy}+\beta^2 u_{yy}] \\ &+\frac{1}{12}(6\nu\tau-h^2)(\nu u_{xxxx}-2\alpha u_{xxx})+\frac{1}{12}(6\nu\tau-k^2)(\nu u_{yyyy}-2\beta u_{yyy}) \\ &+O(\tau^2,h^4,k^4) \end{aligned} \tag{4.43}$$

are added to the classical base scheme, Eq. (4.42), as

$$\frac{u_{i,j}^{n+1}-u_{i,j}^{n}}{\tau}+\alpha\frac{u_{i+1,j}^{n}-u_{i-1,j}^{n}}{2h}+\beta\frac{u_{i,j+1}^{n}-u_{i,j-1}^{n}}{2k}= \\ \nu\left(\frac{u_{i+1,j}^{n}-2u_{i,j}^{n}+u_{i-1,j}^{n}}{h^2}+\frac{u_{i,j+1}^{n}-2u_{i,j}^{n}+u_{i,j-1}^{n}}{k^2}\right)+d_c\ . \tag{4.44}$$

If for simplicity reasons, a regular mesh ($h=k$) is used in computations, then d_c can be further simplified to read

$$\begin{aligned} d_c =&\frac{\tau}{2}[2\nu^2 u_{xxyy}-2\nu(\alpha u_{xyy}+\beta u_{xxy})+\alpha^2 u_{xx}+2\alpha\beta u_{xy}+\beta^2 u_{yy}] \\ &+\frac{1}{12}(6\nu\tau-h^2)(\nu(u_{xxxx}+u_{yyyy})-2\alpha u_{xxx}-2\beta u_{yyy})+O(\tau^2,h^4)\ . \end{aligned} \tag{4.45}$$

As in the previous example, the second term in RHS of Eq. (4.45) can be eliminated by choosing a special time step τ_{sp} as

$$(6\nu\tau - h^2) = 0 \qquad \Rightarrow \qquad \tau_{sp} = \frac{h^2}{6\nu} \ . \tag{4.46}$$

To start the invariantization procedure, we first determine the symmetries of the two-dimensional linear advection-diffusion equation

$$\begin{aligned}
X_1 &= 4\,\nu\,t^2\,\frac{\partial}{\partial\,t} + 4\,\nu\,x\,t\,\frac{\partial}{\partial\,x} + 4\,\nu\,y\,t\,\frac{\partial}{\partial\,y} - u\,[(x-\alpha\,t)^2 + (y-\beta\,t)^2 + 4\nu t]\,\frac{\partial}{\partial\,u} \\
X_2 &= 2\,\nu\,t\,\frac{\partial}{\partial\,x} + 2\,\nu\,t\,\frac{\partial}{\partial\,y} - u\,(x-\alpha\,t+y-\beta\,t)\,\frac{\partial}{\partial\,u} \\
X_3 &= 2\,\nu\,y\,\frac{\partial}{\partial\,x} - 2\,\nu\,x\,\frac{\partial}{\partial\,y} - u\,(\beta\,x-\alpha\,y)\,\frac{\partial}{\partial\,u} \\
X_4 &= 4\,\nu\,t\,\frac{\partial}{\partial\,t} + 2\nu\,x\,\frac{\partial}{\partial\,x} + 2\nu\,y\,\frac{\partial}{\partial\,y} + u[\alpha(x-\alpha\,t) + \beta(y-\beta t)]\frac{\partial}{\partial u} \\
X_5 &= u\,\frac{\partial}{\partial\,u} \\
X_6 &= \frac{\partial}{\partial\,t} \\
X_7 &= \frac{\partial}{\partial\,x} \\
X_8 &= \frac{\partial}{\partial\,y} \ .
\end{aligned} \tag{4.47}$$

For this particular problem, we only consider the symmetry groups X_1, X_6, X_7, and X_8 for preservation in the related numerical algorithms. The transformation expressions obtained from these symmetry groups are

$$\begin{aligned}
\tilde{t} &= \frac{t+s_6}{1-4\,\nu\,s_1\,(t+s_6)} \\
\tilde{x} &= \frac{x+s_7}{1-4\,\nu\,s_1\,(t+s_6)} \\
\tilde{y} &= \frac{y+s_8}{1-4\,\nu\,s_1\,(t+s_6)} \\
\tilde{u} &= u\,(1-4\,\nu\,s_1\,(t+s_6))\,\exp\left[-\frac{s_1\,((x+s_7-\alpha\,(t+s_6))^2 + (y+s_8-\beta\,(t+s_6))^2)}{1-4\,\nu\,s_1\,(t+s_6)}\right] .
\end{aligned} \tag{4.48}$$

We employ a similar procedure as before (the previous test problems) and determine the unknown symmetry parameters s_6, s_7, and s_8 by considering the following normalization conditions

$$\begin{aligned} \tilde{t}^n = 0 \quad &\Rightarrow \quad s_6 = -t^n \\ \tilde{x}_i = 0 \quad &\Rightarrow \quad s_7 = -x_i \\ \tilde{y}_j = 0 \quad &\Rightarrow \quad s_8 = -y_j \end{aligned}$$

that result in a simple computational stencil. As for the projection parameter s_1, there are multiple convenient normalization conditions that can be used. Recall that one of the objectives is to choose a normalization condition that significantly simplifies the discrete form of the modified equation. However, for this particular problem, there are multiple number of normalization conditions that can be used in that context. In order to investigate the effect of selected normalization conditions on the accuracy of constructed invariant schemes, two different (fourth order accurate) invariant numerical schemes are constructed for this problem. Both schemes are defined on regular grids ($h = k$) and special selections of discrete time steps are used when applicable. In the first case, an invariant scheme (referred to as SYM-1) is developed by considering the following normalization condition

$$\partial_{\tilde{x}\tilde{x}}\,\tilde{u} = 0 \quad \Rightarrow \quad \frac{\tilde{u}^n_{i+1,j} - 2\,\tilde{u}^n_{i,j} + \tilde{u}^n_{i-1,j}}{\tilde{h}^2} = 0 \quad \Rightarrow \quad s_1 = -\frac{1}{h^2}\,\ln\left[\frac{2u^n_{i,j}}{u^n_{i+1,j} + u^n_{i-1,j}}\right]. \tag{4.49}$$

This particular normalization condition removes all the terms that include the second derivative with respect to x on the transformed space leading to the following

fourth order accurate invariant scheme

$$\frac{\tilde{u}^{n+1}_{i,j}-\tilde{u}^{n}_{i,j}}{\tilde{\tau}}+\alpha\frac{\tilde{u}^{n}_{i+1,j}-\tilde{u}^{n}_{i-1,j}}{2\tilde{h}}+\beta\frac{\tilde{u}^{n}_{i,j+1}-\tilde{u}^{n}_{i,j-1}}{2\tilde{k}}=\nu\frac{\tilde{u}^{n}_{i,j+1}-2\tilde{u}^{n}_{i,j}+\tilde{u}^{n}_{i,j-1}}{\tilde{k}^2} \\ +\tilde{\tau}[\nu^2\tilde{u}_{\tilde{x}\tilde{x}\tilde{y}\tilde{y}}-\nu(\alpha\tilde{u}_{\tilde{x}\tilde{y}\tilde{y}}+\beta\tilde{u}_{\tilde{x}\tilde{x}\tilde{y}})+\alpha\beta\tilde{u}_{\tilde{x}\tilde{y}}+\beta^2\tilde{u}_{\tilde{y}\tilde{y}}]\ . \tag{4.50}$$

As for the second case, an invariant scheme (referred to as SYM-2) is constructed on a regular mesh ($h=k$) for the linear advection-diffusion equation in 2D with identical characteristic speeds ($\alpha=\beta$) in both x- and y-coordinates. The unknown projection parameter s_1 is determined from the following normalization condition

$$\partial_{\tilde{x}\tilde{x}}\,\tilde{u}+\partial_{\tilde{y}\tilde{y}}\,\tilde{u}=0 \quad \Rightarrow \quad s_1=-\frac{1}{h^2}\ln\left[\frac{4u^n_{i,j}}{u^n_{i+1,j}+u^n_{i,j+1}+u^n_{i-1,j}+u^n_{i,j-1}}\right]. \tag{4.51}$$

By considering this moving frame along with the special time step given in Eq. (4.46), a fourth order accurate scheme is obtained as

$$\frac{\tilde{u}^{n+1}_{i,j}-\tilde{u}^{n}_{i,j}}{\tilde{\tau}}+\alpha\frac{\tilde{u}^{n}_{i+1,j}+\tilde{u}^{n}_{i,j+1}-\tilde{u}^{n}_{i-1,j}-\tilde{u}^{n}_{i,j-1}}{2\tilde{h}}= \\ \tilde{\tau}[\nu^2\tilde{u}_{\tilde{x}\tilde{x}\tilde{y}\tilde{y}}-\nu\alpha(\tilde{u}_{\tilde{x}\tilde{y}\tilde{y}}+\tilde{u}_{\tilde{x}\tilde{x}\tilde{y}})+\alpha^2\tilde{u}_{\tilde{x}\tilde{y}}]\ . \tag{4.52}$$

Both Eq. (4.50) and Eq. (4.52) are invariant under the chosen symmetries and can be expressed in terms of the original variables by using the transformations given in Eq. (4.48).

Note that in all the examples considered here, nuances associated with initial/boundary conditions of PDEs (and associated exact solutions) especially in the context of their smoothness and compatibility with the chosen subgroups are not fully considered as part of the procedure for construction of invariant schemes. We believe that this limitation (which will be addressed as part of future work) might have some effects on the accuracy of constructed invariant schemes. However, as these schemes are constructed based on defect correction and moving frames, it

might be possible to choose moving frames and appropriate base numerical schemes such that the order of accuracy of these invariant schemes is unaffected for different selections of initial/boundary conditions of a given PDE.

4.3 Numerical Experiments

In this section, we evaluate the performance of the proposed invariant numerical schemes constructed for the linear advection-diffusion equation in 1D and 2D, the inviscid Burgers' equation, and the viscous Burgers' equation. In all the linear and nonlinear problems considered here, the results obtained from the proposed invariant schemes (constructed from lower order, non-invariant base schemes) were found to be significantly more accurate than that of the corresponding base numerical schemes. We already noted the advantage associated with the ease of implementation of the proposed invariant schemes, due to the simplifications in numerical representation of the modified form of the equation.

4.3.1 Linear Advection-Diffusion Equation in 1D

We first test the performance of the proposed invariant numerical scheme developed for the one-dimensional linear advection-diffusion equation, Eq. (4.11), over the computational (spatial) domain Γ where $x \in [-2, 4]$. The following analytical solution is used to evaluate the quality of results obtained from the numerical schemes (proposed invariant, FTCS, and modified-FTCS)

$$u(t,x) = \frac{1}{\sqrt{4\,\pi\,(L^2 + \nu\,t)}} \exp\left[-\frac{(x-\alpha\,t)^2}{4\,(L^2+\nu\,t)}\right] \tag{4.53}$$

where L represents the characteristic width of the kernel and assumed to be equal to 0.4 in all test runs. The initial and boundary conditions can be noted from the analytical solution.

Table 4.1
Root mean square error (RMSE) and L_∞ error associated with numerical solutions for linear advection-diffusion equation.

Error	FTCS	MOD-FTCS	SYM
L_∞	2.5×10^{-2}	5.0×10^{-4}	6.0×10^{-4}
RMSE	9.0×10^{-3}	2.0×10^{-4}	4.0×10^{-4}

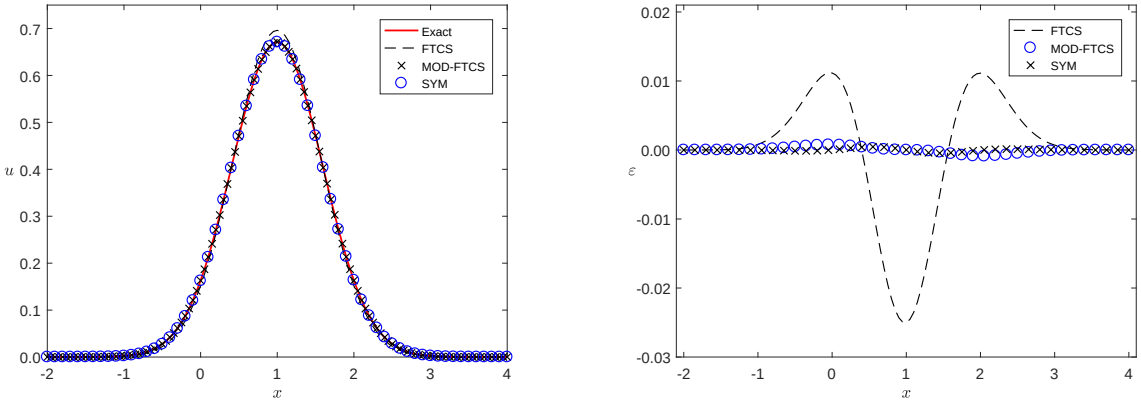

Fig. 4.1. Linear advection-diffusion equation (1D). Comparison of profiles of $u(t,x)$, at $t = 1$, obtained from the analytical solution (Exact), the classical base scheme (FTCS), the modified scheme (MOD-FTCS), and the proposed invariant scheme (SYM) is shown in the left figure. Spatial distribution of errors obtained from these schemes is displayed in the right figure. Parameter settings: $\tau = 0.025$, $h = 0.05$, $\alpha = 1$, and $\nu = 1/60$.

Snapshots of the propagating wave $u(t,x)$, at $t = 1$, that are obtained from the analytical solution (Exact, Eq. (4.53)), the proposed invariant scheme (SYM, Eq. (4.11)), the classical base numerical scheme (FTCS, Eq. (4.2)), and the modified equation (MOD-FTCS, Eq. (4.4)) are shown in figure 4.1 (left). The spatial distribution of errors in these numerical solutions, $\varepsilon = u_a - u_n$, is also displayed in this figure (right), where u_a and u_n denote the analytical and numerical solutions, respectively. It appears that the proposed invariant scheme (SYM) performs significantly better than the classical base scheme (FTCS), in terms of numerical accuracy, especially around the wave crest where the classical scheme seems to be failing to generate reliable results. The invariant scheme also appears to be nearly overlapping with the modified FTCS scheme (MOD-FTCS) that is known to be fourth

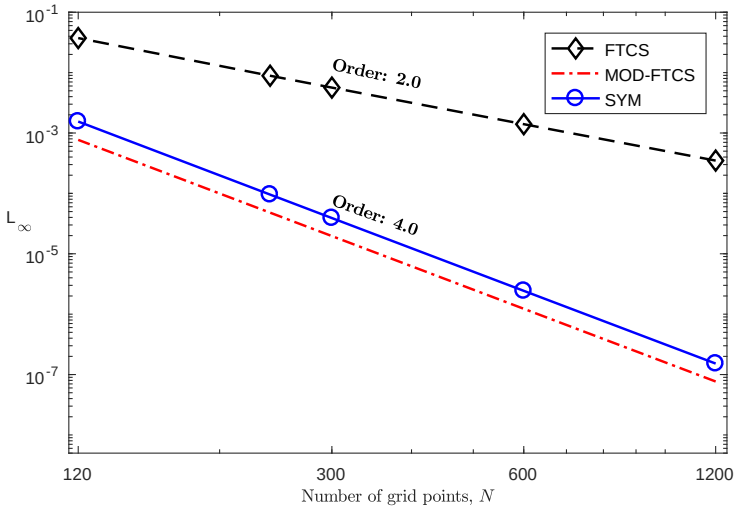

Fig. 4.2. Linear advection-diffusion equation (1D). Comparison of L_∞ errors of numerical schemes as a function of number of grid points.

order accurate. Further error analysis is performed to evaluate the performance of these numerical schemes. L_∞ errors, estimated as $max(|u_a - u_n|)$, and root mean square errors (RMSE), estimated as $\sqrt{\sum (u_a - u_n)^2/N}$, obtained from the proposed invariant scheme, classical base scheme, and the modified scheme, for this particular run, are given in table 4.1. As expected, the proposed invariant scheme performs significantly better than the classical base scheme (FTCS) in terms of numerical accuracy (by two orders of magnitude) and the accuracy of the invariant scheme is comparable to that of the modified scheme. Besides, for this particular simulation, the ratio of simulation times corresponding to the base, modified, and invariant schemes was found to be $0.95 : 1.07 : 1$.

The variations of L_∞ errors, obtained from the proposed invariant scheme, classical base scheme, and the modified equation, with respect to number of spatial grid points are presented in figure 4.2. In this figure, it appears that the proposed invariant scheme is at least two orders more accurate than the classical forward in time and central in space (FTCS) scheme (which is known to be second order accurate), and this increase in numerical accuracy can be attributed to symmetry preservation.

Both the invariant scheme and the numerical scheme for the modified equation appear to be generating fourth order accurate results. However, we note that the proposed invariant scheme has a significantly simpler numerical representation and is constructed on a three-point stencil whereas the numerical scheme developed for the modified equation has a cumbersome numerical representation and is built on a five-point stencil. This feature of invariant schemes, relevant to relative simplicity in numerical representation and implementation along with significant improvement in accuracy, can also be very useful for extensions to development of high order accurate schemes for multidimensional problems.

4.3.2 Inviscid Burgers' Equation

Further, we evaluate the performance of the proposed invariant schemes constructed for the inviscid Burgers' equation by comparing the results with the following analytical solution

$$u(t,x) = \frac{1}{\sqrt{2\,\pi\,\sigma^2}} \exp\left[-\frac{(x-u(t,x)\,t)^2}{2\,\sigma^2}\right] \tag{4.54}$$

where the symbol σ is the characteristic width of the kernel. The problem is defined over the computational domain Γ where $x \in [-3,3]$. The initial and boundary conditions can be noted from the analytical solution given in Eq. (4.54).

Evolution of the profile $u(t,x)$, from a Gaussian initial condition, obtained from the analytical solution (Exact, Eq. (4.54)), the classical base scheme (FTCS, Eq. (4.13)), the modified scheme (MOD-FTCS, Eq. (4.18)), the first proposed invariant scheme that preserves X_1, X_6, and X_7 (SYM-1, Eq. (4.23)), and the second proposed invariant scheme that preserves X_1, X_2, X_6, and X_7 (SYM-2, Eq. (4.26)) is shown in figure 4.3 (left). Numerical errors, along x-coordinate, obtained from these numerical schemes are also shown in this figure (right). It is clear that both

Table 4.2
Root mean square error (RMSE) and L_∞ error associated with numerical solutions for inviscid Burgers' equation.

Error	FTCS	MOD-FTCS	SYM-1	SYM-2
L_∞	6.03×10^{-2}	3.68×10^{-2}	3.66×10^{-2}	2.93×10^{-2}
RMSE	1.99×10^{-2}	8.20×10^{-3}	8.00×10^{-3}	7.40×10^{-3}

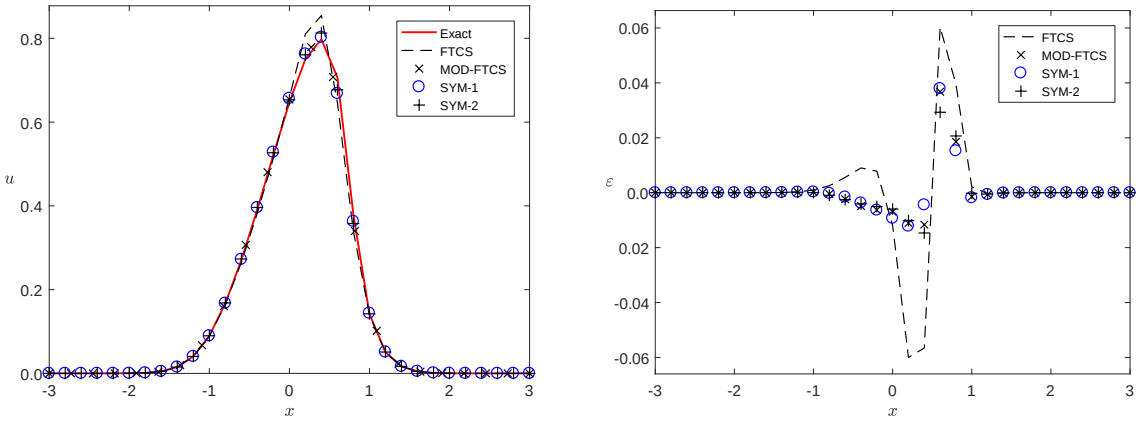

Fig. 4.3. Inviscid Burgers' equation. Comparison of profiles of $u(t,x)$, at $t = 0.5$, obtained from the analytical solution (Exact), the classical base scheme (FTCS), the modified scheme (MOD-FTCS), the proposed invariant scheme SYM-1, and the proposed invariant scheme SYM-2 is shown in the left figure. Spatial distribution of errors is displayed in the right figure. Parameter settings: $\tau = 0.1,\ h = 0.2$.

proposed invariant schemes (SYM-1 and SYM-2) perform better than the classical base scheme (FTCS) and the modified scheme (MOD-FTCS) in terms of numerical accuracy. The invariant schemes capture the wave propagation particularly well around the wave crest in contrast to the classical base scheme. L_∞ error and root mean square error comparisons of these numerical solutions for this particular run are given in table 4.2. The data presented here also verifies that the invariant schemes are comparably more accurate than other non-invariant schemes. For this particular case, the ratio of simulation times corresponding to the FTCS, MOD-FTCS, SYM-1 and SYM-2 schemes was found to be $0.68 : 1.23 : 0.72 : 1$.

Figure 4.4 shows the variation of L_∞ errors, obtained from each numerical scheme, with respect to the number of grid points for a constant ratio of discrete time and space variables, $\tau/h = 0.5$. The classical base scheme (FTCS) is first order

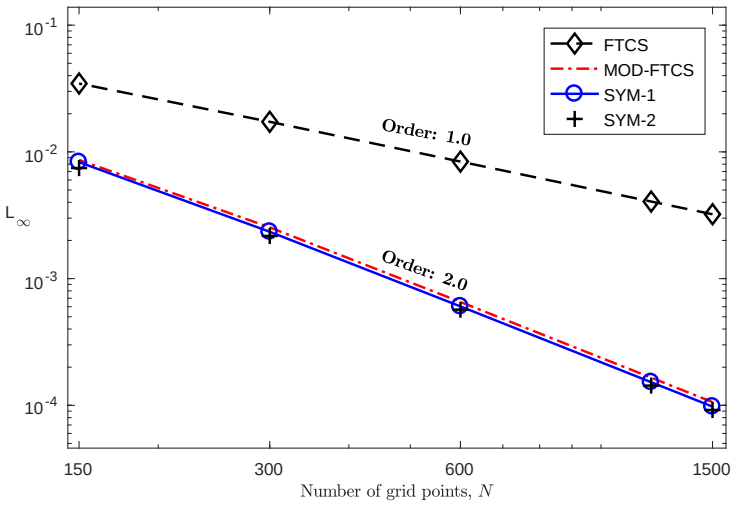

Fig. 4.4. Inviscid Burgers' equation. Comparison of L_∞ errors of numerical schemes as a function of number of grid points for a constant ratio of discrete step variables, $\tau/h = 0.5$.

accurate in time and second order accurate in space. However, the discrete time step variable τ is chosen to be the at the same order of magnitude as the spatial variable h. Therefore, the FTCS scheme is expected to be first order accurate as verified in this figure. On the other hand, the modified equation and both proposed invariant schemes are expected to be second order accurate in time and space. Figure 4.4 clearly shows this improvement. Both invariant schemes are also found to preform slightly better than MOD-FTCS scheme in terms of accuracy. Moreover, recall that SYM-2 represents the invariant scheme that preserves symmetry groups X_1, X_2, X_6, and X_7 and has a very cumbersome numerical algorithm. On the other hand, SYM-1 only preserves X_1, X_6, and X_7, but it has a comparably simpler numerical algorithm. Although SYM-2 performs better than SYM-1, this improvement is negligible. As numerical schemes that preserve more symmetries of underlying continuous equations are likely to have more laborious numerical algorithms, one must consider all advantages and disadvantages of preserving more symmetries in numerical schemes as not all of them will result in significant improvement in numerical accuracy. For this specific test problem (IBE), it appears that preserving one

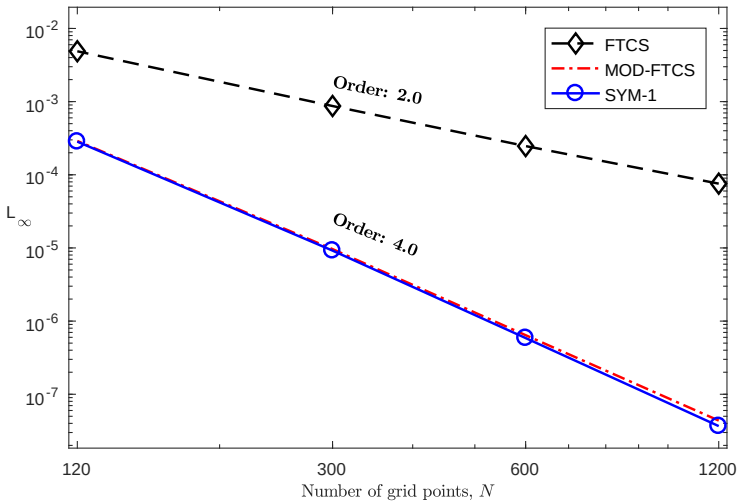

Fig. 4.5. Inviscid Burgers' equation. Comparison of L_∞ errors of numerical schemes as a function of number of grid points for a constant ratio of discrete step variables, $\tau/h = 0.01$.

extra projection symmetry does not improve numerical accuracy notably. Hence, it may be sufficient to only preserve symmetries considered in SYM-1 case if numerical accuracy is the main concern.

Recall that we also constructed a third invariant scheme that is fourth order accurate and only preserves the symmetry groups considered in SYM-1 case. The objective was to check if it was possible to construct a fourth order accurate invariant scheme by only preserving these symmetry groups. As it is clearly seen in figure 4.5 which displays L_∞ error of each numerical scheme against the number of spatial grid points, the invariant scheme (SYM-1) successfully generates accurate results that are slightly better than the results obtained from the modified scheme (MOD-FTCS) which is known to be fourth order accurate. We also note that the invariant scheme, not only generates slightly better results but also has a significantly less complex numerical algorithm compared to the modified scheme which has a very cumbersome numerical algorithm.

4.3.3 Viscous Burgers' Equation

In our next case, we evaluate the performance of the proposed invariant scheme developed for the viscous Burgers' equation over the periodic computational domain Γ where $x \in [0, 2\pi]$. The following analytical solution

$$u(t,x) = -\frac{2\nu}{\phi}\frac{\partial \phi}{\partial x} + 4 \tag{4.55}$$

where

$$\phi = \exp\left(-\frac{(x-4t)^2}{4\nu(t+1)}\right) + \exp\left(-\frac{(x-4t-2\pi)^2}{4\nu(t+1)}\right)$$

is used to evaluate the accuracy of numerical schemes. For this particular problem, periodic boundary condition, $u(0) = u(2\pi)$, is considered and the initial condition is noted from the analytical solution.

Snapshots of the propagating shock, at $t = 0.25$, obtained from the analytical solution (Exact), the proposed invariant scheme (SYM, Eq. (4.40)), the classical base scheme (FTCS, Eq. (4.32)), and the modified scheme (MOD-FTCS, Eq. (4.34)) are shown in figure 4.6 (left). The spatial distribution of errors in each numerical solution is also displayed in this figure (right). Similar to the previous test problems, the performance of the proposed invariant scheme is found to be significantly better than the classical base scheme (FTCS) and slightly better than the modified scheme (MOD-FTCS). Although a coarse grid with 121 grid points is considered for this simulation, the proposed invariant scheme captures the wave propagation with a high degree of accuracy in contrast to the classical base scheme which is not as accurate, and especially fails to reliably capture the numerical behavior around the shock front. Root mean square error and L_∞ error measures corresponding to the proposed invariant scheme, the non-invariant base scheme, and the modified

Table 4.3
Root mean square error (RMSE) and L_∞ error associated with numerical solutions for the viscous Burgers' equation.

Error	FTCS	MOD-FTCS	SYM
L_∞	$2.61 \times 10^{\,0}$	7.29×10^{-1}	6.50×10^{-1}
RMSE	2.75×10^{-1}	8.80×10^{-2}	8.01×10^{-2}

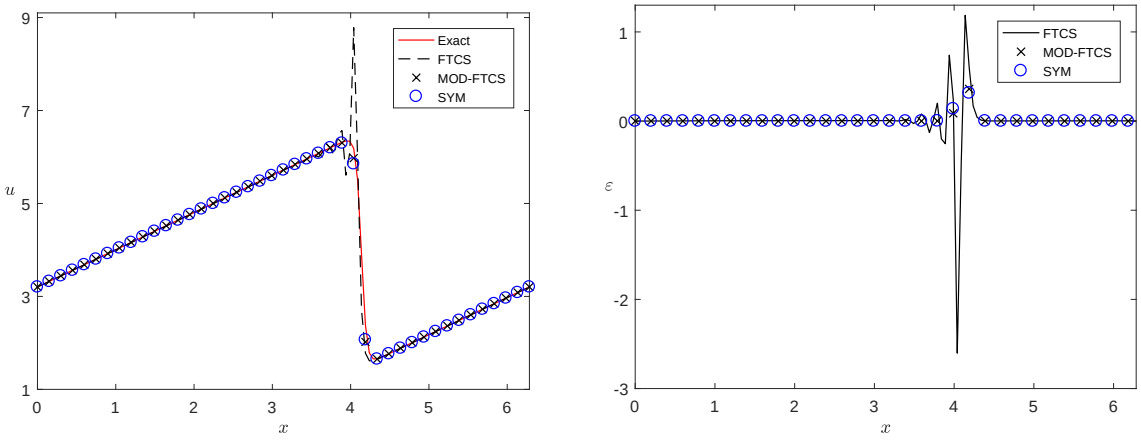

Fig. 4.6. Viscous Burgers' equation. Comparison of shock formation profiles, at $t = 0.25$, obtained from the analytical solution (Exact), the classical base scheme (FTCS), the modified scheme (MOD-FTCS), and the proposed invariant scheme (SYM) is shown in the left figure. Spatial distribution of errors is displayed in the right figure. Parameter settings: $h = 0.05$, $\tau = 0.005$, $\nu = 1/12$.

equation are given in table 4.3. The data shown in this table indicates that the proposed invariant scheme performs significantly better (in terms of accuracy) than the non-invariant base scheme and only slightly better than the modified scheme. Further, for this particular run, the ratio of simulation times corresponding to the base, modified, and invariant schemes was noted as $0.98 : 1.15 : 1$.

L_∞ errors (obtained from the proposed invariant scheme, the classical base scheme, and the modified scheme) with respect to number of spatial grid points is shown in figure 4.7. It appears that the proposed invariant scheme is at least two orders more accurate than the classical base scheme which is known to be second order accurate. Although the results obtained from both the modified scheme and the invariant scheme appear to be nearly overlapping, considering the simplicity of the numerical representation of the latter scheme (which is constructed on a three-

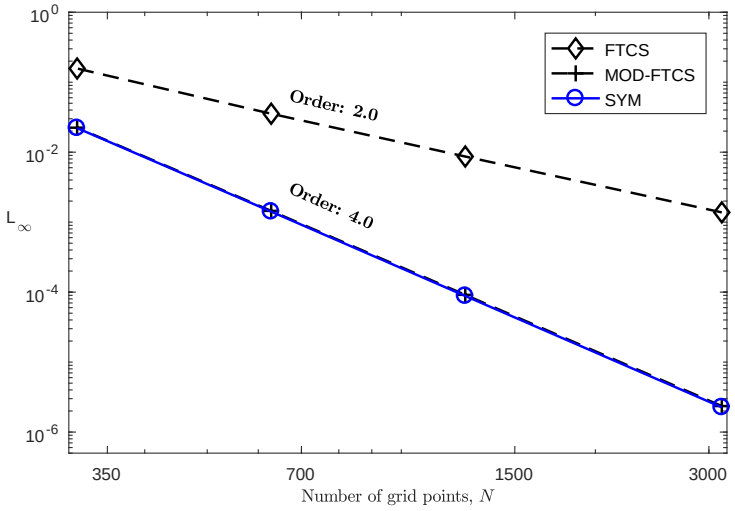

Fig. 4.7. Viscous Burgers' equation. Comparison of L_∞ errors of numerical schemes as a function of number of grid points.

point stencil as opposed to a five-point stencil used for the modified scheme), the advantages of symmetry preservation in numerical algorithms become more evident.

4.3.4 Linear Advection-Diffusion Equation in 2D

In our last test case, we evaluate the performance of the proposed invariant schemes constructed for the two-dimensional linear advection-diffusion equation by comparison with the analytical solution given by the following relation:

$$u(t,x) = \frac{1}{4\pi\,(L^2+\nu\,t)} \exp\left[-\frac{(x-\alpha\,t)^2+(y-\beta\,t)^2}{4\,(L^2+\nu\,t)}\right] . \tag{4.56}$$

Recall that, for this problem, two invariant schemes are constructed by considering different moving frames. In the first invariant scheme which we referred to as SYM-1, the unknown projection parameter s_1 was determined by using the normalization condition given in Eq. (4.49). On the other hand, in the second invariant scheme (referred to as SYM-2), the moving frame given in Eq. (4.51) is used to determine s_1. We test these invariant numerical schemes for accuracy over the computational domain Γ where both x and y are defined in the range $[-2,2]$. The initial and

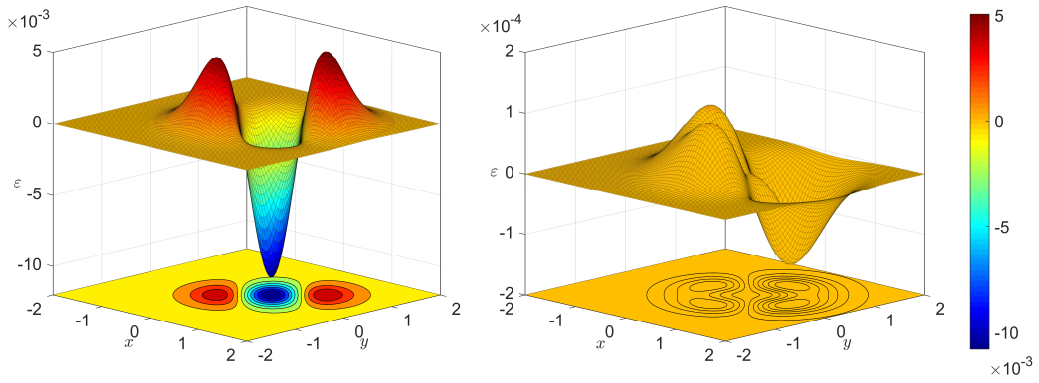

Fig. 4.8. Linear advection-diffusion equation (2D). Spatial distributions of numerical errors, at $t = 0.5$, obtained from the classical base scheme (left) and the proposed invariant scheme (right). Parameter settings: $h = 0.05$, $\tau = 0.005$, $\alpha = 0.5$, $\beta = 0.5$, $\nu = 1/60$.

boundary conditions considered for this problem can be noted from the analytical solution given in Eq. (4.56).

Spatial distributions of numerical errors, at $t = 0.5$, obtained from the proposed invariant scheme (SYM-1) and the classical base scheme are shown in figure 4.8. From this figure, it appears that the invariant scheme performs significantly better than the classical forward in time and central in space finite difference scheme (FTCS). This improvement in numerical accuracy is also verified by error analysis of these schemes. The proposed invariant scheme appears to be two orders of magnitude more accurate than the classical base scheme when we consider L_∞ errors (which are noted as 2×10^{-4} for SYM-1, and 1×10^{-2} for FTCS schemes). Similar results are also observed from comparisons of root mean square errors (which are noted as 2.7×10^{-5} for SYM-1 and 1.3×10^{-3} for FTCS schemes).

We also compared the invariant schemes SYM-1, Eq. (4.50), and SYM-2, Eq. (4.52), constructed for the two-dimensional linear advection-diffusion equation in terms of numerical accuracy. In figure 4.9, L_∞ errors obtained from these invariant schemes, the classical base scheme (FTCS, Eq. (4.42)), and modified scheme (MOD-FTCS, Eq. (4.44)) are illustrated. Both invariant schemes appear to perform significantly

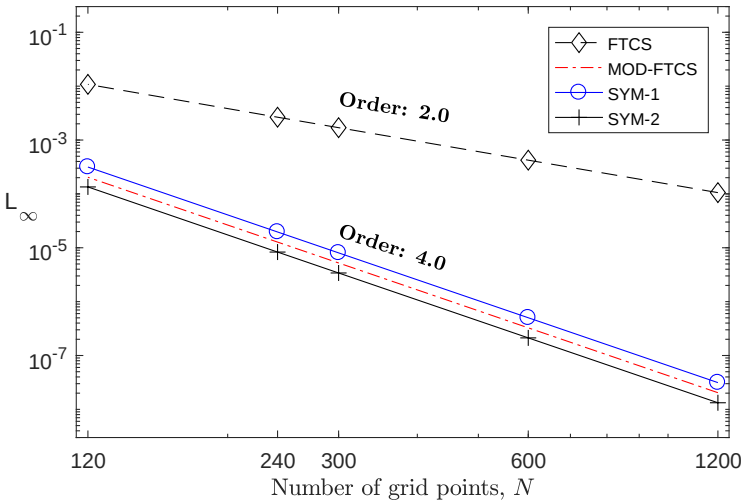

Fig. 4.9. Linear advection-diffusion equation (2D). Comparison of L_∞ errors of numerical schemes as a function of number of grid points.

better than the classical base scheme. The proposed invariant scheme SYM-2 also appears to be perform slightly better than both the invariant scheme SYM-1 and the modified scheme (which is known to be fourth order accurate). Although different selection of moving frames resulted in invariant schemes with different accuracy, we consider this improvement to be negligible for this particular problem. Therefore, we conclude that both moving frames can be considered for construction of high order accurate invariant schemes for this particular problem.

4.4 Chapter Summary

In this chapter, we presented a methodology to construct high order accurate invariant finite difference schemes that inherit Lie symmetry properties of underlying partial differential equations. In contrast to other approaches based on moving frames, the method proposed in this work offers a systematic approach to develop invariant (or Lie symmetry preserving) numerical schemes with desired order of accuracy. The order of accuracy of invariant schemes can be arbitrarily fixed by considering the difference equations associated to the modified forms of equations

instead of their original forms. Modified forms of equations are obtained by addition of defect correction terms (noted from truncation error analysis) to the original forms of equations. These additional terms are then significantly simplified (if not completely eliminated) in the transformed space by considering convenient moving frames. We also found that convenient moving frames (among vast number of possibilities) that increase accuracy of resulting invariant schemes can be systematically identified when the modified forms of equations are considered. This feature of the proposed method suggests that high order accurate invariant schemes with significantly simplified numerical representations can be constructed from standard, low order, non-invariant finite difference schemes. This is particularly important, as high order schemes that are obtained from lower order schemes through defect correction procedures often have cumbersome numerical representations. In this work, high order accurate invariant numerical schemes were developed for some canonical linear and nonlinear PDEs and their performance was evaluated.

In the first test case, a fourth order accurate invariant numerical scheme that is built on a three-point stencil was constructed for the one-dimensional linear advection diffusion equation. In this case, a discrete form of the modified equation in the transformed space was simplified to a discrete form of a linear advection equation through selection of convenient moving frames for which numerical representations of all the defect terms along with the diffusion term of the original linear advection-diffusion equation go to zero. Hence, a fourth order accurate (in space) numerical scheme that is not only invariant but also has a much simpler numerical representation was constructed for the linear advection-diffusion equation in 1D. Based on our implementation of the invariant numerical scheme for this problem, fourth order accuracy (in space) was demonstrated and significant improvement in performance over the classical second order accurate base scheme was also observed (as expected).

As our second test case, we considered the inviscid Burgers' equation and constructed three different high order accurate invariant schemes by modifying some non-invariant base schemes. The first invariant scheme (referred to as SYM-1) which is set to be second order accurate was constructed such that only three symmetries of the original inviscid Burgers' equations are preserved. The second invariant scheme (referred to as SYM-2) which is also set to be second order accurate was developed to preserve one more projection symmetry in addition to the three symmetries preserved in the first invariant scheme. The objective was to understand the effect of different configurations of symmetry preservation on accuracy of schemes and the level of complexity of their numerical representations. Preservation of the extra projection symmetry in the base scheme resulted in an invariant scheme that has a more cumbersome numerical representation compared to the first invariant scheme. However, the numerical results obtained from both invariant schemes show minor differences (that can be ignored) and suggest that preservation of more symmetries in schemes may not always improve numerical accuracy. Furthermore, for the sake of simplicity, the symmetries considered for the first invariant scheme (SYM-1) were used to construct a third invariant scheme for the solution of the inviscid Burgers' equation that is set to be fourth order accurate in both time and space. Results obtained from this scheme indicate that preservation of the symmetries considered for the first invariant scheme (which were projection, translation in time, and translation in space symmetries) was enough to construct a fourth order accurate invariant scheme that has a significantly simplified numerical representation.

We considered the viscous Burgers' equation as our third test case and constructed a fourth order accurate invariant scheme that is built on a three-point stencil. By considering appropriate moving frames, defect correction terms were significantly simplified (leaving only a single term that is of the form of a diffusion) in the transformed space. In addition, the nonlinear transport term of the original

viscous Burgers' equation was also eliminated. The final form of the fourth order accurate invariant scheme in this case contains only a temporal derivative term and a nonlinear diffusion term which has a much simpler discrete representation. As expected, the performance of the proposed invariant scheme was similar to that of the previous problems.

In our last test case, we considered the two-dimensional linear advection diffusion equation and constructed two different fourth order accurate invariant numerical schemes for this problem. The objective was to develop invariant schemes for different choices of moving frames and to compare the results for the effects of these selections. Results indicate that both sets of moving frames lead to invariant numerical schemes that are fourth order accurate with negligible differences.

CHAPTER 5

Construction of Invariant Compact Finite Difference Schemes

5.1 Scope of the Chapter

In this chapter, we propose a novel mathematical approach for construction of high order accurate compact finite difference schemes that preserve Lie symmetry groups of underlying differential equations. In this method, extended symmetry groups of partial differential equations are used to obtain point transformations not only for independent and dependent variables of differential equations, but also for their derivative terms (which is a novel aspect of this work that was not considered in earlier works [85, 87, 91]). Once point transformations for derivatives of differential equations are determined, then these transformations are applied to some (non-invariant) base compact finite difference schemes (of a desired order of accuracy) to obtain the final invariant (or symmetry preserving) forms of these schemes. Here we note that the unknown symmetry parameters that appear in these point transformations are determined by choosing convenient moving frames for which numerical representations of base schemes simplify notably and their accuracy improves. The proposed method is applied to some commonly used linear and nonlinear problems and for all the test problems, these invariant schemes appear to perform significantly better than the selected non-invariant base compact schemes in terms of numerical accuracy verifying the potential advantages of symmetry preservation.

We demonstrate the implementation of the proposed method by considering

fourth order accurate invariant compact finite difference schemes for one- and two-dimensional linear advection-diffusion equations and Burgers' equations (i.e., inviscid, viscous). For numerical simplicity, we use forward differencing to discretize temporal derivatives and fourth order compact schemes based on central differencing to discretize spatial derivatives. Note that the proposed construction of invariant schemes can also be extended to arbitrarily high order temporal and spatial discretization. Results obtained from the proposed invariant compact schemes developed for these test problems suggest that symmetry preservation can lead to significant improvements in numerical accuracy besides storing important geometric information (regarding the underlying differential equations) in associated numerical schemes.

5.2 Mathematical Formulation

In this section, the procedure for construction of invariant compact schemes is presented in detail.

5.2.1 Construction of Compact Schemes

Compact finite difference methods are widely used for high order computations and in some cases are favored over standard finite difference methods due to their ability to achieve high order accuracy over smaller stencils. For instance, while a standard central difference approximation of the first derivative of a function on a three-point stencil is second order accurate, an approximation based on a compact scheme (that is also derived through central differencing) of the same derivative could be of higher orders. The implementation of compact schemes is rather simple. To illustrate construction of compact schemes through an example, let us develop fourth order accurate compact finite difference schemes for the first and second derivatives of a function U. Consider the following Taylor series expansion of the function U at grid

points $(i \pm 1)$:

$$U^{i\pm1} = U^i \pm hU^i_x + \frac{h^2}{2}U^i_{xx} \pm \frac{h^3}{6}U^i_{xxx} + \frac{h^4}{24}U^i_{(\mathrm{IV})} \pm O(h^5) \tag{5.1}$$

where h is the discrete spatial step and the symbol $(\cdot)_x$ denotes derivative with respect to variable x. Similarly, the first and second derivative of U can be expanded in a Taylor series as

$$U^{i\pm1}_x = U^i_x \pm hU^i_{xx} + \frac{h^2}{2}U^i_{xxx} \pm \frac{h^3}{6}U^i_{(\mathrm{IV})} + \frac{h^4}{24}U^i_{(\mathrm{V})} \pm O(h^5) \tag{5.2}$$

$$U^{i\pm1}_{xx} = U^i_{xx} \pm hU^i_{xxx} + \frac{h^2}{2}U^i_{(\mathrm{IV})} \pm \frac{h^3}{6}U^i_{(\mathrm{V})} + \frac{h^4}{24}U^i_{(\mathrm{VI})} \pm O(h^5). \tag{5.3}$$

In order to eliminate the higher order derivatives ($U_{xx}, U_{xxx}, U_{(\mathrm{IV})}$, and $U_{(\mathrm{V})}$) and obtain an implicit relationship between the first derivative U_x and the function U at nodes $(i \pm 1)$, one can multiply Eq. (5.1) with constant a (at point $i+1$) and with constant b (at point $i-1$), and multiply Eq. (5.2) with quantity $c \times h$ (at point $i+1$) and with quantity $d \times h$ (at point $i-1$) and sum up these resulting quantities which eventually simplifies to the following:

$$\begin{aligned} aU^{i+1} + bU^{i-1} + chU^{i+1}_x + dhU^{i-1}_x = {} & (a+b)U^i + (a-b+c+d)hU^i_x \\ & + (a+b+2c-2d)\frac{h^2}{2}U^i_{xx} + (a-b+3c+3d)\frac{h^3}{6}U^i_{xxx} \\ & + (a+b+4c-4d)\frac{h^4}{24}U^i_{(\mathrm{IV})} + (c+d)\frac{h^5}{24}U^i_{(\mathrm{IV})} + O(h^5). \end{aligned} \tag{5.4}$$

Here, a, b, c, and d are arbitrary constants. A particular set of solutions for these constants (for which the higher order derivatives are eliminated) is found as

$$\{a, b, c, d\} = \{\frac{3}{4}, -\frac{3}{4}, -\frac{1}{4}, -\frac{1}{4}\} \ .$$

Hence the final form of Eq. (5.4) (which implicitly relates the function U to its first derivative) can be written as

$$\frac{1}{6}U_x^{i+1} + \frac{2}{3}U_x^i + \frac{1}{6}U_x^{i-1} = \frac{U^{i+1} - U^{i-1}}{2h} + O(h^4) \ . \tag{5.5}$$

Through similar algebraic manipulations, one can obtain the following fourth order accurate implicit approximation for the second derivative of the function U as well

$$\frac{1}{12}U_{xx}^{i+1} + \frac{5}{6}U_{xx}^i + \frac{1}{12}U_{xx}^{i-1} = \frac{U^{i+1} - 2U^i + U^{i-1}}{h^2} + O(h^4). \tag{5.6}$$

Both Eqs. (5.5)–(5.6) yield tridiagonal matrices that can easily be solved to accurately approximate the first and second derivatives of U at all grid points. More information on compact schemes along with compact algorithms for derivatives with higher orders of accuracy and a discussion on the treatment of boundary conditions in this method can be found in the literature [54, 55].

5.2.2 Invariantization of Compact Schemes

In this work, a compact finite difference scheme (corresponding to a surface $L(\mathbf{z}) = 0$) is considered as an invariant compact scheme if its form remains unchanged under the action of a point symmetry group G associated with the surface $L(\mathbf{z}) = 0$. In this context, let $\tilde{N}_c(\mathbf{z}) = 0$ be an invariant compact finite difference scheme, and $\tilde{\phi}_c(\mathbf{z}) = 0$ be a stencil equation for the surface $L(\mathbf{z}) = 0$ where $\mathbf{z} = (\mathbf{x}, \mathbf{u}, \mathbf{p})$ is the vector of the independent/dependent variables and derivatives, respectively. The compact scheme $\tilde{N}_c(\mathbf{z}) = 0$ and the stencil equation $\tilde{\phi}_c(\mathbf{z}) = 0$ are said to be invariant under the action of the group element g (where $g \in G$) if the following condition is

satisfied:

$$\begin{aligned} \tilde{N}_c(\rho(\mathbf{z})\cdot\mathbf{z}) = 0 \quad &\Longleftrightarrow \quad \tilde{N}_c(\mathbf{z}) = 0 \\ \tilde{\phi}_c(\rho(\mathbf{z})\cdot\mathbf{z}) = 0 \quad &\Longleftrightarrow \quad \tilde{\phi}_c(\mathbf{z}) = 0 \end{aligned} \tag{5.7}$$

where $\rho(\mathbf{z})$ represents right moving frames defined on a manifold M such that it is a topological map ($\rho : M \to G$) that satisfies the following condition:

$$\rho(g\cdot\mathbf{z}) = \rho(\mathbf{z})\, g^{-1}$$

for $\forall\, g \in G$. For any given non-invariant compact finite difference scheme $N_c(\mathbf{z}) = 0$ (constructed for a surface $L(\mathbf{z}) = 0$), an invariant form of this scheme $\tilde{N}_c(\mathbf{z}) = 0$ can be obtained by simply transforming every coordinate variable and derivative of the base (non-invariant) compact scheme according to the symmetry group G as $\tilde{N}_c(\mathbf{z}) = N_c(g\cdot\mathbf{z})$ for all $g \in G$. The unknown group parameters (that appear when the action of a particular group element g on the coordinate variables and derivatives is evaluated) can be determined via Cartan's method of normalization.

5.3 Development of Invariant Compact Schemes

In this section, the invariantization of compact finite difference schemes is illustrated through examples. In particular, fourth order accurate invariant compact schemes are constructed for some linear and nonlinear problems.

5.3.1 Inviscid Burgers' Equation

As our first test problem, we consider the inviscid Burgers' equation (IBE) which is of the form

$$u_t + u\, u_x = 0. \tag{5.8}$$

A non-invariant compact scheme can be constructed for the IBE using the compact algorithms developed for the spatial first, Eq. (5.5), and second, Eq. (5.6), derivatives. As for the time derivative, for simplicity, a classical first order forward differencing technique can be considered. The order of accuracy can be improved from first to second order via truncation error analysis or defect correction. Hence the final form of the compact scheme develop for the inviscid Burgers' equation can be found as

$$N_c(\mathbf{z}) = \frac{u^{(i,n+1)} - u^{(i,n)}}{\tau} + uu_x + d_c = 0 \ . \tag{5.9}$$

Here, d_c represents the defect correction terms (obtained from truncation error analysis) that are added to the scheme to improve accuracy and is given by

$$d_c = -\frac{\tau}{2}(u^2\, u_{xx} + 2\, u\, u_x^2) \ + \ O(\tau^2, h^4) \tag{5.10}$$

where τ and h denote the discrete time and space steps, respectively.

Considering the Lie group, Eq. (4.14), associated with the IBE, extended point transformations are found for the independent/dependent variables and derivative terms. Here, we note that in order to find the extended point transformations $\tilde{\mathbf{p}} = (\tilde{u}_{\tilde{x}}, \tilde{u}_{\tilde{x}\tilde{x}})$, one should extend the group operators given in Eq. (4.14) such that it accounts for all the derivative terms before these groups are used in the Lie series given in Eq. (2.23). Alternatively, one can use the chain rule to find the extended point transformations. For instance, the transformation expression for the spatial first derivative can be found using

$$\frac{\partial \tilde{u}}{\partial \tilde{x}} = \frac{\partial \tilde{u}}{\partial x}\frac{\partial x}{\partial \tilde{x}} + \frac{\partial \tilde{u}}{\partial t}\frac{\partial t}{\partial \tilde{x}}$$

once the point transformations for the independent and dependent variables are

found. Similarly, point transformations associated with a multiple number of subgroups can be obtained by substituting each subgroup into Eq. (2.23) in an arbitrary order. Although it is possible to consider the full Lie algebra and obtain global transformations for the coordinate variables and derivatives, it is sometimes practical to choose only certain subgroups as the form of the point transformations obtained from the full Lie algebra could be cumbersome and not practical for preservation in associated compact finite difference schemes [91]. Hence, for this particular problem, we only choose the subgroups X_1, X_3, X_6, and X_7 for preservation in the associated (non-invariant) compact scheme given in Eq. (5.9). The global transformations obtained from these particular subgroups are found via Eq. (2.23) as

$$\begin{aligned}
\tilde{t} &= e^{2s_3}\frac{(t+s_6)}{\lambda} \\
\tilde{x} &= e^{s_3}\frac{x+s_7}{\lambda} \\
\tilde{u} &= e^{-s_3}(\lambda u + s_1(x+s_7)) \\
\tilde{u}_{\tilde{x}} &= e^{-2s_3}(\lambda^2 u_x + s_1\lambda) \\
\tilde{u}_{\tilde{x}\tilde{x}} &= e^{-3s_3}\lambda^3 u_{xx}
\end{aligned} \tag{5.11}$$

where $\lambda = 1 - s_1(t+s_6)$. The compact scheme constructed for the inviscid Burgers' equation, Eq. (5.9), can be invariantized by transforming every coordinate variable and derivative according to the above transformations

$$\tilde{N}_c(\mathbf{z}) = N_c(g\cdot\mathbf{z}) = \frac{\tilde{u}^{(i,n+1)} - \tilde{u}^{(i,n)}}{\tilde{\tau}} + \tilde{u}\tilde{u}_{\tilde{x}} - \frac{\tilde{\tau}}{2}(\tilde{u}^2\,\tilde{u}_{\tilde{x}\tilde{x}} + 2\,\tilde{u}\,\tilde{u}_{\tilde{x}}^2) \;+\; O(\tilde{\tau}^2, \tilde{h}^4) = 0\ . \tag{5.12}$$

Based on the point transformations given in Eq. (5.11), it appears that the symmetry parameter s_3 does not appear in the transformed scheme given in Eq. (5.12). All the other symmetry parameters can be determined through Cartan's method

of normalization. First, we consider convenient normalization conditions that lead to simple stencils. For instance, the particular normalization conditions $\tilde{t}^{(i,n)} = 0$ and $\tilde{x}^{(i,n)} = 0$, among infinite possibilities, yield a simple stencil where the symmetry parameters s_6 and s_7 are $-t^{(i,n)}$ and $-x^{(i,n)}$, respectively. Second, we choose normalization conditions that remove terms from the truncation error of compact schemes under consideration and hence lead to a considerable improvement in numerical accuracy besides simplifying the numerical representations [91]. In this context, the normalization condition $\tilde{u}_{\tilde{x}}^{(i,n)} = 0$ can be used to determine the symmetry parameter s_1

$$\tilde{u}_{\tilde{x}}^{(i,n)} = 0 \quad \Rightarrow \quad u_x^{(i,n)} + s_1 = 0 \quad \Rightarrow \quad s_1 = -u_x^{(i,n)} \tag{5.13}$$

and remove all the terms that include the spatial first derivative from the compact scheme given in Eq. (5.12) in the transformed space as shown in the following:

$$\tilde{N}_c(\mathbf{z}) = N_c(g \cdot \mathbf{z}) = \frac{\tilde{u}^{(i,n+1)} - \tilde{u}^{(i,n)}}{\tilde{\tau}} - \frac{\tilde{\tau}}{2}\tilde{u}^2\, \tilde{u}_{\tilde{x}\tilde{x}} + O(\tilde{\tau}^2, \tilde{h}^4) = 0 \ . \tag{5.14}$$

The compact scheme given in Eq. (5.14) is invariant under the symmetry groups X_1, X_3, X_6, and X_7 and can also be expressed in original variables as

$$u^{(i,n+1)} = \frac{1}{\lambda_{n+1}} \left(u^{(i,n)} + \frac{\tau^2}{2\lambda_{n+1}^2} (u^{(i,n)})^2 u_{xx} \right) \tag{5.15}$$

where $\lambda_{n+1} = 1 - s_1\tau$. Note that for most of the test problems considered in this work, we use a time-space orthogonal mesh, $t^{(i+1,n)} - t^{(i,n)} = 0$ and $x^{(i,n+1)} - x^{(i,n)} = 0$, and hence, for simplicity, we will replace $t^{(i,n)}$ with t^n, and $x^{(i,n)}$ with x^i in the following examples. Invariance of the compact scheme constructed for the inviscid Burgers' equation, Eq. (5.15), can be verified by transforming every variable in this scheme according to the transformations given in Eq. (5.11) and the resulting

transformed scheme should be identical to Eq. (5.15).

Here we also note that for this particular problem, for simplicity, we considered first order forward differencing for the time derivative and used the method of modified equations to improve the accuracy of the approximation from first to second order. However, one could also use higher order approximations or other discretization techniques (e.g. Runge-Kutta algorithms) for the time derivative if desired. A particularly interesting case occurs when a TVD-RK2 discretization technique is used for the time derivative in Eq. (5.8). In this case, the final form of the invariant compact scheme constructed using the transformations and moving frames considered for the IBE would be identical to the invariant compact scheme given in Eq. (5.15).

5.3.2 Linear Advection-Diffusion Equation in 1D

As our second test problem, we choose the one-dimensional linear advection-diffusion equation of the form

$$u_t + \alpha\, u_x = \nu\, u_{xx}. \tag{5.16}$$

which describes the evolution of a quantity u due to linear advection and diffusion processes. The symbols α and ν denote the constant characteristic speed and diffusion coefficient, respectively. A non-invariant compact numerical scheme can be developed for Eq. (5.16) as

$$\frac{u^{(i,n+1)} - u^{(i,n)}}{\tau} + \alpha\, u_x = \nu\, u_{xx} \tag{5.17}$$

where forward differencing is considered for the time derivative, and the spatial first and second derivatives are approximated according to Eq. (5.5) and Eq. (5.6), respectively. The symmetry group G associated with the one-dimensional advection-

diffusion equation is given in Eq. (4.5). Considering the subgroups X_1, X_5, and X_6, the following point transformations can be obtained

$$\begin{aligned}
\tilde{t} &= \frac{t+s_5}{\lambda} \\
\tilde{x} &= \frac{x+s_6}{\lambda} \\
\tilde{u} &= \lambda^{\frac{1}{2}} u \exp\left(-\frac{s_1\,\gamma^2}{2\lambda\nu}\right) \\
\tilde{u}_{\tilde{x}} &= \lambda^{\frac{1}{2}}\nu^{-1}(s_1\gamma u + \lambda\nu u_x)\exp\left(-\frac{s_1\,\gamma^2}{2\lambda\nu}\right) \\
\tilde{u}_{\tilde{x}\tilde{x}} &= \lambda^{\frac{1}{2}}\nu^{-2}(s_1^2\gamma^2 u - s_1\lambda\nu u - 2s_1\lambda\gamma\nu u_x + \lambda^2\nu^2 u_{xx})\exp\left(-\frac{s_1\,\gamma^2}{2\lambda\nu}\right)
\end{aligned} \tag{5.18}$$

where $\lambda = 1 - 2\,s_1\,(t+s_5)$ and $\gamma = x + s_6 - \alpha\,(t+s_5)$. The other subgroups are neglected as their inclusion leads to point transformations of cumbersome structures that are difficult to implement. The normalization conditions $\tilde{t}^n = 0$ and $\tilde{x}^i = 0$ can be used to determine the symmetry parameters s_5 and s_6, respectively. The symmetry parameter s_1 (corresponding to the projection group X_1) can be found by considering the normalization condition

$$\tilde{u}^{(i,n)}_{\tilde{x}\tilde{x}} = 0 \quad \Rightarrow \quad s_1 = \frac{\nu}{u^{(i,n)}}\,u^{(i,n)}_{xx}. \tag{5.19}$$

As all the unknown symmetry parameters are defined, the point transformations given in Eq. (5.18) can be implemented to the base compact numerical scheme, Eq. (5.17). This implementation appears to reduce the scheme to a form of linear advection equation in the transformed space as

$$\frac{\tilde{u}^{(i,n+1)} - \tilde{u}^{(i,n)}}{\tilde{\tau}} + \alpha\,\tilde{u}^{(i,n)}_{\tilde{x}} = 0 \tag{5.20}$$

where the spatial second derivative is removed from the scheme owing to the normalization condition given in Eq. (5.19). Hence, the transformed compact scheme given

in Eq. (5.20) that is constructed for the one-dimensional linear advection-diffusion equation and is invariant under the subgroups X_1, X_5, and X_6 can be expressed in the original discrete variables as follows

$$u^{(i,n+1)} = \lambda_{n+1}^{-\frac{3}{2}} \left(\lambda_{n+1} u^{(i,n)} - \tau\, \alpha\, u_x^{(i,n)}\right) \exp\left(\frac{s_1 \alpha^2 \tau^2}{2\nu\lambda_{n+1}}\right) \tag{5.21}$$

where $\lambda_{n+1} = 1 - 2s_1\tau$.

5.3.3 Viscous Burgers' Equation

As our third test problem, let us consider the viscous Burgers' equation that is of the form

$$u_t + u\, u_x = \nu\, u_{xx} \tag{5.22}$$

and develop an invariant compact numerical scheme for this particular PDE. Similar to the one-dimensional linear advection-diffusion equation, we consider forward differencing for the time derivative and use Eqs. (5.5)–(5.6) for the spatial derivatives to construct the non-invariant base compact scheme for the solution of this PDE as shown in the following

$$\frac{u^{(i,n+1)} - u^{(i,n)}}{\tau} + u u_x = \nu u_{xx}\ . \tag{5.23}$$

The symmetry group G associated with the viscous Burgers' equation is noted in Eq. (4.36). The point transformations that account for the projection group X_1, Galilean transformation group X_2, scaling group X_3, and translation groups X_4 and X_5 can be found as

$$\tilde{t} = e^{2s_3} \frac{(t + s_4)}{\lambda}$$

$$
\begin{aligned}
\tilde{x} &= e^{s_3}\frac{x + s_5 + s_2(t + s_4)}{\lambda} \\
\tilde{u} &= e^{-s_3}(\lambda u + s_1(x + s_5) + s_2) \\
\tilde{u}_{\tilde{x}} &= e^{-2s_3}(\lambda^2 u_x + s_1\lambda) \\
\tilde{u}_{\tilde{x}\tilde{x}} &= e^{-3s_3}\lambda^3 u_{xx}
\end{aligned}
\tag{5.24}
$$

where $\lambda = 1 - s_1(t + s_4)$. As similar to the inviscid Burgers' equation, the scaling symmetry parameter s_3 does not occur when these transformations are implemented to the compact scheme given in Eq. (5.23). The symmetry parameters associated with the translation groups X_4 and X_5 can be found by considering the same normalization conditions used for the previous problems. The Galilean parameter s_2 can be found by using the normalization condition $\tilde{u}^{(i,n)} = 0$. And finally, the projection parameter s_1 can be found by choosing a moving frame for which the approximation for the first derivative goes to zero in the transformed space

$$
\tilde{u}_{\tilde{x}}^{(i,n)} = 0 \quad \Rightarrow \quad s_1 = -u_x^{(i,n)} \ . \tag{5.25}
$$

The above normalization condition indicates that all terms in the base (non-invariant) compact scheme, Eq. (5.23), that include the spatial first derivative will be removed from the compact scheme in the transformed space leading to the following reduced form

$$
\tilde{u}^{(i,n+1)} = \nu\,\tilde{\tau}\,\tilde{u}_{\tilde{x}\tilde{x}} \tag{5.26}
$$

where $\tilde{\tau} = \tilde{t}^{(i,n+1)}$. The transformed compact numerical scheme, Eq. (5.26), that is invariant under all the symmetry groups of the viscous Burgers' equation can also

be expressed in the original variables as

$$u^{(i,n+1)} = \frac{1}{\lambda_{n+1}} \left(u^{(i,n)} - s_1 (x^{(i,n+1)} - x^{(i,n)}) + \frac{\tau \nu}{\lambda_{n+1}} u_{xx}^{(i,n)} \right) \tag{5.27}$$

where $\lambda_{n+1} = 1 - s_1 \tau$.

5.3.4 Linear Advection-Diffusion Equation in 2D

As our last test problem, we choose the two-dimensional linear advection-diffusion equation that is of the form

$$u_t + \alpha\, u_x + \beta\, u_y = \nu\, (u_{xx} + u_{yy}) \tag{5.28}$$

to demonstrate the applicability of the proposed method to a multidimensional problem. Here α and β denote constant characteristic wave speeds along x- and y-coordinates, respectively. For this particular PDE, two different compact numerical schemes that are invariant under the same symmetry groups but are constructed using different moving frames are developed. Similar to the previous problems, the base (non-invariant) compact numerical scheme considered for this PDE is also developed considering forward differencing for the temporal derivative and fourth order compact finite difference algorithms, given in Eq. (5.5)–(5.6), for the spatial derivatives as shown in the following:

$$\frac{u^{(i,j,n+1)} - u^{(i,j,n)}}{\tau} + \alpha\, u_x + \beta\, u_y = \nu\, (u_{xx} + u_{yy})\ . \tag{5.29}$$

Considering the symmetry group associated with the two-dimensional linear advection-diffusion equation given in Eq. (4.47), the following point transformations that are

based on the subgroups X_1, X_6, X_7, and X_8, are found

$$\begin{aligned}
\tilde{t} &= \frac{t+s_6}{\lambda}, \qquad \tilde{x} = \frac{x+s_7}{\lambda}, \qquad \tilde{y} = \frac{y+s_8}{\lambda} \\
\tilde{u} &= \lambda\, u \exp\left[-\frac{s_1\,(\gamma^2+\theta^2)}{\lambda}\right] \\
\tilde{u}_{\tilde{x}} &= (2\,\lambda\,\gamma\,s_1\,u + \lambda^2\,u_x) \exp\left[-\frac{s_1\,(\gamma^2+\theta^2)}{\lambda}\right] \\
\tilde{u}_{\tilde{y}} &= (2\,\lambda\,\theta\,s_1\,u + \lambda^2\,u_y) \exp\left[-\frac{s_1\,(\gamma^2+\theta^2)}{\lambda}\right] \\
\tilde{u}_{\tilde{x}\tilde{x}} &= (4\,\lambda\,\gamma^2\,s_1^2\,u - 2\,\lambda^2\,s_1\,u + 4\,\lambda^2\,\gamma\,s_1\,u_x + \lambda^3\,u_{xx}) \exp\left[-\frac{s_1\,(\gamma^2+\theta^2)}{\lambda}\right] \\
\tilde{u}_{\tilde{y}\tilde{y}} &= (4\,\lambda\,\theta^2\,s_1^2\,u - 2\,\lambda^2\,s_1\,u + 4\,\lambda^2\,\theta\,s_1\,u_y + \lambda^3\,u_{yy}) \exp\left[-\frac{s_1\,(\gamma^2+\theta^2)}{\lambda}\right]
\end{aligned} \tag{5.30}$$

where

$$\begin{aligned}
\lambda &= 1 - 4\,\nu\,s_1\,(t+s_6) \\
\gamma &= x + s_7 - \alpha\,(t+s_6) \\
\theta &= y + s_8 - \beta\,(t+s_6)\ .
\end{aligned}$$

The base compact scheme given in Eq. (5.29) can be transformed according to the above transformations as follows

$$\frac{\tilde{u}^{(i,j,n+1)} - \tilde{u}^{(i,j,n)}}{\tilde{\tau}} + \alpha\,\tilde{u}_{\tilde{x}} + \beta\,\tilde{u}_{\tilde{y}} = \nu\,(\tilde{u}_{\tilde{x}\tilde{x}} + \tilde{u}_{\tilde{y}\tilde{y}})\ . \tag{5.31}$$

Here we note that, for simplicity, we ignore the Galilean (X_2 and X_3) and scaling (X_4 and X_5) groups and do not consider them for determination of the point transformations as their inclusion (besides the other symmetry groups) result in transformations that are laborious to implement. The symmetry parameters s_6, s_7, and s_8 can be determined by considering the normalization conditions $\tilde{t}^n = 0$, $\tilde{x}_i = 0$, and $\tilde{y}_j = 0$, respectively. As for the determination of the symmetry parameter s_1,

we consider two different normalization conditions to evaluate the effect of these selections on the numerical accuracy of the resulting invariant schemes. We choose

$$\partial_{\tilde{x}\tilde{x}}\tilde{u}^{(i,j,n)} = 0 \quad \Rightarrow \quad s_1 = \frac{\partial_{xx}u^{(i,j,n)}}{2\,u^{(i,j,n)}} \tag{5.32}$$

as the first normalization condition and construct an invariant compact scheme (referred to as SYM-1) as follows

$$\frac{\tilde{u}^{(i,j,n+1)} - \tilde{u}^{(i,j,n)}}{\tilde{\tau}} + \alpha\tilde{u}_{\tilde{x}} + \beta\tilde{u}_{\tilde{y}} = \nu\tilde{u}_{\tilde{y}\tilde{y}} \ . \tag{5.33}$$

In the second case, we consider the normalization condition

$$\partial_{\tilde{x}\tilde{x}}\tilde{u}^{(i,j,n)} + \partial_{\tilde{y}\tilde{y}}\tilde{u}^{(i,j,n)} = 0 \quad \Rightarrow \quad s_1 = \frac{\partial_{xx}u^{(i,j,n)} + \partial_{yy}u^{(i,j,n)}}{4\,u^{(i,j,n)}} \tag{5.34}$$

and construct another invariant compact scheme (referred to as SYM-2) as

$$\frac{\tilde{u}^{(i,j,n+1)} - \tilde{u}^{(i,j,n)}}{\tilde{\tau}} + \alpha\tilde{u}_{\tilde{x}} + \beta\tilde{u}_{\tilde{y}} = 0 \ . \tag{5.35}$$

Here we note that both Eq. (5.33) and Eq. (5.35) can also be expressed in the original variables by implementing the transformations given in Eq. (5.30).

5.4 Results and Discussion

In this section, the performance of the proposed invariant compact finite difference schemes developed for the inviscid Burgers' equation, linear advection-diffusion equation (in 1D and 2D), and viscous Burgers' equation are evaluated. Results obtained from these invariant schemes are compared with standard schemes for numerical accuracy.

Table 5.1
Root mean square error (RMSE) and L_∞ error associated with numerical solutions (based on compact schemes) for the inviscid Burgers' equation.

Error	FTCS	COMP	SYM
L_∞	4.0×10^{-2}	5.8×10^{-3}	5.1×10^{-3}
RMSE	9.7×10^{-3}	1.3×10^{-3}	1.1×10^{-3}

5.4.1 Inviscid Burgers' Equation

We first evaluate the performance of the invariant compact scheme constructed for the inviscid Burgers' equation, Eq. (5.15), by comparing the results with the analytical solution given in Eq. (4.54) over the spatial domain Γ where $x \in [-3, 3]$. The initial and boundary conditions are noted from the analytical solution.

Snapshots of the propagating wave that are obtained from the exact solution, the proposed invariant (compact) scheme (SYM), standard fourth order accurate compact scheme (COMP), and the classical second order accurate forward in time central in space (FTCS) scheme are shown in figure 5.1 (left plot). The associated numerical errors of these schemes, which are estimated as $N_{exact} - N_{numeric}$, are also given in this figure 5.1 (right plot). It appears that the results obtained from the proposed invariant compact scheme (SYM) are significantly more accurate than the results obtained from classical finite difference (FTCS) scheme and are slightly better than those obtained from the compact finite difference (COMP) scheme. Further, the root mean square error (RMSE), estimated as $\sqrt{\sum (u_a - u_n)^2 / N}$, and L_∞ error, estimated as $max(|u_a - u_n|)$, of these numerical schemes, for this particular run, are given in table 5.1. According to the error analysis presented in this table, the L_∞ errors obtained from the FTCS scheme, compact finite difference scheme, and the invariant scheme are 4.0×10^{-2}, 5.8×10^{-3}, and 5.1×10^{-3}, respectively. Similarly, the root mean square errors for these numerical schemes are found as 9.7×10^{-3} (FTCS), 1.3×10^{-3} (COMP), and 1.1×10^{-3} (SYM). As expected, the proposed invariant scheme (SYM) which preserves the symmetries of the underlying PDE has

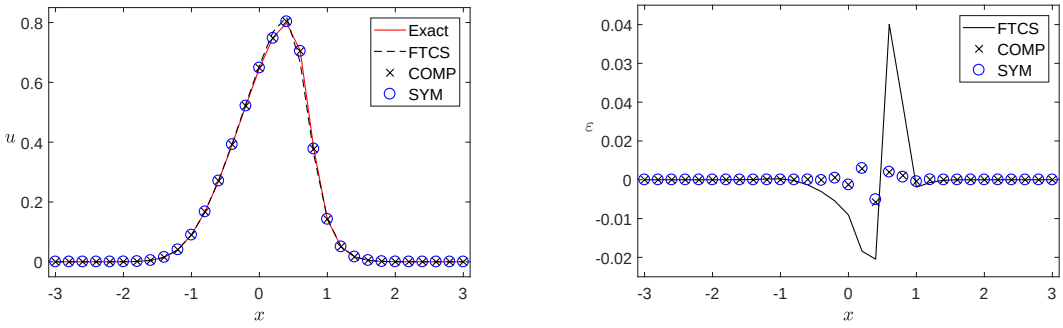

Fig. 5.1. Inviscid Burgers' equation. Comparison of velocity profiles, at $t = 0.5$, obtained from the analytical solution (Exact), the classical forward in time central in space (FTCS) scheme, the standard compact scheme (COMP), and the proposed invariant compact scheme (SYM) is shown in the left plot. Spatial distribution of errors for these numerical schemes is shown in the right figure. Parameter settings: $h = 0.2$, $\tau = 0.001$, and $\sigma = 0.5$.

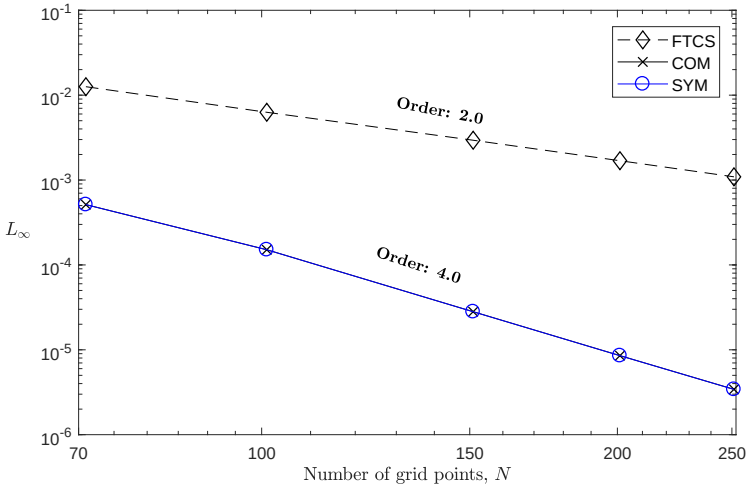

Fig. 5.2. Inviscid Burgers' equation. Comparison of L_∞ errors of numerical schemes versus number of grid points.

significantly less error compared to the standard FTCS scheme ans has slightly less error than the standard compact finite difference scheme.

The variation of L_∞ errors (obtained from the standard FTCS scheme, standard compact finite difference scheme, and the invariant scheme) with respect to the number of spatial grid points is demonstrated in figure 5.2. The proposed invariant scheme (SYM) appears to be two orders more accurate than the standard

second order FTCS scheme and is at the same order as the standard compact finite difference scheme which is known to be fourth order accurate. Here, we note that a sufficiently small time step is considered for this simulation as the fourth order compact algorithms (given in Eq. (5.5) and Eq. (5.6)) are only considered for the spatial derivatives.

5.4.2 Linear Advection-Diffusion Equation in 1D

Further, we evaluated the performance of the proposed method by developing a fourth order accurate invariant compact finite difference scheme for the one-dimensional linear advection-diffusion equation and compared the results with the analytical solution given in Eq. (4.53).

For this particular problem, evolution of the profile $u(t, x)$ (from a given Gaussian initial profile) obtained from the proposed invariant scheme (SYM), standard FTCS scheme and compact finite difference (COMP) scheme is depicted in figure 5.3 (left plot). The spatial distribution of errors obtained from these particular numerical solutions is also shown in this figure (right plot). The invariant compact scheme appears to be capturing the wave propagation significantly better than the FTCS scheme and slightly better than the compact scheme. Additionally, L_∞ error and root mean square error measures corresponding to the proposed invariant compact scheme, FTCS scheme and standard compact finite difference scheme are presented in table 5.2. It appears that the invariant compact scheme is two orders of magnitude more accurate than the FTCS scheme and is one order of magnitude more accurate than the standard compact finite difference scheme.

Additionally, figure 5.4 shows the variation of L_∞ errors associated to the invariant compact scheme, FTCS scheme and standard non-invariant compact scheme with respect to the number of spatial grid points. The invariant scheme appears to be two orders more accurate than the standard second order FTCS scheme. More-

Table 5.2
Root mean square error (RMSE) and L_∞ error associated with numerical solutions (based on compact schemes) for the one-dimensional linear advection-diffusion equation.

Error	FTCS	COMP	SYM
L_∞	2.9×10^{-2}	1.2×10^{-3}	4.6×10^{-4}
RMSE	1.2×10^{-2}	3.7×10^{-4}	2.1×10^{-4}

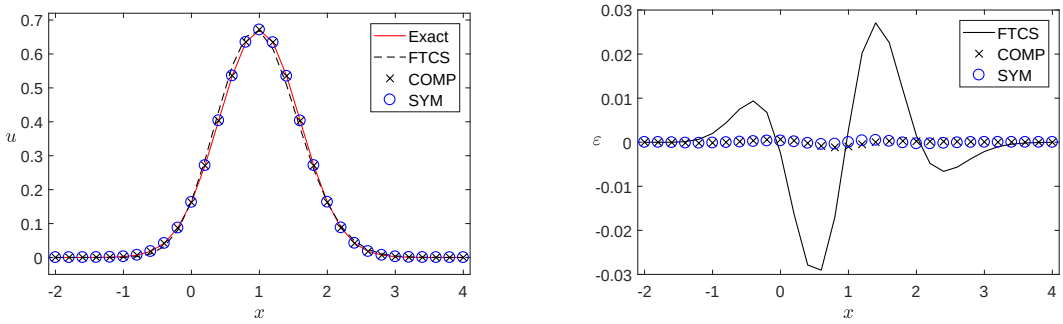

Fig. 5.3. Advection-diffusion equation (1D). Snapshots of velocity profiles, at $t = 1.0$, obtained from the analytical solution (Exact), the classical forward in time central in space (FTCS) scheme, the standard compact scheme (COMP), and the proposed invariant compact scheme (SYM) are displayed in the left figure. Spatial distribution of errors is displayed in the right figure. Parameter settings: $h = 0.2$, $\tau = 0.001$, $\nu = 1/60$. .

over, although both the invariant and standard non-invariant compact schemes are fourth order accurate, the invariant scheme appears to have slightly less numerical error.

5.4.3 Viscous Burgers' Equation

In our next test case, we considered the viscous Burgers' equation and developed a fourth order accurate invariant compact scheme that preserves the whole symmetry group, Eq. (4.14), associated with this PDE. The results are compared with the analytical solution given in Eq. (4.55).

Snapshots of the propagating shock, at $t = 0.25$, along with the spatial distribution of numerical errors, obtained from the fourth order accurate invariant compact scheme (SYM), standard second order FTCS scheme, and non-invariant fourth or-

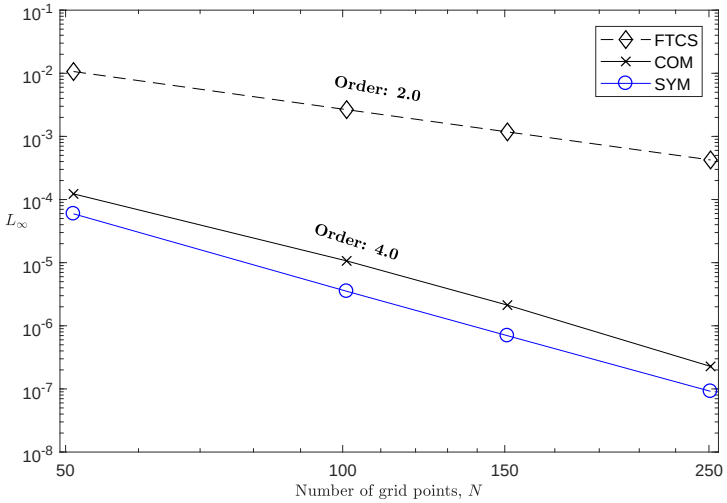

Fig. 5.4. Advection-diffusion equation (1D). Comparison of L_∞ errors of numerical schemes versus number of grid points.

der compact finite difference scheme (COMP) are depicted in figure 5.5. Although a coarse grid with 101 nodes is used for this particular run, it appears that the invariant scheme performs well and captures the shock propagation significantly better than the standard FTCS scheme, particularly near the shock-front. Further, L_∞ error and root mean square error analysis given in table 5.3 also confirms that the invariant compact scheme performs better than the standard FTCS scheme. For this particular run, root mean square errors corresponding to the invariant compact scheme, standard FTCS scheme, and non-invariant compact finite difference scheme are found to be 0.0140, 0.1251, and 0.0143, respectively. Similarly, L_∞ errors of these schemes were determined as 0.1060 (SYM), 0.8962 (FTCS), and 0.0994 (COMP).

The variation of L_∞ errors obtained from these numerical schemes with respect to number of spatial grid points is shown in figure 5.6. As expected, the results obtained from the invariant scheme are indeed fourth order accurate and are two orders more accurate than the standard FTCS scheme which is known to be a second order accurate scheme. Also, both the invariant scheme and the standard fourth order compact scheme yield results of comparable order of accuracy with negligible

Table 5.3
Root mean square error (RMSE) and L_∞ error associated with numerical solutions (based on compact schemes) for the viscous Burgers' equation.

Error	FTCS	COMP	SYM
L_∞	0.8962	0.0994	0.1060
RMSE	0.1251	0.0143	0.0140

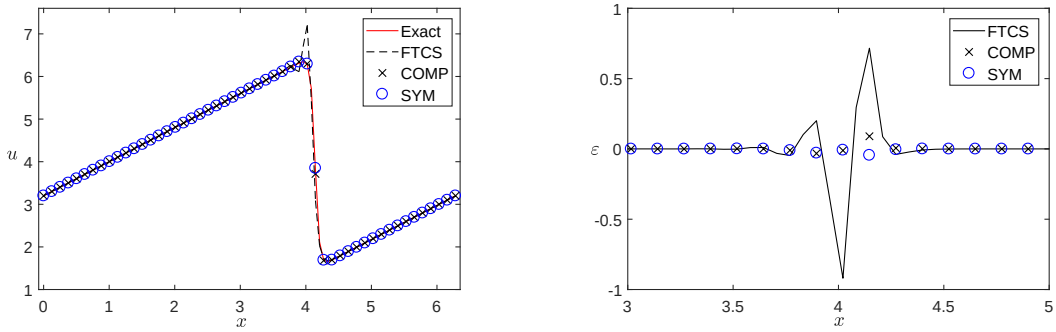

Fig. 5.5. Viscous Burgers' equation. **Left**: snapshots of shock formation profiles, at $t = 0.25$, obtained from the analytical solution, the classical FTCS scheme, the standard compact scheme (COMP), and the proposed invariant compact scheme (SYM). **Right**: spatial distribution of errors for these numerical schemes (right). Parameter settings: $h = 0.063$, $\tau = 0.0001$, $\nu = 1/12$. .

differences.

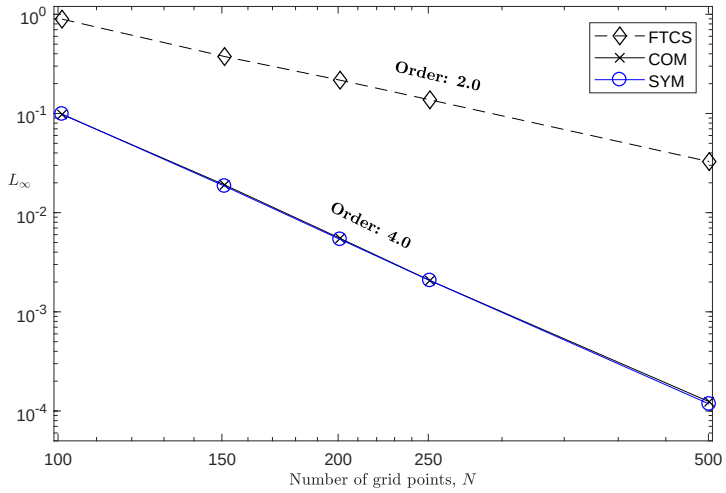

Fig. 5.6. Viscous Burgers' equation. Comparison of L_∞ errors of numerical schemes versus number of grid points.

Table 5.4
Variation of RMSE and L_∞ errors associated with numerical solutions presented in figure 5.7 (left) with respect to the Galilean parameter c.

c	Error	FTCS	COMP	SYM
0	L_∞	0.1157	0.0100	0.0120
	RMSE	0.0213	0.0023	0.0022
0.5	L_∞	0.5543	0.5131	0.0120
	RMSE	0.2424	0.2417	0.0022
1.0	L_∞	0.9033	0.9166	0.0120
	RMSE	0.3232	0.3206	0.0022

Table 5.5
Variation of RMSE and L_∞ errors associated with numerical solutions presented in figure 5.7 (right) with respect to the Galilean parameter c.

c	Error	FTCS	COMP	SYM
0	L_∞	0.2384	0.0269	0.0217
	RMSE	0.0339	0.0041	0.0034
0.3	L_∞	2.1117	2.0058	0.0217
	RMSE	0.7521	0.7451	0.0034
0.75	L_∞	2.2750	2.0118	0.0217
	RMSE	1.2066	1.2027	0.0034

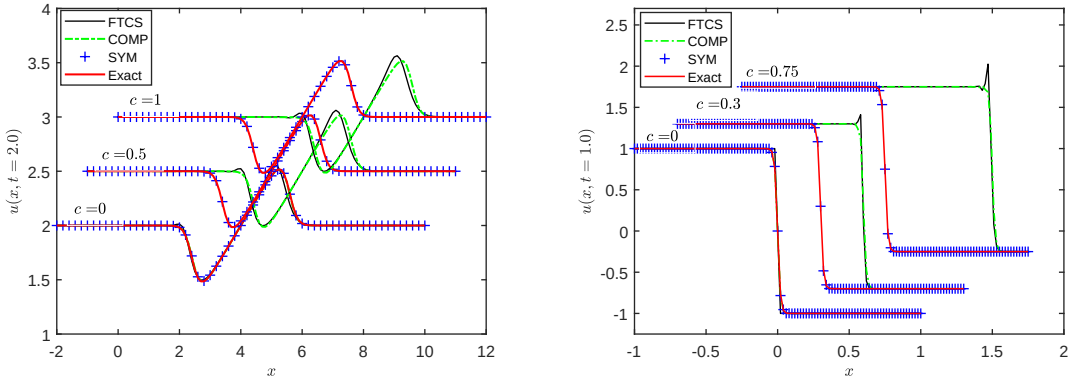

Fig. 5.7. Viscous Burgers' equation. Snapshots of numerical solutions, obtained from the analytical solution (Exact), classical forward in time central in space (FTCS) scheme, standard compact scheme (COMP), and proposed invariant compact scheme (SYM), evolving from various initial profiles for different values of the Galilean parameter c. **Left:** $h = 0.1$, $\tau = 0.0001$, $\nu = 0.05$, **Right:** $h = 0.02$, $\tau = 0.0005$, $\nu = 0.01$.

As the proposed invariant compact scheme given in Eq. (5.27) preserves all the symmetry groups of the viscous Burgers' equation, under transformations based on these symmetry groups, the invariant scheme is expected to perform significantly better than the standard numerical schemes that do not preserve these symmetry groups. For instance, under a Galilean transformation of the form

$$\hat{x} = x + ct, \qquad \hat{t} = t, \qquad \hat{u} = u + c \tag{5.36}$$

the proposed invariant scheme (SYM) is likely to capture the evolution of the velocity profile significantly better than both the standard FTCS and compact schemes. This is expected as the invariant scheme preserves the Galilean transformation group X_2 given in Eq. (4.36) whereas the standard schemes do not. To test this particular advantage of the invariant scheme, we applied the Galilean transformation given in Eq. (5.36) to these numerical schemes and presented the snapshots of the evolution of the numerical solutions from (two different) given initial profiles in figure 5.7. Additionally, root mean square errors and L_∞ errors associated with these numerical solutions are given in table 5.4 and table 5.5. These particular initial conditions along with the associated analytical solutions considered for the left and right plots in figure 5.7 can be found in reference [88]. Based on figure 5.7 and relevant error tables, it appears that when the Galilean parameter c is equal to zero, all the numerical schemes capture the evolution of the solution well which is expected. However, for the cases when the Galilean parameter c is nonzero, both the standard FTCS scheme and compact finite difference scheme appear to overpredict the solution leading to a significant lag in the solution, particularly for large values of c. On the other hand, the invariant scheme, as it preserves the Galilean symmetry group, captures the evolution of the solution well even for nonzero values of the Galilean parameter c. In fact, in the case of a numerical precision considered in table 5.4 and table 5.5, the results obtained from the invariant scheme for nonzero values of c are found to be identical to the results of the case where $c = 0$. The latter indicates that the Galilean invariance property of the viscous Burgers' equation is indeed preserved in the relevant difference equation. This property of symmetry preservation in numerical schemes can be particularly useful when differential equations associated to more complex symmetries are solved through difference equations.

Table 5.6
Root mean square error (RMSE) and L_∞ error associated with numerical solutions (based on compact schemes) for two-dimensional linear advection-diffusion equation.

Error	FTCS	COMP	SYM-1	SYM-2
L_∞	2.4×10^{-3}	3.8×10^{-5}	3.4×10^{-5}	3.3×10^{-5}
RMSE	2.7×10^{-4}	3.4×10^{-6}	3.3×10^{-6}	3.1×10^{-6}

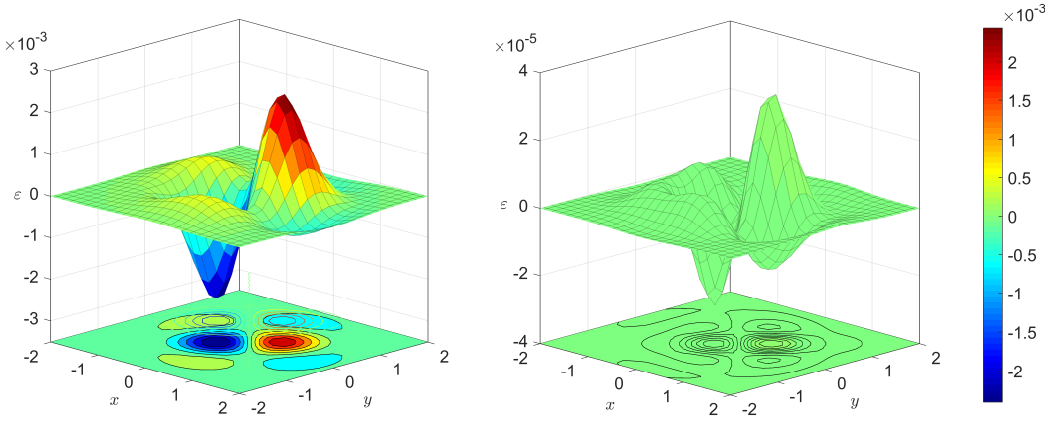

Fig. 5.8. Linear advection-diffusion equation (2D). Spatial distributions of numerical errors, at $t = 0.1$, obtained from the classical base scheme (left) and the proposed invariant scheme (right). Parameter settings: $h = 0.16,\ \tau = 0.0001,\ \alpha = 1.0,\ \beta = 1.0,\ \nu = 1/60$.

5.4.4 Linear Advection-Diffusion Equation in 2D

As our last test case, we considered the two-dimensional linear advection-diffusion equation and constructed two different fourth order accurate invariant compact finite difference scheme (SYM-1 and SYM-2) for this PDE. The main difference between the constructed invariant schemes are that both are developed via selections of different moving frames and the details of these selections are given in Section 5.3. The objective is to investigate the effect of these selections on the accuracy of the resulting invariant schemes. The analytical solution given in Eq. (4.56) is used to evaluate the quality of results obtained from the invariant SYM-1 and SYM-2 schemes.

Spatial distribution of numerical errors corresponding to the proposed invariant

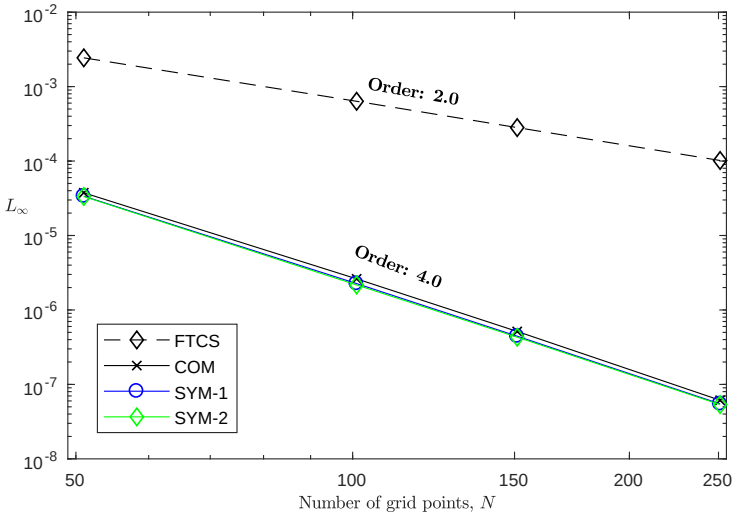

Fig. 5.9. Advection-diffusion equation in 2D. Comparison of L_∞ errors of numerical schemes versus number of grid points.

compact finite difference scheme (SYM-2) and standard non-invariant FTCS scheme is given in figure 5.8. Based on this figure, it appears that the invariant scheme has significantly less numerical error compared to the standard non-invariant FTCS scheme in this case as well. This improvement in numerical accuracy is also verified by the error analysis given in table 5.6 where both invariant schemes (SYM-1 and SYM-2) perform better than the standard schemes. L_∞ errors obtained from the invariant scheme SYM-1, invariant scheme SYM-2, FTCS scheme, and standard non-invariant compact scheme are noted as 3.4×10^{-5}, 3.3×10^{-5}, 2.4×10^{-3}, and 3.8×10^{-5}, respectively. It appears that the invariant schemes are at least two orders of magnitude more accurate than the standard FTCS scheme. Root mean square error measures of these numerical schemes also yield similar results that are 3.3×10^{-6} and 3.1×10^{-6} for the invariant schemes SYM-1 and SYM-2, 2.7×10^{-4} for the FTCS scheme, and 3.4×10^{-6} for the non-invariant compact finite difference scheme.

The variation of L_∞ errors (obtained from the proposed invariant schemes, standard FTCS scheme, and non-invariant compact scheme) with respect to the number

of spatial grid points is presented in figure 5.9. As expected, both of the proposed invariant compact schemes constructed for the two-dimensional linear advection-diffusion equation are indeed fourth order accurate and perform significantly better than the second order standard forward in time central in space (FTCS) finite difference scheme. Moreover, these invariant schemes also perform with slightly less error compared to the non-invariant compact scheme which is known to be fourth order accurate. Further, the invariant scheme SYM-2 appears to be slightly more accurate than the invariant scheme SYM-1 which indicates that the selection of moving frames could affect the accuracy of resulting invariant schemes. Although for this particular problem, the differences in the results obtained from the invariant schemes appear to be minor, in general the moving frames must be chosen carefully.

5.5 Chapter Summary

In this chapter, we presented a method, that is based on moving frames, for construction of invariant compact finite difference schemes that preserve Lie symmetry groups of underlying partial differential equations. In this method, we first determine the extended symmetry groups of PDEs and obtain point transformations based on these symmetry groups. These transformations are then applied to some (non-invariant) base compact finite difference schemes such that all the system variables (i.e., independent and dependent variables) and derivatives of these compact schemes are transformed. We then determine the unknown symmetry parameters that exist in these symmetry-based point transformations by considering convenient moving frames that are obtained through Cartan's method of normalization. In most cases, such convenient moving frames not only result in significant improvement in numerical accuracy but also notably simplify the numerical representations of the resulting invariant schemes and eventually make them easier to program. The performance of the proposed method was evaluated via construction of high or-

der accurate invariant compact finite difference schemes (built on simple three-point stencils) for some linear and nonlinear PDEs. Based on our evaluation, we concluded that symmetry preservation has the potential to significantly improve numerical accuracy of compact schemes besides embedding important geometric properties of underlying PDEs.

As our first test case, we considered the inviscid Burgers' equation and constructed a high order accurate invariant compact finite difference scheme for this PDE. Although the order of accuracy of compact schemes can be arbitrarily set by considering suitable compact finite difference algorithms, for this particular problem, we chose fourth order accurate compact algorithms to approximate the spatial derivatives and constructed an invariant scheme based on these algorithms. In all the test problems, the temporal derivatives were handled through standard forward differencing. For this particular PDE, in order to improve the numerical accuracy from first to second order in time, the base scheme was modified using defect correction techniques. The results obtained from this fourth order accurate invariant compact scheme were found to be slightly better than the results obtained from the standard compact scheme and notably better than those of the standard FTCS scheme. For all the test cases, the computation times required to run a simulation with a numerical error of comparable order were found to be similar for both the proposed invariant scheme and standard compact scheme and the differences were negligible.

As our next test problem, we considered the one-dimensional linear advection-diffusion equation and developed a fourth order accurate invariant compact scheme for this problem as well. For this particular problem, through the use of convenient moving frames (i.e., $\tilde{u}_{\tilde{x}\tilde{x}} = 0$), the numerical representation of the base scheme were reduced to a form of the linear advection equation ($\tilde{u}_{\tilde{t}} + \alpha \tilde{u}_{\tilde{x}} = 0$) in the transformed space. Similar to the previous problem, the quality of results obtained from this

invariant compact scheme (in terms of numerical accuracy) was found to be better than that of the standard FTCS and compact schemes.

Next we constructed a fourth order accurate invariant compact finite difference scheme for the viscous Burgers' equation (which is of the form of a linear heat equation, $\tilde{u}_{\tilde{t}} = \nu \tilde{u}_{\tilde{x}\tilde{x}}$, in the transformed space for the normalization condition $\tilde{u}_{\tilde{x}} = 0$) that preserves all the symmetries of the Burgers' equation and compared our results with the standard schemes. As expected, the proposed invariant compact scheme developed for this problem yielded more accurate results than standard schemes in this case as well. In particular, the performance of the proposed invariant scheme was significantly better than that of the standard schemes when a Galilean transformation is applied to these schemes (see figure 5.7 and tables 5.4–5.5) to test how these schemes are affected by such transformations that are based on symmetries of the underlying differential equation. This is due to the fact that the invariant scheme preserves the Galilean symmetry group of the viscous Burgers' equation, whereas the standard schemes do not.

In order to demonstrate the implementation of the proposed method to a multidimensional problem, as our last test case, we considered the two-dimensional linear advection-diffusion equation and constructed a couple of fourth order accurate invariant compact schemes for this problem where different moving frames are used in the construction of each invariant scheme to evaluate how this action effects the accuracy of the resulting schemes. For the first invariant scheme SYM-1, a normalization condition of the form $\tilde{u}_{\tilde{x}\tilde{x}} = 0$ is used to determine the projection group parameter s_1 whereas for the other invariant scheme (SYM-2), this particular parameter was determined using the normalization condition $\tilde{u}_{\tilde{x}\tilde{x}} + \tilde{u}_{\tilde{y}\tilde{y}} = 0$. Although both normalization conditions simplify the base compact scheme considered for this PDE notably, the latter condition reduces the base scheme to the form of two-dimensional linear advection equation ($\tilde{u}_{\tilde{t}} + \alpha \tilde{u}_{\tilde{x}} + \beta \tilde{u}_{\tilde{y}} = 0$) in the transformed

space. As for the results obtained from these invariant schemes, SYM-2 appears to be slightly more accurate than SYM-1 where both of these schemes are notably more accurate than standard schemes. Although for this particular problem, selection of different moving frames in the construction of invariant schemes did not affect the accuracy of these schemes significantly, this may not be the case for other problems as there are usually infinitely many applicable moving frames and not all of them will result in accurate invariant schemes.

CHAPTER 6

Construction of Invariant Schemes for Euler Equations

6.1 Scope of the Chapter

In this chapter, we put forth a procedure for construction of symmetry preserving numerical schemes for the solution of one- and two-dimensional Euler equations. Point transformations derived from the Lie symmetry groups underlying the Euler equations are implemented into some selected non-invariant base numerical schemes to obtain their invariant forms. The unknown symmetry parameters that occur in the definition of the derived point transformations are fully resolved through Cartan's method of normalizations where convenient normalization conditions are used to determine each symmetry parameter. The proposed procedure is implemented in two different standard, non-invariant, base numerical schemes namely Lax-Friedrichs and van Leer flux splitting schemes developed for the one- and two-dimensional Euler equations. The performance of these numerical schemes is evaluated through implementations to several different shock-tube problems (in 1D and 2D). Based on our results, it appears that these invariant numerical schemes not only preserve geometric properties of the underlying equations, which could be quite beneficial in some cases, but also accurately predict approximate numerical solutions for the selected multidimensional test problems as well.

6.2 Introduction

For the past several decades, a great deal of effort was devoted to design of high order accurate numerical schemes for solutions of nonlinear hyperbolic conservation laws [109–130]. The main challenge in the design of such numerical schemes is due to the presence of discontinuities that are commonly encountered in solutions of hyperbolic equations. Several methodologies have been proposed for constructions of numerical schemes that are capable of capturing discontinuities (up to a certain degree) that might be present in solutions of such systems [131–151]. Among these methods, there are approaches based on traditional low order schemes such as the first order Godunov scheme [132], Lax-Friedrichs scheme [39], or the Roe scheme [115]. There are also approaches based on second (or higher) orders schemes such as the Lax-Wendroff, MacCormack's, Richtmyer schemes, or upwind schemes (i.e., van Leer, Steger-Warming, Osher schemes) that are usually based on vector flux-splitting algorithms [39, 152]. The performance of most of these numerical schemes when implemented to the Euler equations in one- and two-dimensions is well-reviewed in the literature [39, 111, 118, 126, 149, 152, 153].

In this chapter, we present a systematic approach for construction of Lie symmetry preserving numerical schemes for the numerical solution of the one- and two-dimensional Euler equations which, to the best of our knowledge, has never been considered in earlier works. Point transformations obtained from selected Lie symmetry groups associated with the one- and two-dimensional Euler equations are implemented to some non-invariant base numerical schemes, namely Lax-Friedrichs scheme and van Leer flux vector splitting scheme, constructed for these equations to obtain their symmetry preserving forms. Note that we consider the method of equivariant moving frames and Cartan's method of normalization to fully resolve the unknown symmetry parameters that occur in point transformations when these

transformations are determined through Lie series approach [83,84,93,95]. Although, in this work we choose Lax-Friedrichs and van Leer schemes for the invariantization procedure, there is no such specific requirement and one can always choose some other base numerical schemes for the invariantization procedure. We evaluate the performance of the proposed invariant schemes in the case of various initial value configurations and compare our results with those obtained from standard, non-invariant based schemes considered in this work.

For the one-dimensional Euler equations, we implement the constructed invariant Lax-Friedrichs and van Leer schemes to three different shock-tube problems. Similarly, for the two-dimensional case, we evaluate the performance of the invariant Lax-Friedrichs scheme through implementations to four different two-dimensional shock-tube problems. For both one- and two-dimensional cases, the proposed invariant schemes lead to accurate numerical predictions for the solution of considered shock-tube problems. Additionally, these invariant schemes were found to be also more accurate than their non-invariant counterparts.

This chapter is organized as follows. The mathematical formulation of the one- and two-dimensional Euler equations along with a detailed discussion of associated Lie symmetry groups are discussed in Section 6.3. A discussion on construction of invariant numerical schemes is also included in this section. In the following section, Section 6.4, a systematic approach for construction of invariant schemes for the Euler equations is presented in detail. This is followed by Section 6.5 which includes some results and a discussion on the performance of the constructed numerical schemes. And finally, concluding remarks are noted in Section 6.6.

6.3 Mathematical background and Symmetry Methods

6.3.1 Euler Equations in 1D

Let us first consider the one-dimensional Euler equations given by the following conservative form

$$\mathbf{U}_t + \mathbf{F}(\mathbf{U})_x = 0 \ , \tag{6.1}$$

where the vector of conserved variables $\mathbf{U}$ and fluxes $\mathbf{F}(\mathbf{U})$ are given by

$$\mathbf{U} = \begin{bmatrix} \rho \\ \rho u \\ E \end{bmatrix} \ , \qquad \mathbf{F}(\mathbf{U}) = \begin{bmatrix} \rho u \\ \rho u^2 + p \\ u(E+p) \end{bmatrix} \ . \tag{6.2}$$

Here, u is the particle velocity, ρ is the density, p is the pressure, and E is the total energy per unit volume that is given by

$$E = \frac{p}{\gamma - 1} + \frac{1}{2}\rho u^2 \ ,$$

where the parameter $\gamma = c_p/c_v$ represents the ratio of specific heats.

The one-dimensional Euler equations given in Eq. (6.1) admits the following 6 parameters Lie group [14]:

$$\begin{aligned} X_1 &= \frac{\partial}{\partial t} \\ X_2 &= \frac{\partial}{\partial x} \\ X_3 &= t\frac{\partial}{\partial x} + \frac{\partial}{\partial u} \\ X_4 &= x\frac{\partial}{\partial x} + t\frac{\partial}{\partial t} \end{aligned} \tag{6.3}$$

$$X_5 = t\frac{\partial}{\partial t} - u\frac{\partial}{\partial u} + 2\rho\frac{\partial}{\partial \rho}$$
$$X_6 = p\frac{\partial}{\partial p} + \rho\frac{\partial}{\partial \rho} \ ,$$

where X_1 and X_2 represent invariance under translations in time and space, respectively, X_3 represents invariance under Galilean transformation, and finally, X_4, X_5, and X_6 represent invariance under scaling transformations. For simplicity, let us linearly combine the above scaling groups, $X_4 - 2X_5 + X_6$, to obtain a general scaling group of the form

$$X_7 = x\frac{\partial}{\partial x} - t\frac{\partial}{\partial t} + 2u\frac{\partial}{\partial u} + p\frac{\partial}{\partial p} - 3\rho\frac{\partial}{\partial \rho} \ . \tag{6.4}$$

The conservative form of the Euler equations given in Eq. (6.1) also admits the following projection group

$$X_8 = tx\frac{\partial}{\partial x} + t^2\frac{\partial}{\partial t} + (x - tu)\frac{\partial}{\partial u} - 3tp\frac{\partial}{\partial p} - t\rho\frac{\partial}{\partial \rho} \ , \tag{6.5}$$

for the special case where $\gamma = 3$ which corresponds to isentropic flow of a monatomic gas with one degree of freedom where molecules are constrained to move on a line. This particular value of γ is obtained from the relation

$$\gamma = \frac{n+2}{n} \ , \tag{6.6}$$

where n represents the degree of freedom [151]. The occurrence of the projection symmetry group X_8 for this specific value of γ indicates that the Lie symmetry groups associated with the Euler equations is somehow connected to the relation given in Eq. (6.6) which is systematically obtained from the kinetic theory. Similarly, for the two- and three-dimensional Euler equations, additional projection groups are obtained for specific values of $\gamma = 2$ (for 2D) and $\gamma = 5/3$ (for 3D). Although the

particular type of one-dimensional flow that corresponds to $\gamma = 3$ is not physically realizable, it has been the subject of numerous studies in discrete particle simulations [14].

6.3.2 Euler Equations in 2D

As our second problem, we consider the two-dimensional Euler equations given by

$$\mathbf{U}_t + \mathbf{F}(\mathbf{U})_x + \mathbf{G}(\mathbf{U})_y = 0 \ . \tag{6.7}$$

Here, the vectors $\mathbf{U}$, $\mathbf{F}(\mathbf{U})$, and $\mathbf{G}(\mathbf{U})$ denote the conserved variables, and fluxes in x- and y -directions, respectively, and are given as

$$\mathbf{U} = \begin{bmatrix} \rho \\ \rho u \\ \rho v \\ E \end{bmatrix} \qquad \mathbf{F}(\mathbf{U}) = \begin{bmatrix} \rho u \\ \rho u^2 + p \\ \rho uv \\ u(E+p) \end{bmatrix} \qquad \mathbf{G}(\mathbf{U}) = \begin{bmatrix} \rho v \\ \rho uv \\ \rho v^2 + p \\ v(E+p) \end{bmatrix} . \tag{6.8}$$

Further, u and v represents particle velocities in x- and y-coordinates, respectively, and the total energy per unit volume in this case is given by the following relation

$$E = \frac{p}{\gamma - 1} + \frac{1}{2}\rho(u^2 + v^2) \ .$$

The conservative form of the two-dimensional Euler equations given in Eq. (6.7) admits the following 9 parameters Lie group [14]:

$$\begin{aligned} X_1 &= \frac{\partial}{\partial t} \ , \qquad X_2 = \frac{\partial}{\partial x} \ , \qquad X_3 = \frac{\partial}{\partial y} \\ X_4 &= t\frac{\partial}{\partial x} + \frac{\partial}{\partial u} \ , \qquad X_5 = t\frac{\partial}{\partial y} + \frac{\partial}{\partial v} \\ X_6 &= x\frac{\partial}{\partial x} + y\frac{\partial}{\partial y} + t\frac{\partial}{\partial t} \end{aligned}$$

$$
\begin{aligned}
X_7 &= t\frac{\partial}{\partial t} - u\frac{\partial}{\partial u} - v\frac{\partial}{\partial v} + 2\rho\frac{\partial}{\partial \rho} \\
X_8 &= p\frac{\partial}{\partial p} + \rho\frac{\partial}{\partial \rho} \\
X_9 &= y\frac{\partial}{\partial x} - x\frac{\partial}{\partial y} + v\frac{\partial}{\partial u} - u\frac{\partial}{\partial v}
\end{aligned}
\tag{6.9}
$$

where X_1, X_2, and X_3 represent invariance under translations in time and space, respectively, X_4 and X_5 represent invariance under Galilean transformation, X_6, X_7, and X_8 represent invariance under scaling transformations, and finally, X_9 represent invariance under rotation. Let us combine the scaling groups, $X_6 - 2X_7 + X_8$, to obtain a general scaling group as given in the following

$$
X_{10} = x\frac{\partial}{\partial x} + y\frac{\partial}{\partial y} - t\frac{\partial}{\partial t} + 2u\frac{\partial}{\partial u} + 2v\frac{\partial}{\partial v} + p\frac{\partial}{\partial p} - 3\rho\frac{\partial}{\partial \rho} \ . \tag{6.10}
$$

$$
\tag{6.11}
$$

Similar to the one-dimensional case, the two-dimensional Euler equations given in Eq. (6.7) admit the following additional symmetry group

$$
X_{11} = tx\frac{\partial}{\partial x} + ty\frac{\partial}{\partial y} + t^2\frac{\partial}{\partial t} + (x - tu)\frac{\partial}{\partial u} + (y - tv)\frac{\partial}{\partial v} - 4tp\frac{\partial}{\partial p} - 2t\rho\frac{\partial}{\partial \rho} \tag{6.12}
$$

for the special case of $\gamma = 2$ which corresponds to isentropic flow of a monatomic gas with two-degrees of freedom where molecules are constrained to move on a plane.

6.4 Invariant schemes

In this section, we show the implementation of the proposed procedure for construction of symmetry preserving numerical schemes for solution of one- and two-dimensional Euler equations. As our non-invariant base numerical schemes, we consider a Lax-Friedrichs scheme and a van Leer flux vector splitting scheme for one-

dimensional Euler equations, and a Lax-Friedrichs scheme for the two-dimensional Euler equations. However, the implementation of the proposed procedure is straightforward and could be applied to other numerical schemes of choice as well.

6.4.1 Invariant Lax-Friedrichs Scheme

As our first non-invariant base scheme, we choose the standard Lax-Friedrichs scheme which is of the form

$$\mathbf{U}^{i,n+1} = \frac{1}{2}\left(\mathbf{U}^{i+1,n} + \mathbf{U}^{i-1,n}\right) - \frac{\tau}{2h}\left(\mathbf{F}^{i+1,n} - \mathbf{F}^{i-1,n}\right) \tag{6.13}$$

for the conservative form of the one-dimensional Euler equations where τ and h are discrete time and space steps. The point transformations associated with the selected symmetry groups of the one-dimensional Euler equations can be obtained through the Lie series expansion given in Eq. (2.23). In this particular case, for simplicity, we ignore the Galilean group X_3 and determine point symmetries based on all the other groups of the one-dimensional Euler equations, given in Eq. (6.3), as follows:

$$\begin{aligned}
\tilde{t} &= \frac{t + s_1}{\lambda}\, e^{-s_7} \\
\tilde{x} &= \frac{x + s_2}{\lambda}\, e^{s_7} \\
\tilde{u} &= [\lambda\, u + s_8(x + s_2)]\, e^{2s_7} \\
\tilde{p} &= \lambda^3\, p\, e^{s_7} \\
\tilde{\rho} &= \lambda\, \rho\, e^{-3s_7}
\end{aligned} \tag{6.14}$$

where $\lambda = 1 - s_8(t + s_1)$. The unknown symmetry parameters s_1, s_2, s_7, and s_8 in the above point transformations could be determined through convenient selections of moving frames. As discussed in the previous section, there are infinitely

many applicable moving frames. However, not all of these moving frames will result in accurate numerical solutions. We suggest the use of moving frames that lead to convenient grids and remove the leading error terms from truncation error of difference equations. For instance, for this particular problem of one-dimensional Euler equations, the normalization conditions $\tilde{t}^{i,n} = 0$ and $\tilde{x}^{i,n} = 0$ lead to a grid that is practical and easy to implement. From these normalization conditions, the symmetry parameters s_1 and s_2 are found as

$$s_1 = -t^{i,n}, \qquad s_2 = -x^{i,n} \ .$$

The symmetry parameter s_7 does not appear in the transformed form of the Lax-Friedrichs scheme. As for the last symmetry parameter s_8, we can choose two different normalization conditions to investigate the effect of these choices on the accuracy of the final invariant scheme. We first choose a normalization condition for which the discrete definition of the spatial derivative of the first element of the flux vector $\mathbf{F}(\mathbf{U})$ goes to zero as shown in the following:

$$\left.\frac{\partial(\tilde{\rho}\tilde{u})}{\partial\tilde{x}}\right|^{i,n} \equiv \frac{(\tilde{\rho}\tilde{u})^{i+1,n} - (\tilde{\rho}\tilde{u})^{i-1,n}}{\tilde{x}^{i+1,n} - \tilde{x}^{i-1,n}} = 0 \quad \Leftrightarrow \quad s_8 = -\frac{(\rho u)^{i+1,n} - (\rho u)^{i-1,n}}{h(\rho^{i+1,n} + \rho^{i+1,n})} \tag{6.15}$$

where $\tilde{x}^{i+1,n} - \tilde{x}^{i-1,n} = x^{i+1,n} - x^{i-1,n} = 2h$. The invariant scheme constructed for the Euler equations based on this particular normalization condition is referred to as SYM-1. Similarly, we select another normalization condition (that leads to the invariant scheme SYM-2) for which only the spatial first derivative of the velocity goes to zero

$$\left.\frac{\partial\tilde{u}}{\partial\tilde{x}}\right|^{i,n} \equiv \frac{\tilde{u}^{i+1,n} - \tilde{u}^{i-1,n}}{\tilde{x}^{i+1,n} - \tilde{x}^{i-1,n}} = 0 \quad \Leftrightarrow \quad s_8 = -\frac{u^{i+1,n} - u^{i-1,n}}{2h} \ . \tag{6.16}$$

As all the unknown symmetry parameters are determined, the fully defined point

transformations given in Eq.(6.14) can be implemented to the standard non-invariant Lax-Friedrichs scheme, Eq (6.13), to obtain its invariant form as follows:

$$\tilde{\mathbf{U}}^{i,n+1} = \frac{1}{2}\left(\tilde{\mathbf{U}}^{i+1,n} + \tilde{\mathbf{U}}^{i-1,n}\right) - \frac{\tilde{\tau}}{2\tilde{h}}\left(\tilde{\mathbf{F}}^{i+1,n} - \tilde{\mathbf{F}}^{i-1,n}\right). \tag{6.17}$$

The above difference equation, Eq. (6.17), is invariant under the selected symmetries of the one-dimensional Euler equations.

Similarly, for the two-dimensional Euler equations, the Lax-Friedrichs scheme is given by

$$\begin{aligned}\mathbf{U}^{i,j,n+1} =& \frac{1}{4}\left(\mathbf{U}^{i+1,j,n} + \mathbf{U}^{i-1,j,n} + \mathbf{U}^{i,j+1,n} + \mathbf{U}^{i,j-1,n}\right) \\ & - \frac{\tau}{2h_x}\left(\mathbf{F}^{i+1,j,n} - \mathbf{F}^{i-1,j,n}\right) - \frac{\tau}{2h_y}\left(\mathbf{G}^{i,j+1,n} - \mathbf{G}^{i,j-1,n}\right) \ , \end{aligned} \tag{6.18}$$

where h_x and h_y are discrete space steps for x- and y-coordinates, respectively. Similar to the one-dimensional case, for simplicity, we ignore the rotation group X_9 and the Galilean groups X_4 and X_5. We then construct point transformations based on the rest of the symmetry groups given in Eq. (6.9) through Lie series expansion as

$$\begin{aligned}\tilde{t} &= \frac{t + s_1}{\lambda}\, e^{-s_{10}} \\ \tilde{x} &= \frac{x + s_2}{\lambda}\, e^{s_{10}} \\ \tilde{y} &= \frac{y + s_3}{\lambda}\, e^{s_{10}} \\ \tilde{u} &= \left[\lambda\, u + s_{11}(x + s_2)\right] e^{2s_{10}} \\ \tilde{v} &= \left[\lambda\, v + s_{11}(y + s_3)\right] e^{2s_{10}} \\ \tilde{p} &= \lambda^4\, p\, e^{s_{10}} \\ \tilde{\rho} &= \lambda^2\, \rho\, e^{-3s_{10}} \ , \end{aligned} \tag{6.19}$$

where $\lambda = 1 - s_{11}(t - s_1)$. Recall that the scaling parameter s_{10} does not appear in the Lax-Friedrichs scheme in the transformed space. Additionally, the translation parameters s_1, s_2, and s_3 can be found by considering the following normalization conditions

$$\tilde{t}^{i,j,n} = 0, \qquad \tilde{x}^{i,j,n} = 0, \qquad \tilde{y}^{i,j,n} = 0 \ .$$

And the projection parameter s_{11} can be found by setting the sum of discrete definition of spatial first derivatives to zero as shown in the following:

$$\begin{aligned} \frac{\partial \tilde{u}}{\partial \tilde{x}} + \frac{\partial \tilde{v}}{\partial \tilde{y}} &\equiv \frac{\tilde{u}^{i+1,j,n} - \tilde{u}^{i-1,j,n}}{\tilde{x}^{i+1,j,n} - \tilde{x}^{i-1,j,n}} + \frac{\tilde{v}^{i,j+1,n} - \tilde{v}^{i,j-1,n}}{\tilde{y}^{i,j+1,n} - \tilde{y}^{i,j-1,n}} = 0 \\ s_{11} &= -\frac{2d_y(u^{i+1,j,n} - u^{i-1,j,n}) + 2d_x(v^{i,j+1,n} - v^{i,j-1,n})}{8h_x h_y} \ . \end{aligned}$$

Finally, the invariant form of the Lax-Friedrichs scheme for the two-dimensional Euler equations can be found as

$$\begin{aligned} \tilde{\mathbf{U}}^{i,j,n+1} =& \frac{1}{4}\left(\tilde{\mathbf{U}}^{i+1,j,n} + \tilde{\mathbf{U}}^{i-1,j,n} + \tilde{\mathbf{U}}^{i,j+1,n} + \tilde{\mathbf{U}}^{i,j-1,n}\right) \\ & - \frac{\tilde{\tau}}{2\tilde{h}_x}\left(\tilde{\mathbf{F}}^{i+1,j,n} - \tilde{\mathbf{F}}^{i-1,j,n}\right) - \frac{\tilde{\tau}}{2\tilde{h}_y}\left(\tilde{\mathbf{G}}^{i,j+1,n} - \tilde{\mathbf{G}}^{i,j-1,n}\right) \ . \end{aligned} \tag{6.20}$$

6.4.2 Invariant van Leer Flux Splitting scheme

In order to show the applicability of the proposed method to an arbitrary base numerical scheme, we constructed an invariant form of the van Leer flux splitting scheme for the one-dimensional Euler equations as well. The non-invariant form of the van Leer scheme for this particular problem is as follows:

$$\frac{\partial \mathbf{U}}{\partial t} + \frac{\partial \mathbf{F}^+}{\partial x} + \frac{\partial \mathbf{F}^-}{\partial x} \tag{6.21}$$

where the fluxes are defined as

$$\mathbf{F}^{+} = \frac{\rho c}{4}(M+1)^2 \begin{bmatrix} 1 \\ \frac{2c}{\gamma}\left(1+\frac{\gamma-1}{2}M\right) \\ \frac{2c^2}{\gamma^2-1}\left(1+\frac{\gamma-1}{2}M\right)^2 \end{bmatrix}$$

$$\mathbf{F}^{-} = -\frac{\rho c}{4}(M-1)^2 \begin{bmatrix} 1 \\ \frac{2c}{\gamma}\left(-1+\frac{\gamma-1}{2}M\right) \\ \frac{2c^2}{\gamma^2-1}\left(1-\frac{\gamma-1}{2}M\right)^2 \end{bmatrix},$$

where $c = \sqrt{\gamma p/\rho}$ is the speed of sound and $M = u/c$ is the Mach number. Hence the final form of the van Leer upwind scheme can be found as

$$\mathbf{U}_i^{n+1} = \mathbf{U}_i^n - \frac{\tau}{h}\left[(\mathbf{F}^{+})_i^n - (\mathbf{F}^{+})_{i-1}^n + (\mathbf{F}^{-})_{i+1}^n - (\mathbf{F}^{-})_i^n\right] . \tag{6.22}$$

The point transformations obtained for the one-dimensional Euler equations in the previous subsection, Eq. (6.14), can be directly implemented to the above van Leer scheme as well. Hence the final invariant form of the van Leer flux splitting scheme can be found as

$$\tilde{\mathbf{U}}_i^{n+1} = \tilde{\mathbf{U}}_i^n - \frac{\tilde{\tau}}{\tilde{h}}\left[(\tilde{\mathbf{F}}^{+})_i^n - (\tilde{\mathbf{F}}^{+})_{i-1}^n + (\tilde{\mathbf{F}}^{-})_{i+1}^n - (\tilde{\mathbf{F}}^{-})_i^n\right] . \tag{6.23}$$

6.5 Results and Discussion

In this section, performance of the invariant numerical schemes developed for the one- and two-dimensional Euler equations are evaluated. In the case of one-dimensional Euler equations, three different Riemann problems are considered, and results obtained from standard Lax-Friedrichs scheme, van Leer flux vector splitting scheme, and proposed invariant schemes (SYM-1 and SYM-2) are compared with available exact solutions for accuracy. As expected, the invariant schemes that preserve se-

Table 6.1
Initial configurations for one-dimensional Euler equations.

	ρ_L	ρ_R	u_L	u_R	p_L	p_R
case 1 :	1.0	0.125	0.0	0.0	1.0	0.1
case 2 :	1.0	1.0	0.0	0.0	7.0	10.0
case 3 :	1.0	2.5	−2.0	−2.0	40.0	40.0

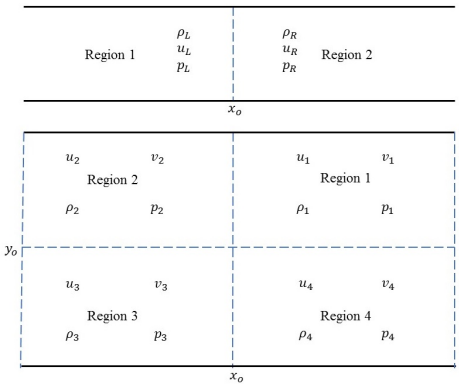

Fig. 6.1. Representation of a shock-tube in 1D (top) and 2D (bottom) at $t = 0$.

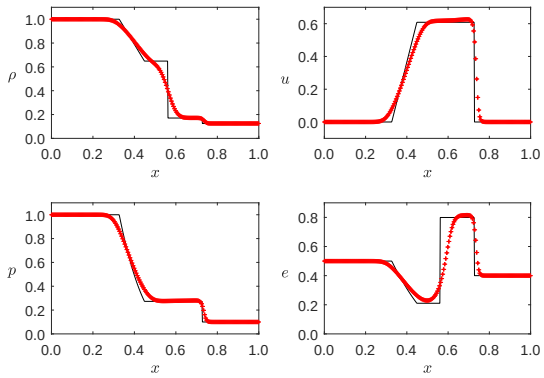

Fig. 6.2. Euler equations in 1D (*case* 1). Snapshots of exact solution (solid line) and numerical solution based on Lax-Friedrichs scheme (+) at $t = 0.1$. Parameter settings: $h = 0.0025$, $CFL = 0.4$.

lected Lie symmetry groups of the one-dimensional Euler equations lead to accurate approximate solutions for the considered shock-tube configurations given in table 6.1. Similarly, for two-dimensional Euler equations, an invariant form if the Lax-Friedrichs scheme is constructed and implemented to four different Riemann problems. Similar to the one-dimensional case, the proposed invariant scheme constructed for this case also leads to accurate approximate solutions for each Riemann problem (considered in this work) as well.

As our first test problem in the one-dimensional case, we consider the well-known Shock-Tube problem of Sod [111] that is demonstrated in figure 6.1 (top plot). Initial values for this case are noted in *case* 1 of table 6.1. Additionally, for this particular problem configuration, numerical tests are performed on a mesh with 400 grid points and the CFL number is set to be 0.4. Snapshots of the density ρ, velocity

Table 6.2
L_∞ and RMSE errors (based on velocity u) for Euler equations in 1D.

	case 1		*case* 2		*case* 3	
	L_∞	RMSE	L_∞	RMSE	L_∞	RMSE
Lax-Friedrichs :	0.4884	0.0536	0.2001	0.0437	0.8512	0.2298
Lax-Friedrichs (SYM-1) :	0.2882	0.0459	0.1964	0.0433	0.7848	0.2380
Lax-Friedrichs (SYM-2) :	0.3959	0.0416	0.1966	0.0433	0.7736	0.2345
van Leer :	0.4726	0.0380	0.2514	0.0376	0.8431	0.1546
van Leer (SYM-2) :	0.2582	0.0177	0.2465	0.0367	0.7783	0.1514

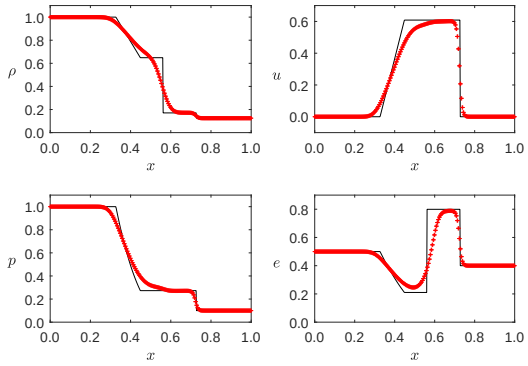

Fig. 6.3. Euler equations in 1D (*case* 1). Snapshots of exact solution (solid line) and numerical solution based on invariant Lax-Friedrichs scheme (+), SYM-1, at $t = 0.1$. Parameter settings: $h = 0.0025$, $CFL = 0.4$.

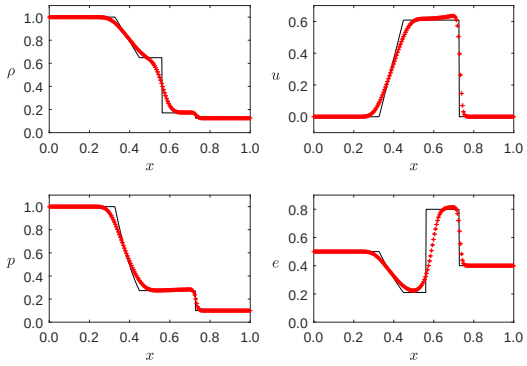

Fig. 6.4. Euler equations in 1D (*case* 1). Snapshots of exact solution (solid line) and numerical solution based on invariant Lax-Friedrichs scheme (+), SYM-2, at $t = 0.1$. Parameter settings: $h = 0.0025$, $CFL = 0.4$.

u, pressure p, and energy e (at $t = 0.1$) obtained from the exact solution (solid line) and the standard non-invariant Lax-Friedrichs scheme (+), Eq. (6.13), is shown in figure 6.2. Similarly, the results obtained from the proposed invariant Lax-Friedrichs schemes, Eq. (6.17), that are constructed using the normalization conditions given in Eq. (6.15) (SYM-1), and Eq. (6.16) (SYM-2), are demonstrated in figures 6.3 and 6.4, respectively. Further, figures 6.5 and 6.6 depict numerical solutions obtained from the standard non-invariant van Leer scheme, Eq. (6.21), and the proposed invariant scheme, Eq. (6.23), that is constructed based on the standard van Leer scheme through the use of normalization condition given in Eq. (6.16). Furthermore, root mean square error (RMSE), estimated as $\sqrt{\frac{1}{N}\sum(u_{exact} - u_{numeric})^2}$, and

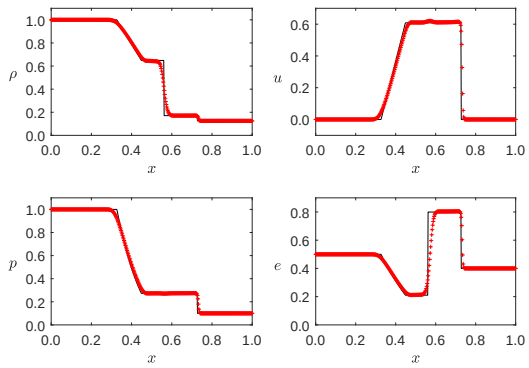

Fig. 6.5. Euler equations in 1D (*case* 1). Snapshots of exact solution (solid line) and numerical solution based on van Leer flux vector splitting scheme (+), at $t = 0.1$. Parameter settings: $h = 0.0025$, $CFL = 0.4$.

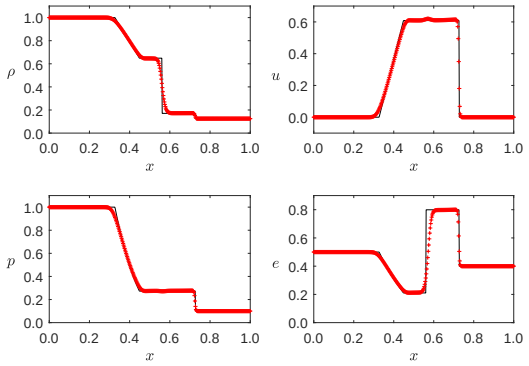

Fig. 6.6. Euler equations in 1D (*case* 1). Snapshots of exact solution (solid line) and numerical solution based on invariant van Leer flux vector splitting scheme (+), SYM-2, at $t = 0.1$. Parameter settings: $h = 0.0025$, $CFL = 0.4$.

L_∞ error, estimated as $max(|u_{exact} - u_{numeric}|)$, measurements obtained from these numerical schemes are presented in table 6.2. Based on these results, it appears that the proposed invariant schemes accurately capture shock propagations evolving from considered initial conditions. In particular, the L_∞ and root mean square error measurements given in table 6.2 indicate that both invariant Lax-Friedrichs scheme and invariant van Leer scheme perform notably better than their non-invariant counterparts. This improvement in numerical accuracy is particularly significant in the case of van Leer scheme. As our second test problem for the one-dimensional Euler equations, we again consider a shock-tube problem for which initial conditions are noted in *case* 2 of table 6.1. Similar to the previous case, a grid with 400 points is considered for this case as well and simulations are run until $t = 0.05$. Profiles of density (ρ), velocity (u), pressure (p), and internal energy (e) are shown in figure 6.7 through figure 6.10. In particular, numerical solution obtained from the Lax-Friedrichs scheme and invariant scheme based on the moving frames given in Eq. (6.16) (SYM-2) and their comparisons with the exact solution are shown in figure 6.7 and figure 6.8, respectively. Similarly, numerical solutions obtained from

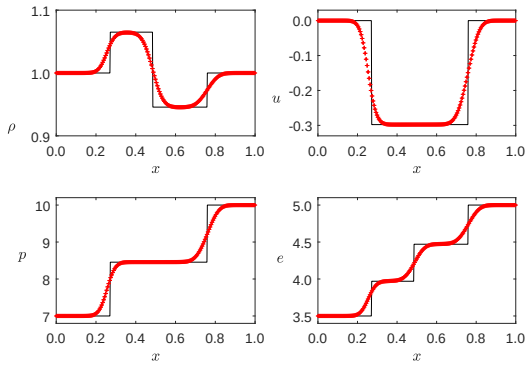

Fig. 6.7. Euler equations in 1D (*case* 2). Snapshots of exact solution (solid line) and numerical solution based on Lax-Friedrichs scheme (+), at $t = 0.05$. Parameter settings: $h = 0.0025$, $CFL = 0.4$.

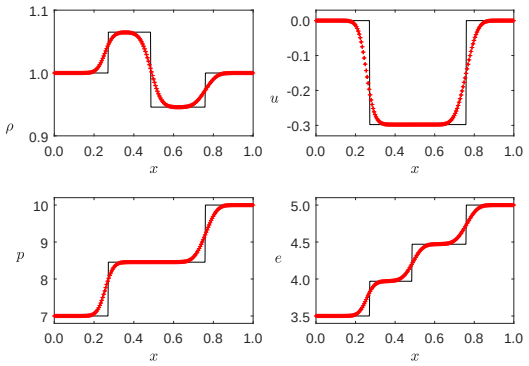

Fig. 6.8. Euler equations in 1D (*case* 2). Snapshots of exact solution (solid line) and numerical solution based on invariant Lax-Friedrichs scheme (+), SYM-2, at $t = 0.05$. Parameter settings: $h = 0.0025$, $CFL = 0.4$.

the standard van Leer scheme and its proposed invariant form are demonstrated in figure 6.9 and figure 6.10, respectively. Root mean square error and L_∞ error measurements obtained from these numerical solutions (which are computed based on velocity u) are presented in *case* 2 of table 6.2. From these results, it appears that the proposed invariant Lax-Friedrichs scheme and invariant van Leer schemes perform better than standard non-invariant lax-Friedrichs and van Leer schemes in terms of numerical accuracy.

As our last test problem for one-dimensional Euler equations, we consider the shock-tube problem, figure 6.1 (top plot), with initial configuration given in *case* 3 of table 6.1. Similar to previous cases, a mesh with 400 grid points is used for this case as well. Numerical solutions obtained from the standard Lax-Friedrichs and invariant Lax-Friedrichs schemes are demonstrated in figure 6.11 and figure 6.12, respectively. Similarly, figure 6.13 and figure 6.14 show the numerical solutions obtained from the standard van Leer scheme and the proposed invariant van Leer scheme. Additionally, RMSE and L_∞ error measurements for this case are also provided in the table 6.2 under *case* 3. As expected, both the invariant Lax-Friedrichs scheme and invariant van Leer scheme accurately capture the propagation of density,

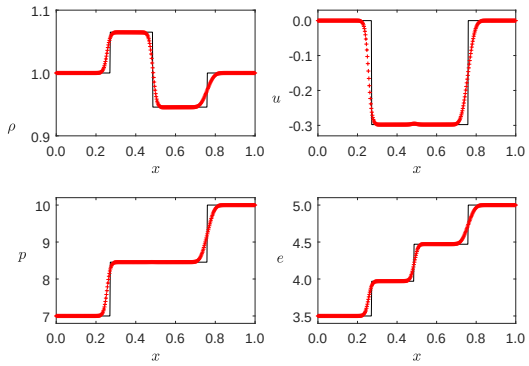

Fig. 6.9. Euler equations in 1D (*case* 2). Snapshots of exact solution (solid line) and numerical solution based on van Leer flux vector splitting scheme (+), at $t = 0.05$. Parameter settings: $h = 0.0025$, $CFL = 0.4$.

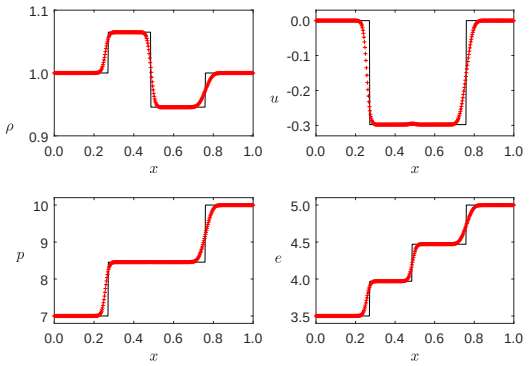

Fig. 6.10. Euler equations in 1D (*case* 2). Snapshots of exact solution (solid line) and numerical solution based on invariant van Leer flux vector splitting scheme (+), at $t = 0.05$. Parameter settings: $h = 0.0025$, $CFL = 0.4$.

velocity, pressure, and internal energy in this case as well. Similar to the previous cases, these invariant schemes also appear to be slightly more accurate than standard non-invariant schemes considered in this work.

In this study, we also demonstrated the procedure for construction of an invariant MUSCL scheme with minmod limiter for the solution of one-dimensional Euler equations. The details of this procedure and the results obtained from the constructed invariant MUSCL scheme can be found in Appendix A.

Next, we evaluate the performance of the proposed invariant Lax-Friedrichs scheme, Eq. (6.20), developed for the two-dimensional Euler equations. In this case, four different Riemann problems are considered, and results obtained from the standard and invariant Lax-Friedrichs schemes are compared with high-resolution numerical solutions for accuracy (as no analytical solution exists for these cases). Here we note that, the Riemann problems are defined on a square domain that is divided into four regions as shown in figure 6.1 (bottom plot).

As our first test problem (*case* 1) for numerical solution of the two-dimensional Euler equations, we consider the Riemann problem with initial data given in table 6.3. For further discussion on this particular Riemann problem, the reader is re-

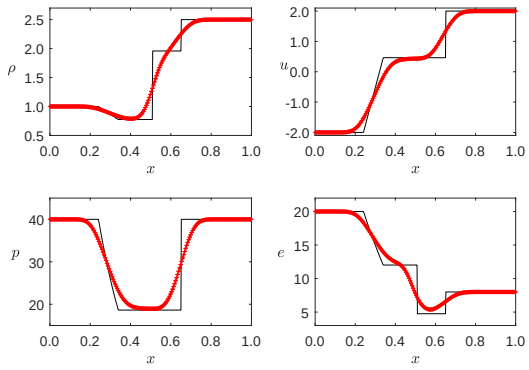

Fig. 6.11. Euler equations in 1D (*case* 3). Snapshots of exact solution (solid line) and numerical solution based on Lax-Friedrichs scheme (+), at $t = 0.02$. Parameter settings: $h = 0.0025$, $CFL = 0.4$.

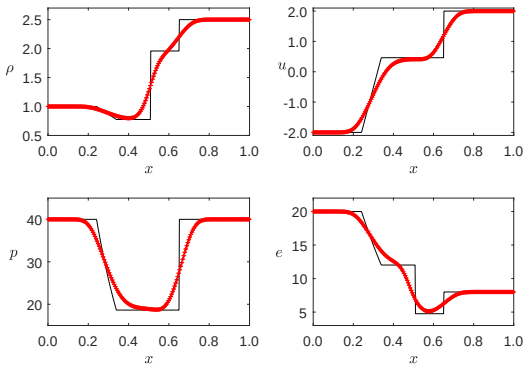

Fig. 6.12. Euler equations in 1D (*case* 3). Snapshots of exact solution (solid line) and numerical solution based on invariant Lax-Friedrichs scheme (+), SYM-2, at $t = 0.02$. Parameter settings: $h = 0.0025$, $CFL = 0.4$.

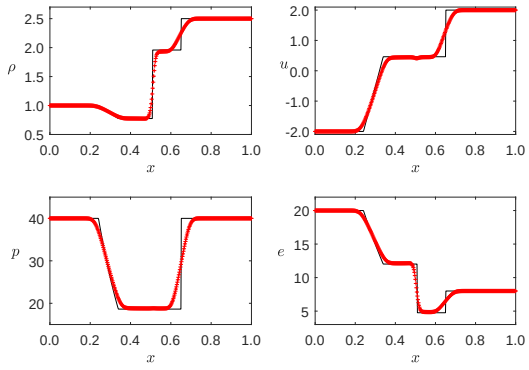

Fig. 6.13. Euler equations in 1D (*case* 3). Snapshots of exact solution (solid line) and numerical solution based on van Leer flux vector splitting scheme (+), at $t = 0.02$. Parameter settings: $h = 0.0025$, $CFL = 0.4$.

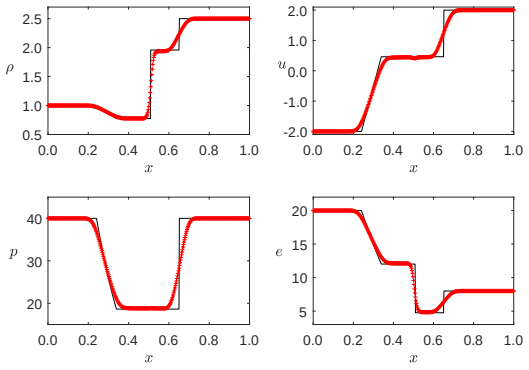

Fig. 6.14. Euler equations in 1D (*case* 3). Snapshots of exact solution (solid line) and numerical solution based on invariant van Leer flux vector splitting scheme (+), at $t = 0.02$. Parameter settings: $h = 0.0025$, $CFL = 0.4$.

ferred to the reference [153]. For this simulation, a constant $CFL = 0.475$ number is considered and a stencil with 800×800 grid points is utilized. The snapshots (for density) of the numerical solutions (at $t = 0.2$) obtained from the standard non-invariant Lax-Friedrichs scheme given in Eq. (6.18) and the proposed invariant Lax-Friedrichs scheme given in Eq. (6.20) developed for the two-dimensional Euler equations are shown in figure 6.15. We also included a relatively high-resolution (with 1500×1500 grid points) solution as a reference solution in this figure as well.

Table 6.3
Two-dimensional Euler equations. Initial data for *case* 1.

	ρ	p	u	v
Region 1 :	1.1	1.1	0.0	0.0
Region 2 :	0.5065	0.35	0.8939	0.0
Region 3 :	1.1	1.1	0.8939	0.8939
Region 4 :	0.5065	0.35	0.0	0.8939

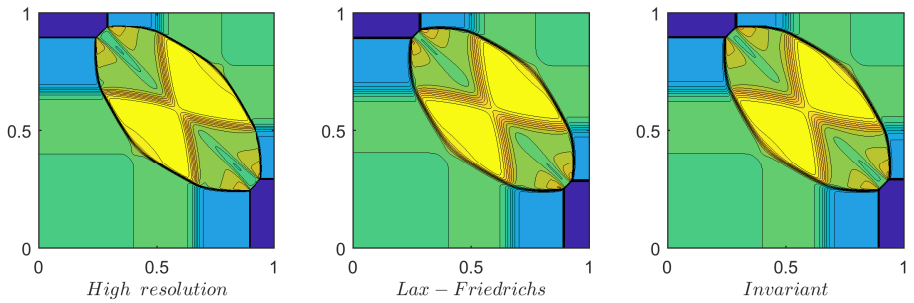

Fig. 6.15. Euler equations in 2D (*case* 1). Snapshots of numerical solutions, at $t = 0.2$, obtained from a high resolution reference scheme (left), standard Lax-Friedrichs scheme (middle), and invariant Lax-Friedrichs scheme (right). Parameter settings: $h = 0.00125$, $CFL = 0.475$.

Based on these results, it appears that the proposed invariant schemes are successfully capturing an approximate solution for the two-dimensional Euler equations as well. Further, the L_∞ error measurements that are obtained through comparisons with the high-resolution solution are determined to be 6.22×10^{-1} and 3.815×10^{-1} for the standard and invariant Lax-Friedrichs schemes, respectively. Similarly, the root mean square error measurements obtained from these schemes, in the same order, are noted as 2.77×10^{-2} and 1.28×10^{-2}. Although, for this particular test problem, the improvement in numerical accuracy with respect to the standard non-invariant Lax-Friedrichs scheme appears to be minor, we believe that the potential advantages owing to symmetry preserving nature of the proposed invariant Lax-Friedrichs scheme are quite valuable.

As our second test problem (*case* 2) for the numerical solution of the two-dimensional Euler equations, we again consider the two-dimensional shock-tube

Table 6.4
Two-dimensional Euler equations. Initial data for *case* 2.

	ρ	p	u	v
Region 1 :	1.5	1.5	0.0	0.0
Region 2 :	0.5323	0.3	1.206	0.0
Region 3 :	0.138	0.029	1.206	1.206
Region 4 :	0.5323	0.3	0.0	1.206

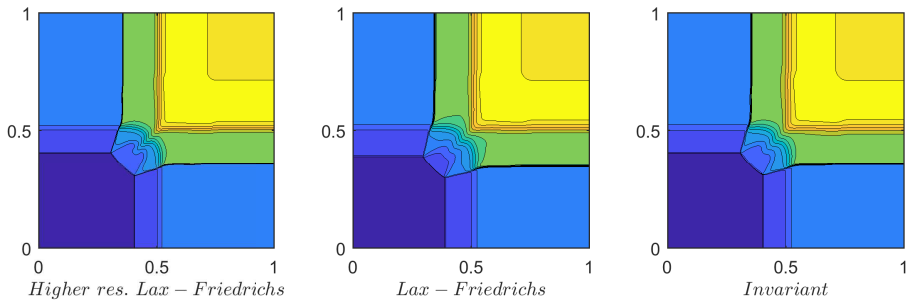

Fig. 6.16. Euler equations in 2D (*case* 2). Snapshots of numerical solutions, at $t = 0.2$, obtained from a high resolution reference scheme (left), standard Lax-Friedrichs scheme (middle), and invariant Lax-Friedrichs scheme (right). Parameter settings: $h = 0.00125$, $CFL = 0.475$.

problem demonstrated in figure 6.1 (bottom plot) with initial data given in table 6.4. For this simulation, the parameter settings are identical to the previous case. Snapshots of the propagating shocks (based on density computation) obtained from the standard and invariant Lax-Friedrichs schemes and a reference high resolution solution are depicted in figure 6.16. Moreover, L_∞ error measurements computed for the standard and invariant Lax-Friedrichs schemes (based on this reference solution) are determined to be 5.60×10^{-1} and 2.18×10^{-1}, respectively. And similarly, the root mean square error measurements for these numerical schemes are noted as 5.56×10^{-2} (standard) and 1.21×10^{-2} (invariant). Similar to the previous case, the invariant scheme performs slightly better than the standard scheme for this case as well. Further discussions on the numerical solution of this Riemann problem can also be found in reference [153].

As our next test problem (*case* 3), we consider the shock-tube problem with ini-

Table 6.5
Two-dimensional Euler equations. Initial data for *case* 3.

	ρ	p	u	v
Region 1 :	0.5313	0.4	0.0	0.0
Region 2 :	1.0	1.0	0.7276	0.0
Region 3 :	0.8	1.0	0.0	0.0
Region 4 :	1.0	1.0	0.0	0.7276

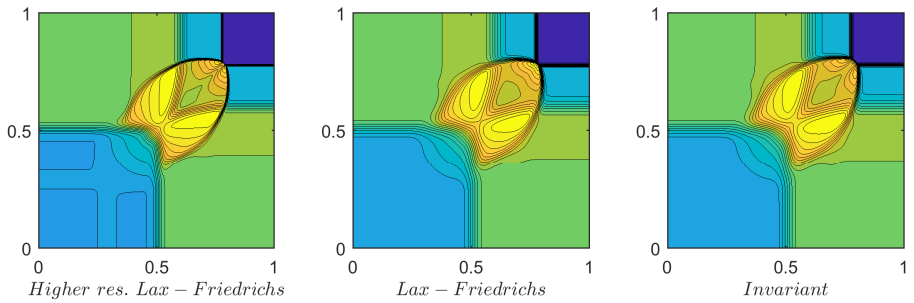

Fig. 6.17. Euler equations in 2D (*case* 3). Snapshots of numerical solutions, at $t = 0.15$, obtained from a high resolution reference scheme (left), standard Lax-Friedrichs scheme (middle), and invariant Lax-Friedrichs scheme (right). Parameter settings: $h = 0.0025$, $CFL = 0.475$.

tial data given in table 6.5. For this case, a grid with 400×400 points is considered and the CFL number is kept at 0.475. The snapshots of the numerical approximations for the density (ρ) at $t = 0.15$ are presented in figure 6.17. Further, L_∞ errors for these schemes are noted as 3.92×10^{-1} (standard) and 5.46×10^{-1} (invariant). And similarly, the root mean square errors are found as 1.15×10^{-2} (standard) and 1.83×10^{-2} (invariant). The invariant scheme still appears to accurately capture the density profile for this problem as well.

And as our last test problem (*case* 4), we again consider the shock-tube problem with initial data given in table 6.6. For this simulation, the parameter settings are identical to the first two Riemann problems (*case* 1 and *case* 2). The numerical solutions for density obtained from the standard and invariant schemes are given in figure 6.18. Similar to the previous cases, a high-resolution solution is again included in this figure as reference solution. For this case, the L_∞ error measure-

Table 6.6
Two-dimensional Euler equations. Initial data for *case* 4.

	ρ	p	u	v
Region 1 :	0.5197	0.4	0.1	0.1
Region 2 :	1.0	1.0	-0.6259	0.1
Region 3 :	0.8	1.0	0.1	0.1
Region 4 :	1.0	1.0	0.1	-0.6259

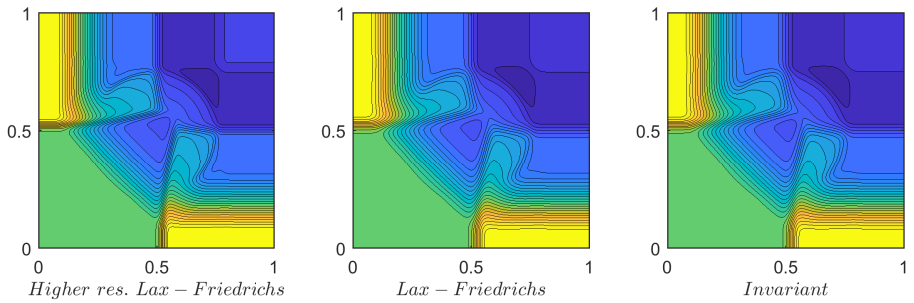

Fig. 6.18. Euler equations in 2D (*case* 4). Snapshots of numerical solutions, at $t = 0.2$, obtained from a high resolution reference scheme (left), standard Lax-Friedrichs scheme (middle), and invariant Lax-Friedrichs scheme (right). Parameter settings: $h = 0.00125$, $CFL = 0.475$.

ments obtained from the standard and invariant Lax-Friedrichs schemes are found as 2.29×10^{-2} and 2.27×10^{-2}, respectively. And similarly, the root mean square errors are found as 4.4×10^{-3} (standard) and 4.28×10^{-3} (invariant). Based on these results, it appears that the invariant scheme is still performing slightly better that the standard non-invariant base scheme in terms of numerical accuracy.

The numerical solutions of the one- and two-dimensional Euler equations through invariant schemes further verified that the proposed method for symmetry preservation in numerical schemes could be effectively used to improve numerical accuracy of some arbitrary base schemes besides retaining important geometric properties of the underlying differential equations in associated schemes. Although we only considered standard Lax-Friedrichs and van Leer schemes as base schemes in this work, it is important to note that the proposed method is not limited to these base schemes.

6.6 Chapter Summary

In this chapter, we presented a method for construction of invariant numerical schemes (for the solution of one- and two-dimensional Euler equations) that inherit Lie symmetry properties of the underlying equations. The proposed method is based on the method of equivariant moving frames and involves implementation of point transformations (that are derived through Lie symmetry groups of Euler equations) to arbitrarily selected non-invariant base numerical schemes such as Lax-Friedrichs and van Leer schemes. Although in this work we selected Lax-Friedrichs and van Leer schemes as our non-invariant base numerical schemes, these selections are arbitrary, and one can always choose other (more convenient) base schemes.

For the one-dimensional Euler equations, we evaluated the performance of the proposed invariant schemes via implementation to three different shock-tube problems. For each of these test problems, the proposed invariant schemes successfully captured solutions that were more accurate than considered non-invariant base numerical schemes. Here we also note that, for the one-dimensional Euler equations, we constructed two different forms of invariant schemes that are based on different moving frames to investigate the effects of these selections on the accuracy of the resulting invariant schemes. Similarly, we tested the performance of the invariant scheme constructed for the two-dimensional Euler equations via implementation to four different shock-tube problems. As expected, the proposed invariant scheme performed better than the standard non-invariant base scheme in this case as well. Based on these results, it appears that symmetry preservation in numerical schemes might lead to significant improvements in quality of results obtained from these schemes not only in terms of numerical accuracy but also in terms of error measures that might be related to geometric properties (such as symmetries) of the underlying differential equations.

CHAPTER 7

Summary and Future Work

7.1 Scope of the Chapter

In this chapter, we will attempt to summarize the main highlights of this dissertation and relate them to the primary objectives of the research. To this end, in the following section, the main results of the dissertation will be briefly discussed. This will be followed (in Section 7.3) with recommendations for future work where possible shortcomings of the proposed methodologies are discussed and ideas for future research are briefly explored.

7.2 Research Highlights

In this dissertation, we investigated Lie symmetry groups in the context of their applications in computational fluid dynamics. Recall that most numerical schemes do not consider Lie symmetry properties of associated differential equations as order of accuracy is usually the primary concern in the development of these schemes. In this dissertation, we addressed this limitation, and proposed novel methodologies for construction of invariant finite difference schemes with a desired order of accuracy, including compact schemes, that inherit Lie symmetry properties of underlying differential equations. We demonstrated the implementation of the proposed methodologies through linear and nonlinear canonical problems, including implementations for Euler equations (in 1D and 2D), that are commonly used in fluid mechanics. For the selected test problems, invariant (or symmetry preserving) numerical schemes

with a desired order of accuracy were constructed. In all the test cases considered in this work, the proposed invariant schemes were found to be more accurate than the standard non-invariant numerical schemes. In some cases, this improvement in the accuracy/performance was found to be quite significant. Based on our observations, we concluded that the proposed procedures for Lie symmetry preservation in finite difference schemes can be used not only for retaining geometric properties of differential equations in relevant numerical approximations but also for achievement of significant improvements in numerical accuracy of these approximations.

7.2.1 Chapter Summaries

We provided a detailed discussion on Lie symmetry analysis in Chapter 2, where a step by step guide for determination of symmetry groups of differential equations was presented. Use of Lie groups for obtaining group invariant solutions through similarity variables based on these groups was also discussed in this chapter. To demonstrate the implementation of Lie symmetry analysis for identification of group invariant solutions, we considered three different flow problems such as a) a boundary layer flow over an exponentially stretching porous flat surface, b) a boundary layer flow over a wedge with slip boundaries, and c) analysis of stagnation point state of an inviscid blunt-body flow. For all these test problems, similarity variables that lead to self-similar solutions were identified from relevant Lie symmetry groups. These similarity variables were implemented in the associated governing equations to obtain reduced form solutions for all these cases. Results obtained based on Lie symmetry analysis were found to be in good agreement with those available in the literature. Further, as Lie symmetry analysis allows for a systematic approach of determining similarity variables for underlying differential equations, identification of other reduced forms (for these equations) with this method is notably more convenient.

In the following chapter (Chapter 3), an effective method for construction of finite difference schemes that retain certain Lie symmetry groups of underlying differential equations is presented in detail. Our method for such constructions is based on the method of equivariant moving frames and modified equations. In order to contribute to the current state of knowledge regarding symmetry preservation through moving frames, several questions related to the use of moving frames for this purpose are addressed thoroughly. The implementation of the proposed method is demonstrated via application to some linear and nonlinear canonical problems (i.e, linear advection equation in 1D/2D and inviscid Burgers' equation). Numerical tests were also conducted in this chapter where results were compared with available analytical solutions (to verify the benefits of symmetry preservation in numerical schemes) and found to be promising. More details on this topic can also be found in reference [90].

In Chapter 4, a novel method for construction of high order accurate invariant finite difference schemes (those that inherit symmetry properties of associated differential equations) is proposed. The novelty of this method relies on the notion that it enables construction of high order accurate invariant numerical schemes with a desired order of accuracy. To achieve this goal, the advantages of the method of modified equations and equivariant moving frames are conveniently utilized. The high order accurate invariant schemes that were constructed (via the proposed method) on base schemes with cumbersome numerical representations were often found to have comparably simpler numerical representations. The application of this method to some commonly used linear and nonlinear PDEs (such as linear advection diffusion equation in 1D/2D and inviscid/viscous Burgers' equations) is also presented in this chapter. Results obtained from these high order invariant schemes indicate that symmetry preservation could lead to significant improvements in accuracy besides improvements in the overall quality of results. Further details on this work can also be found in reference [91].

Another approach (besides the method of modified equations) for construction of high order schemes is the use of compact finite difference schemes where high order accuracy is usually achieved with smaller stencils. In Chapter 5, a novel methodology for construction of high order accurate invariant compact finite difference schemes that preserve Lie symmetry groups of underlying equations up to a desired order of accuracy is proposed. The construction of such invariant compact schemes involves the use of extended symmetry groups of differential equations to determine point transformations not only for independent and dependent variables of relevant compact schemes but also for their spatial derivatives. The latter is a novel aspect of the proposed method that was not considered in earlier works. Numerical tests were conducted to evaluate the performance of the constructed invariant compact numerical schemes, using one- and two-dimensional linear advection diffusion equations and inviscid/viscous Burgers' equation. As expected, the proposed invariant compact schemes were found to be significantly more accurate than their standard non-invariant counterparts.

In Chapter 6, we considered one- and two-dimensional Euler equations and proposed a procedure to construct numerical schemes that preserve selected Lie symmetry groups of the Euler equations. We considered two non-invariant numerical schemes (i.e, Lax-Friedrichs and Van Leer schemes) as our base schemes and converted them into their symmetry preserving forms through point transformations obtained from the underlying symmetries. To evaluate the performance of the constructed invariant schemes, we conducted numerical experiments where well-known problems (i.e., Sod's shock-tube problem) were successfully simulated through these invariant schemes.

7.3 Future Research

In this section, we briefly summarize the recommendations for addressing limitations of the available methods (for symmetry preservation in numerical schemes) along with a discussion on extensions to more general problems. In the latter, we discuss possible implementation of the proposed methods in the three-dimensional Euler equations, ENO/WENO schemes, and compressible/incompressible Navier-Stokes equations. We also briefly discuss possible implementations of Lie symmetry analysis in turbulence, where symmetry preserving subgrid-scale turbulence models and symmetry-based identification of exact coherent structures in turbulent flows are mentioned.

7.3.1 Extensions of Scope to Address Limitations

While the proposed methods appear to be very effective for construction of invariant (or symmetry preserving) numerical schemes with a desired (or fixed) order of accuracy, there are several issues that need to be investigated in more detail. Further research is needed to understand how accuracy of these invariant numerical schemes for PDEs is affected by the following considerations:

i. choice of subgroups (or subalgebras),

ii. choice of moving frames (for any selected subgroup),

iii. choice of base numerical discretization schemes,

iv. and nature of initial/boundary conditions (and associated exact solutions) of PDEs, in context of their compatibility with the selected subgroups and chosen base numerical discretization schemes.

Based on our simulations presented in Chapter 4 and Chapter 5, we observed that although it is possible to consider the whole symmetry group of a PDE for preser-

vation in difference equations, this often leads to cumbersome numerical representations without notably enhancing numerical accuracy. For instance, in the case of the viscous Burgers' equation in Chapter 5, the whole symmetry group of the PDE is preserved in the related difference equation. However, the advantages owing to the inclusion of the Galilean subgroup only become significant when the invariant scheme is actually transformed under a Galilean transformation (as demonstrated in figure 5.7). Further, the choice of moving frames which are used to determine the unknown group parameters could affect the accuracy of resulting invariant schemes. To our knowledge, there is no systematic approach to select the best moving frame and one must consider all the pros and cons of a particular moving frame before making a selection. Based on our observations, we found that a moving frame that removes the leading order terms from truncation error of a difference equation is usually a good choice, as such a moving frame also simplifies the base scheme (in the transformed space). Moreover, the performance of the constructed invariant schemes might be affected by the chosen initial/boundary conditions, especially if these conditions are not compatible with the chosen subgroups. This might be due to the fact that some of the limitations of base difference equations carry over to the constructed invariant schemes. For instance, for cases where discontinuities develop in solutions, the performance of the constructed invariant schemes will undoubtedly depend on the chosen base numerical schemes. This obstacle could be avoided by selecting base schemes that are better suited to handle such discontinuities. In this context, conservative numerical schemes could be chosen as base schemes for construction of invariant schemes.

7.3.2 Extensions to More General Problems

In Chapter 6, we demonstrated the implementation of the proposed methods to selected problems. In particular, we developed invariant numerical schemes for

the one- and two-dimensional Euler equations (in Chapter 6) with consideration of different shock-tube configurations as initial conditions. However, the proposed methods could also be implemented in more general problems such as the three-dimensional Euler equations. Future work, in this regard, involves construction of Lie symmetry preserving (invariant) numerical schemes (including compact schemes) for this problem. We expect that these invariant schemes would perform better than standard schemes in this case as well, especially when error measures based on symmetries underlying the three-dimensional Euler equations are considered. Some preliminary results in this regard are presented in the Appendix B, where we note the Lie symmetry groups and relevant point transformations for these equations.

Additionally, the methods proposed in this dissertation could also be implemented to numerical schemes that are proven to be ideal for simulations of problems that include discontinuities (i.e., shocks) in solutions. For instance, Essentially Non-Oscillatory (ENO) schemes and Weighted Essentially Non-Oscillatory (WENO) schemes are among the first examples that are showed to be well suited for capturing discontinuities [108, 121, 145, 154]. In ENO schemes, approximate solutions are obtained from essentially non-oscillatory piecewise polynomial reconstructions where a highly nonlinear adaptive procedure is used to automatically choose the locally smoothest stencil among several candidates. Such a reconstruction procedure naturally results in a high order accurate solution in smooth regions and leads to a stable solution at discontinuities by avoiding oscillations (i.e., Gibbs phenomena). Similarly, WENO schemes are also developed via piecewise polynomial reconstruction procedures. Although WENO schemes are fundamentally based on ENO schemes, the main difference is attributed to the use of a weighted combination of multiple number of stencils in the reconstruction process of schemes. Smoothness indicators and weighted coefficients are used to increase the order of accuracy in smooth regions of solutions. Construction of high order ENO or WENO schemes that also account

for the Lie symmetry properties of underlying differential equations could be of significant interest to the fluid dynamics community. In addition, through selection of convenient moving frames, invariant ENO/WENO schemes could be constructed such that these schemes are not only arbitrarily high order accurate but also have notably simpler numerical representations (as observed for the invariant schemes developed in Chapter 4). Such schemes would also be expected to perform notably better than their non-invariant forms when an error measure based on symmetries of underlying equations are considered.

Implementation of the proposed methods to compressible/incompressible Navier-Stokes equations could also be of great interest. Navier-Stokes equations are particularly important as these equations describe the physics of many important phenomena in science and engineering related fields. Considering the Lie symmetry groups associated with the Navier-Stokes equations, numerical schemes could be developed for these equations that are more compatible with the underlying physics. The advantages that become available with such invariantization operations could be quite significant. For instance, in the case of turbulent flows, direct numerical simulations (DNS), that are usually based on Navier-Stokes equations, are often used to simulate such flows. It is widely accepted that the computational cost of such simulations can be quite expensive. To avoid such computational loads, various approaches based on large-eddy simulation (LES) or reduced-order models (ROM) have been proposed and successfully tested in the literature. Simulation of such turbulent flows on symmetry preserving stencils could be significantly more accurate and efficient as such behaviors were observed in simulations of simpler cases (as presented in Chapter 4 and 5). Further research is needed to investigate possible advantages in the numerical solution of the Navier-Stokes equations through symmetry preserving high order accurate (invariant) schemes. To this end, some preliminary results on Lie groups and point transformations associated with the multidimensional, incom-

pressible Navier-Stokes equations are presented in Appendix C.

Further, in the context of turbulence modeling, attempts have been made to develop subgrid-scale models that are compatible with the symmetries of the Navier-Stokes equations [155–158]. The primary motivation behind these approaches is that such models would preserve fundamental properties of the Navier-Stokes equations and hence be more accurate than those that ignore such properties. In this context, Lie symmetry analysis could be systematically used to develop subgrid-scale models that inherit symmetry properties of the underlying equations. In the sparse literature on symmetry preserving models, the symmetry groups associated with the Navier-Stokes equations are considered instead of the symmetries of the relevant filtered equations. More accurate models could be developed based on symmetries of the filtered equations that are essentially derived from the Navier-Stokes equations. In this regard, symmetry methods could be connected to modern tools such as artificial neural networks (ANN) and data-driven machine learning frameworks. These methods that are shown to be quite useful for turbulence modeling [159–163] could be used to developed symmetry preserving subgrid-scale models where machine learning strategies are used to determine relevant model parameters.

Furthermore, a great deal of effort has been devoted to the study of coherent structures observed in near-wall regions of turbulent flows at low Reynolds numbers [164–166]. These coherent structures are known to be self-sustaining mechanisms and are usually in the form of traveling-waves [167–169]. The procedure for identification of such coherent states involve determination of traveling-wave solutions for the Navier-Stokes equations. In general, traveling-wave solutions for equations can be systematically identified via Lie symmetry analysis. Hence, a symmetry-based approach could lead to significant advancements on the current state of knowledge regarding the coherent structures in turbulent flows. As symmetry methods are concerned with geometric properties of equations, such methods

could be used not only to identify traveling-wave solutions but also other invariant solutions that are based on different symmetry groups which will eventually lead to different coherent states.

Bibliography

[1] G. Zhong and J. E. Marsden. Lie-Poisson Hamilton-Jacobi theory and Lie-Poisson integrators. *Physics Letters A*, 133(3):134–139, 1988.

[2] P. J. Channell and C. Scovel. Symplectic integration of Hamiltonian systems. *Nonlinearity*, 3(2):231–259, 1990.

[3] R. I. McLachlan. Explicit Lie-Poisson integration and the Euler equations. *Physical Review Letters*, 71(19):3043–3046, 1993.

[4] S. Reich. Momentum conserving symplectic integrators. *Physica D: Nonlinear Phenomena*, 76(4):375–383, 1994.

[5] M. P. Calvo and E. Hairer. Accurate long-term integration of dynamical systems. *Applied Numerical Mathematics*, 18(1):95–105, 1995.

[6] O. Gonzalez and J. C. Simo. On the stability of symplectic and energy-momentum algorithms for non-linear Hamiltonian systems with symmetry. *Computer Methods in Applied Mechanics and Engineering*, 134(3):197–222, 1996.

[7] E. Hairer, C. Lubich, and G. Wanner. *Geometric Numerical Integration: Structure-Preserving Algorithms for Ordinary Differential Equations*, volume 31. Springer, 2006.

[8] R. I. McLachlan, K. Modin, and O. Verdier. Symplectic integrators for spin systems. *Physical Review E*, 89(6):061301, 2014.

[9] S. D. Webb. Symplectic integration of magnetic systems. *Journal of Computational Physics*, 270:570–576, 2014.

[10] Y. Gong, J. Cai, and Y. Wang. Some new structure-preserving algorithms for general multi-symplectic formulations of Hamiltonian PDEs. *Journal of Computational Physics*, 279:80–102, 2014.

[11] Y. He, Y. Sun, J. Liu, and H. Qin. Volume-preserving algorithms for charged particle dynamics. *Journal of Computational Physics*, 281:135–147, 2015.

[12] G. M. Webb and S. C. Anco. Vorticity and symplecticity in multi-symplectic, Lagrangian gas dynamics. *Journal of Physics A: Mathematical and Theoretical*, 49(7):075501, 2016.

[13] Y. Li and X. Wu. Functionally fitted energy-preserving methods for solving oscillatory nonlinear Hamiltonian systems. *SIAM Journal on Numerical Analysis*, 54(4):2036–2059, 2016.

[14] B. Cantwell. *Introduction to Symmetry Analysis*, volume 29. Cambridge University Press, 2002.

[15] I. M. Yaglom, H. Grant, and A. Shenitzer. *Felix Klein and Sophus Lie: Evolution of the Idea of Symmetry in the Nineteenth Century*. Birkhauser, 1988.

[16] E. Noether. Invariant variation problems. *Transport Theory and Statistical Physics*, 1(3):186–207, 1971.

[17] R. K. Gazizov and N. H. Ibragimov. Lie symmetry analysis of differential equations in finance. *Nonlinear Dynamics*, 17(4):387–407, 1998.

[18] J. M. Cornwall, D. N. Levin, and G. Tiktopoulos. Derivation of gauge invariance from high-energy unitarity bounds on the S matrix. *Physical Review D*, 10(4):1145, 1974.

[19] M. S. E. Naschie. The exceptional Lie symmetry groups hierarchy and the expected number of Higgs bosons. *Chaos, Solitons & Fractals*, 35(2):268–273, 2008.

[20] L. V. Ovsiannikov. *Group Analysis of Differential Equations*. Academic Press, 2014.

[21] N. H. Ibragimov. *CRC Handbook of Lie Group Analysis of Differential Equations*, volume 3. CRC press, 1995.

[22] F. Oliveri. Lie symmetries of differential equations: classical results and recent contributions. *Symmetry*, 2(2):658–706, 2010.

[23] P. J. Olver. Symmetry groups and group invariant solutions of partial differential equations. *Journal of Differential Geometry*, 14(4):497–542, 1979.

[24] M. Torrisi and A. Valenti. Group properties and invariant solutions for infinitesimal transformations of a non-linear wave equation. *International Journal of Non-Linear Mechanics*, 20(3):135–144, 1985.

[25] M. Oberlack. Similarity in non-rotating and rotating turbulent pipe flows. *Journal of Fluid Mechanics*, 379:1–22, 1999.

[26] A. H. Kara and F. M. Mahomed. Relationship between symmetries and conservation laws. *International Journal of Theoretical Physics*, 39(1):23–40, 2000.

[27] L. Shao-Kai and J. Li-Qun. A set of Lie symmetrical conservation law for rotational relativistic Hamiltonian systems. *Communications in Theoretical Physics*, 40(3):265–268, 2003.

[28] K. Fakhar, C. Yi, J. Xiaoda, and L. Xiaodong. Lie symmetry analysis and some new exact solutions for rotating flow of a second-order fluid on a porous plate. *International Journal of Engineering Science*, 44(13-14):889–896, 2006.

[29] S. Asghar, M. Mushtaq, and A. H. Kara. Exact solutions using symmetry methods and conservation laws for the viscous flow through expanding–contracting channels. *Applied Mathematical Modelling*, 32(12):2936–2940, 2008.

[30] R. K. Gazizov, A. A. Kasatkin, and S. Y. Lukashchuk. Symmetry properties of fractional diffusion equations. *Physica Scripta*, 2009(T136):014016, 2009.

[31] T. Aziz, F. M. Mahomed, and A. Aziz. Group invariant solutions for the unsteady MHD flow of a third grade fluid in a porous medium. *International Journal of Non-Linear Mechanics*, 47(7):792–798, 2012.

[32] H. Jafari, N. Kadkhoda, and D. Baleanu. Fractional Lie group method of the time-fractional Boussinesq equation. *Nonlinear Dynamics*, 81(3):1569–1574, 2015.

[33] B. J. Cantwell. Similarity transformations for the two-dimensional, unsteady, stream-function equation. *Journal of Fluid Mechanics*, 85(2):257–271, 1978.

[34] Y. Z. Boutros, M. B. Abd-el Malek, N. A. Badran, and H. S. Hassan. Lie-group method solution for two-dimensional viscous flow between slowly expanding or contracting walls with weak permeability. *Applied Mathematical Modelling*, 31(6):1092–1108, 2007.

[35] A. A. Avramenko, D. G. Blinov, and I. V. Shevchuk. Self-similar analysis of fluid flow and heat-mass transfer of nanofluids in boundary layer. *Physics of Fluids*, 23(8):082002, 2011.

[36] M. Jalil and S. Asghar. Flow of power-law fluid over a stretching surface: A Lie group analysis. *International Journal of Non-Linear Mechanics*, 48:65–71, 2013.

[37] R. H. Pletcher, J. C. Tannehill, and D. Anderson. *Computational Fluid Mechanics and Heat Transfer*. CRC Press, 2012.

[38] P. Wesseling. *Principles of Computational Fluid Dynamics*, volume 29. Springer Science & Business Media, 2009.

[39] R. J. LeVeque. *Finite Volume Methods for Hyperbolic Problems*, volume 31. Cambridge University Press, 2002.

[40] C. Johnson, U. Nävert, and J. Pitkäranta. Finite element methods for linear hyperbolic problems. *Computer Methods in Applied Mechanics and Engineering*, 45(1-3):285–312, 1984.

[41] G. Strang and G. J. Fix. *An Analysis of the Finite Element Method*, volume 212. Prentice-Hall Englewood Cliffs, 1973.

[42] J. L. Steger. Implicit finite-difference simulation of flow about arbitrary two-dimensional geometries. *AIAA Journal*, 16(7):679–686, 1978.

[43] J. D. Hoffman and S. Frankel. *Numerical Methods for Engineers and Scientists*. CRC press, 2001.

[44] R. F. Warming and B. J. Hyett. The modified equation approach to the stability and accuracy analysis of finite-difference methods. *Journal of Computational Physics*, 14(2):159–179, 1974.

[45] G. D. Smith. *Numerical Solution of Partial Differential Equations: Finite Difference Methods*. Oxford University Press, 1985.

[46] B. Koren. Defect correction and multigrid for an efficient and accurate computation of airfoil flows. *Journal of Computational Physics*, 77(1):183–206, 1988.

[47] K. T. Chu. Boosting the accuracy of finite difference schemes via optimal time step selection and non-iterative defect correction. *Applied Mathematics and Computation*, 218(7):3596–3614, 2011.

[48] A. P. Engsig-Karup. Analysis of efficient preconditioned defect correction methods for nonlinear water waves. *International Journal for Numerical Methods in Fluids*, 74(10):749–773, 2014.

[49] M. Razi, P. J. Attar, and P. Vedula. Grid adaptation and non-iterative defect correction for improved accuracy of numerical solutions of PDEs. *Applied Mathematics and Computation*, 269:473–487, 2015.

[50] H. Qiu, L. Mei, H. Liu, and S. Cartwright. A defect-correction stabilized finite element method for Navier–Stokes equations with friction boundary conditions. *Applied Numerical Mathematics*, 90:9–21, 2015.

[51] M. Wasserman, Y. Mor-Yossef, and J. B. Greenberg. A positivity-preserving, implicit defect-correction multigrid method for turbulent combustion. *Journal of Computational Physics*, 316:303–337, 2016.

[52] Z. Si, S. Jing, and Y. Wang. Defect correction finite element method for the stationary incompressible Magnetohydrodynamics equation. *Applied Mathematics and Computation*, 285:184–194, 2016.

[53] D. Erkmen and A. E. Labovsky. Defect-deferred correction method for the two-domain convection-dominated convection–diffusion problem. *Journal of Mathematical Analysis and Applications*, 450(1):180–196, 2017.

[54] R. S. Hirsh. Higher order accurate difference solutions of fluid mechanics problems by a compact differencing technique. *Journal of Computational Physics*, 19(1):90–109, 1975.

[55] S. K. Lele. Compact finite difference schemes with spectral-like resolution. *Journal of Computational Physics*, 103(1):16–42, 1992.

[56] M. Ciment and S. H. Leventhal. Higher order compact implicit schemes for the wave equation. *Mathematics of Computation*, 29(132):985–994, 1975.

[57] K. Mahesh. A family of high order finite difference schemes with good spectral resolution. *Journal of Computational Physics*, 145(1):332–358, 1998.

[58] W. Dai and R. Nassar. A compact finite difference scheme for solving a three-dimensional heat transport equation in a thin film. *Numerical Methods for Partial Differential Equations*, 16(5):441–458, 2000.

[59] S. E. Sherer and J. N. Scott. High-order compact finite-difference methods on general overset grids. *Journal of Computational Physics*, 210(2):459–496, 2005.

[60] R. K. Shukla, M. Tatineni, and X. Zhong. Very high-order compact finite difference schemes on non-uniform grids for incompressible Navier–Stokes equations. *Journal of Computational Physics*, 224(2):1064–1094, 2007.

[61] D. P. Rizzetta, M. R. Visbal, and P. E. Morgan. A high-order compact finite-difference scheme for large-eddy simulation of active flow control. *Progress in Aerospace Sciences*, 44(6):397–426, 2008.

[62] M. Cui. Compact finite difference method for the fractional diffusion equation. *Journal of Computational Physics*, 228(20):7792–7804, 2009.

[63] A. Shah, L. Yuan, and A. Khan. Upwind compact finite difference scheme for time-accurate solution of the incompressible Navier–Stokes equations. *Applied Mathematics and Computation*, 215(9):3201–3213, 2010.

[64] H. Yoshida. Construction of higher order symplectic integrators. *Physics Letters A*, 150(5-7):262–268, 1990.

[65] A. L. Islas, D. A. Karpeev, and C. M. Schober. Geometric integrators for the nonlinear Schrödinger equation. *Journal of Computational Physics*, 173(1):116–148, 2001.

[66] R. I. McLachlan and G. R. W. Quispel. Geometric integrators for ODEs. *Journal of Physics A: Mathematical and General*, 39(19):5251, 2006.

[67] E. Gagarina, V. R. Ambati, S. Nurijanyan, J. J. W. Van der Vegt, and O. Bokhove. On variational and symplectic time integrators for Hamiltonian systems. *Journal of Computational Physics*, 306:370–389, 2016.

[68] V. A. Dorodnitsyn. Finite difference models entirely inheriting continuous symmetry of original differential equations. *International Journal of Modern Physics C*, 05(04):723–734, 1993.

[69] M. I. Bakirova, V. A. Dorodnitsyn, and R. V. Kozlov. Symmetry-preserving difference schemes for some heat transfer equations. *Journal of Physics A: Mathematical and General*, 30(23):8139–8155, 1997.

[70] V. A. Dorodnitsyn and P. Winternitz. Lie point symmetry preserving discretizations for variable coefficient Korteweg–de Vries equations. *Nonlinear Dynamics*, 22(1):49–59, 2000.

[71] V. A. Dorodnitsyn and R. Kozlov. A heat transfer with a source: the complete set of invariant difference schemes. *Journal of Nonlinear Mathematical Physics*, 10(1):16–50, 2003.

[72] V. A. Dorodnitsyn. *Applications of Lie groups to Difference Equations*. CRC Press, 2010.

[73] X. Xiang-Peng, C. Yong, and W. Yun-Hu. A symmetry-preserving difference scheme for high dimensional nonlinear evolution equations. *Chinese Physics B*, 22(6):060201, 2013.

[74] R. Campoamor-Stursberg, M. A. Rodríguez, and P. Winternitz. Symmetry preserving discretization of ordinary differential equations. Large symmetry groups and higher order equations. *Journal of Physics A: Mathematical and Theoretical*, 49(3):035201, 2015.

[75] V. A. Dorodnitsyn, R. Kozlov, S. V. Meleshko, and P. Winternitz. Lie group classification of first-order delay ordinary differential equations. *Journal of Physics A: Mathematical and Theoretical*, 51(20):205202, 2018.

[76] C. Budd and V. A. Dorodnitsyn. Symmetry-adapted moving mesh schemes for the nonlinear Schrödinger equation. *Journal of Physics A: Mathematical and General*, 34(48):10387, 2001.

[77] F. Valiquette and P. Winternitz. Discretization of partial differential equations preserving their physical symmetries. *Journal of Physics A: Mathematical and General*, 38(45):9765, 2005.

[78] D. Levi and P. Winternitz. Continuous symmetries of difference equations. *Journal of Physics A: Mathematical and General*, 39(2):R1–R63, 2005.

[79] A. Bourlioux, C. Cyr-Gagnon, and P. Winternitz. Difference schemes with point symmetries and their numerical tests. *Journal of Physics A: Mathematical and General*, 39(22):6877, 2006.

[80] Z. Ran. Lie symmetry preservation and shock-capturing methods. *SIAM Journal on Numerical Analysis*, 46(1):325–343, 2008.

[81] R. O. Popovych and A. Bihlo. Symmetry preserving parameterization schemes. *Journal of Mathematical Physics*, 53(7):073102, 2012.

[82] D. Levi, L. Martina, and P. Winternitz. Lie-point symmetries of the discrete Liouville equation. *Journal of Physics A: Mathematical and Theoretical*, 48(2):025204, 2014.

[83] M. Fels and P. J. Olver. Moving coframes: I. A practical algorithm. *Acta Applicandae Mathematica*, 51(2):161–213, 1998.

[84] M. Fels and P. J. Olver. Moving coframes: II. Regularization and theoretical foundations. *Acta Applicandae Mathematica*, 55(2):127–208, 1999.

[85] P. Kim. Invariantization of numerical schemes using moving frames. *BIT Numerical Mathematics*, 47(3):525–546, 2007.

[86] P. Kim. Invariantization of the Crank–Nicolson method for Burgers' equation. *Physica D: Nonlinear Phenomena*, 237(2):243–254, 2008.

[87] P. Kim. *Invariantization of Numerical Schemes for Differential Equations Using Moving Frames*. University of Minnesota, 2006.

[88] M. Chhay and A. Hamdouni. Lie symmetry preservation by finite difference schemes for the Burgers equation. *Symmetry*, 2(2):868–883, 2010.

[89] M. Chhay, E. Hoarau, A. Hamdouni, and P. Sagaut. Comparison of some Lie-symmetry-based integrators. *Journal of Computational Physics*, 230(5):2174–2188, 2011.

[90] E. Ozbenli and P. Vedula. Numerical solution of modified differential equations based on symmetry preservation. *Physical Review E*, 96(6):063304, 2017.

[91] E. Ozbenli and P. Vedula. High order accurate finite difference schemes based on symmetry preservation. *Journal of Computational Physics*, 349:376–398, 2017.

[92] E. Ozbenli and P. Vedula. Construction of compact finite difference schemes. *Physical Review E*, (in preparation for submission), 2018.

[93] P. J Olver. Moving frames. *Journal of Symbolic Computation*, 36(3):501–512, 2003.

[94] A. Bihlo and F. Valiquette. Symmetry-preserving numerical schemes. In *Symmetries and Integrability of Difference Equations*, pages 261–324. Springer, 2017.

[95] É. Cartan. La méthode du repere mobile, la théorie des groupes continus, et les espaces généralisés. In *Exposés de Géometrié*, volume 5. 1935.

[96] J. Butcher, J. Carminati, and K. T. Vu. A comparative study of some computer algebra packages which determine the Lie point symmetries of differential equations. *Computer Physics Communications*, 155(2):92–114, 2003.

[97] K. T. Vu, G. F. Jefferson, and J. Carminati. Finding higher symmetries of differential equations using the MAPLE package DESOLVII. *Computer Physics Communications*, 183(4):1044–1054, 2012.

[98] S. Mukhopadhyay, M. G. Arif, and M. W. Ali. Effects of partial slip on chemically reactive solute transfer in the boundary layer flow over an exponentially stretching sheet with suction/blowing. *Journal of Applied Mechanics and Technical Physics*, 54(6):928–936, 2013.

[99] L. J. Crane. Flow past a stretching plate. *Zeitschrift für angewandte Mathematik und Physik ZAMP*, 21(4):645–647, 1970.

[100] E. Magyari and B. Keller. Heat and mass transfer in the boundary layers on an exponentially stretching continuous surface. *Journal of Physics D: Applied Physics*, 32(5):577, 1999.

[101] W. A. Khan and I. Pop. Boundary-layer flow of a nanofluid past a stretching sheet. *International Journal of Heat and Mass Transfer*, 53(11-12):2477–2483, 2010.

[102] A. Noghrehabadi, R. Pourrajab, and M. Ghalambaz. Effect of partial slip boundary condition on the flow and heat transfer of nanofluids past stretching sheet prescribed constant wall temperature. *International Journal of Thermal Sciences*, 54:253–261, 2012.

[103] M. J. Martin and I. D. Boyd. Falkner-Skan flow over a wedge with slip boundary conditions. *Journal of thermophysics and heat transfer*, 24(2):263–270, 2010.

[104] M. Vinokur. On stagnation-point conditions in non-equilibrium inviscid blunt-body flows. *Journal of Fluid Mechanics*, 43(1):49–75, 1970.

[105] R. Gilmore. Baker-Campbell-Hausdorff formulas. *Journal of Mathematical Physics*, 15(12):2090–2092, 1974.

[106] G. Strang. On the construction and comparison of difference schemes. *Journal on Numerical Analysis*, 5(3):506–517, 1968.

[107] R. Glowinski and P. L. Tallec. *Augmented Lagrangian and Operator-Splitting Methods in Nonlinear Mechanics*, volume 9. SIAM, 1989.

[108] X. Liu, S. Osher, and T. Chan. Weighted essentially non-oscillatory schemes. *Journal of Computational Physics*, 115(1):200–212, 1994.

[109] J. Gray. On certain finite difference schemes for hyperbolic systems. *Mathematics of Computation*, 18(85):1–18, 1964.

[110] B. Van Leer. Towards the ultimate conservative difference scheme. II. Monotonicity and conservation combined in a second-order scheme. *Journal of Computational Physics*, 14(4):361–370, 1974.

[111] G. A. Sod. A survey of several finite difference methods for systems of nonlinear hyperbolic conservation laws. *Journal of Computational Physics*, 27(1):1–31, 1978.

[112] A. Jameson. Numerical computation of transonic flows with shock waves. In *Symposium Transsonicum II*, pages 384–414. Springer, 1976.

[113] A. Rizzi and H. Viviand. *Numerical methods for the computation of inviscid transonic flows with shock waves: A AGAMM workshop*, volume 3. Springer-Verlag, 2013.

[114] A. Jameson, W. Schmidt, and E. Turkel. Numerical solution of the Euler equations by finite volume methods using Runge Kutta time stepping schemes. In *14th Fluid and Plasma Dynamics Conference*, page 1259, 1981.

[115] P. L. Roe. Approximate Riemann solvers, parameter vectors, and difference schemes. *Journal of Computational Physics*, 43(2):357–372, 1981.

[116] J. L. Steger and R. F. Warming. Flux vector splitting of the inviscid gas-dynamic equations with application to finite-difference methods. *Journal of Computational Physics*, 40(2):263–293, 1981.

[117] A. Jameson. Solution of the Euler equations for two dimensional transonic flow by a multigrid method. *Appl. Math. Comput*, 13(3-4):327–355, 1983.

[118] P. Woodward and P. Colella. The numerical simulation of two-dimensional fluid flow with strong shocks. *Journal of Computational Physics*, 54(1):115–173, 1984.

[119] P. L. Roe. Characteristic-based schemes for the Euler equations. *Annual Review of Fluid Mechanics*, 18(1):337–365, 1986.

[120] W. K. Anderson, J. L. Thomas, and B. Van Leer. Comparison of finite volume flux vector splittings for the Euler equations. *AIAA Journal*, 24(9):1453–1460, 1986.

[121] C. Shu and S. Osher. Efficient implementation of essentially non-oscillatory shock-capturing schemes. *Journal of Computational Physics*, 77(2):439–471, 1988.

[122] C. W. Shu and S. Osher. Efficient implementation of essentially non-oscillatory shock-capturing schemes, II. In *Upwind and High-Resolution Schemes*, pages 328–374. Springer, 1989.

[123] H. Nessyahu and E. Tadmor. Non-oscillatory central differencing for hyperbolic conservation laws. *Journal of Computational Physics*, 87(2):408–463, 1990.

[124] T. Zhang and Y. X. Zheng. Conjecture on the structure of solutions of the Riemann problem for two-dimensional gas dynamics systems. *SIAM Journal on Mathematical Analysis*, 21(3):593–630, 1990.

[125] F. Bassi and S. Rebay. High-order accurate discontinuous finite element solution of the 2D Euler equations. *Journal of Computational Physics*, 138(2):251–285, 1997.

[126] P. D. Lax and X. D. Liu. Solution of two-dimensional Riemann problems of gas dynamics by positive schemes. *SIAM Journal on Scientific Computing*, 19(2):319–340, 1998.

[127] G. Luo and T. Y. Hou. Potentially singular solutions of the 3D axisymmetric Euler equations. *Proceedings of the National Academy of Sciences*, 111(36):12968–12973, 2014.

[128] J. A. Carrillo, Y. P. Choi, E. Tadmor, and C. Tan. Critical thresholds in 1D Euler equations with non-local forces. *Mathematical Models and Methods in Applied Sciences*, 26(01):185–206, 2016.

[129] J. Bedrossian and N. Masmoudi. Inviscid damping and the asymptotic stability of planar shear flows in the 2D Euler equations. *Publications mathématiques de l'IHÉS*, 122(1):195–300, 2015.

[130] E. Feireisl, P. Gwiazda, A. Świerczewska-Gwiazda, and E. Wiedemann. Regularity and energy conservation for the compressible Euler equations. *Archive for Rational Mechanics and Analysis*, 223(3):1375–1395, 2017.

[131] J. VonNeumann and R. D. Richtmyer. A method for the numerical calculation of hydrodynamic shocks. *Journal of Applied Physics*, 21(3):232–237, 1950.

[132] S. K. Godunov. A difference method for numerical calculation of discontinuous solutions of the equations of hydrodynamics. *Matematicheskii Sbornik*, 89(3):271–306, 1959.

[133] P. D. Lax. *Hyperbolic systems of conservation laws and the mathematical theory of shock waves*, volume 11. SIAM, 1973.

[134] A. Harten, J. M. Hyman, P. D. Lax, and B. Keyfitz. On finite-difference approximations and entropy conditions for shocks. *Communications on Pure and Applied Mathematics*, 29(3):297–322, 1976.

[135] S. Osher and S. Chakravarthy. Upwind schemes and boundary conditions with applications to Euler equations in general geometries. *Journal of Computational Physics*, 50(3):447–481, 1983.

[136] S. Osher. Riemann solvers, the entropy condition, and difference. *SIAM Journal on Numerical Analysis*, 21(2):217–235, 1984.

[137] B. Van Leer. *Upwind-difference methods for aerodynamic problems governed by the Euler equations*. Technische Hogeschool Delft. Onderafdeling der Wiskunde en Informatica, 1984.

[138] A. Harten, P. D. Lax, and B. Van Leer. On upstream differencing and Godunov-type schemes for hyperbolic conservation laws. *SIAM review*, 25(1):35–61, 1983.

[139] A. Harten. On a class of high resolution total-variation-stable finite-difference schemes. *SIAM Journal on Numerical Analysis*, 21(1):1–23, 1984.

[140] P. Colella. A direct Eulerian MUSCL scheme for gas dynamics. *SIAM Journal on Scientific and Statistical Computing*, 6(1):104–117, 1985.

[141] M. Liou and C. J. Steffen Jr. A new flux splitting scheme. *Journal of Computational physics*, 107(1):23–39, 1993.

[142] R. D. Richtmyer and K. W. Morton. Difference methods for initial-value problems. *Malabar, Fla.: Krieger Publishing Co.,| c1994, 2nd ed.*, 1994.

[143] M. Liou. A sequel to AUSM: AUSM+. *Journal of Computational Physics*, 129(2):364–382, 1996.

[144] B. Van Leer. Flux-vector splitting for the Euler equation. In *Upwind and High-Resolution Schemes*, pages 80–89. Springer, 1997.

[145] C. W. Shu. Essentially non-oscillatory and weighted essentially non-oscillatory schemes for hyperbolic conservation laws. In *Advanced numerical approximation of nonlinear hyperbolic equations*, pages 325–432. Springer, 1998.

[146] B. Cockburn and C. W. Shu. The Runge–Kutta discontinuous Galerkin method for conservation laws V: Multidimensional systems. *Journal of Computational Physics*, 141(2):199–224, 1998.

[147] L. Wang and D. J. Mavriplis. Implicit solution of the unsteady Euler equations for high-order accurate discontinuous Galerkin discretizations. *Journal of Computational Physics*, 225(2):1994–2015, 2007.

[148] Z. J. Wang, Y. Liu, G. May, and A. Jameson. Spectral difference method for unstructured grids II: Extension to the Euler equations. *Journal of Scientific Computing*, 32(1):45–71, 2007.

[149] C. W. Shu. High order weighted essentially nonoscillatory schemes for convection dominated problems. *SIAM review*, 51(1):82–126, 2009.

[150] X. Zhang and C. W. Shu. On positivity-preserving high order discontinuous Galerkin schemes for compressible Euler equations on rectangular meshes. *Journal of Computational Physics*, 229(23):8918–8934, 2010.

[151] E. F. Toro and M. E. Vázquez-Cendón. Flux splitting schemes for the Euler equations. *Computers & Fluids*, 70:1–12, 2012.

[152] E. F. Toro. *Riemann Solvers and Numerical Methods for Fluid Dynamics: A Practical Introduction*. Springer Science & Business Media, 2013.

[153] A. Kurganov and E. Tadmor. Solution of two-dimensional Riemann problems for gas dynamics without Riemann problem solvers. *Numerical Methods for Partial Differential Equations: An International Journal*, 18(5):584–608, 2002.

[154] A. Harten, B. Engquist, S. Osher, and S. R. Chakravarthy. Uniformly high order accurate essentially non-oscillatory schemes, III. In *Upwind and high-resolution schemes*, pages 218–290. Springer, 1987.

[155] D. Razafindralandy, A. Hamdouni, and M. Oberlack. Analysis and development of subgrid turbulence models preserving the symmetry properties of the Navier–Stokes equations. *European Journal of Mechanics-B/Fluids*, 26(4):531–550, 2007.

[156] N. Al Sayed, A. Hamdouni, E. Liberge, and D. Razafindralandy. The symmetry group of the non-isothermal Navier–Stokes equations and turbulence modelling. *Symmetry*, 2(2):848–867, 2010.

[157] R. Verstappen. On the inertial subrange of symmetry-preserving regularization models for turbulent flow. In *PAMM: Proceedings in Applied Mathematics and Mechanics*, volume 7, pages 1100901–1100902. Wiley Online Library, 2007.

[158] M. H. Silvis, R. A. Remmerswaal, and R. Verstappen. Physical consistency of subgrid-scale models for large-eddy simulation of incompressible turbulent flows. *Physics of Fluids*, 29(1):015105, 2017.

[159] J. Ling, A. Kurzawski, and J. Templeton. Reynolds averaged turbulence modelling using deep neural networks with embedded invariance. *Journal of Fluid Mechanics*, 807:155–166, 2016.

[160] J. N. Kutz, S. L. Brunton, B. W. Brunton, and J. L. Proctor. *Dynamic mode decomposition: Data-driven modeling of complex systems*, volume 149. SIAM, 2016.

[161] B. D. Tracey, K. Duraisamy, and J. J. Alonso. A machine learning strategy to assist turbulence model development. In *53rd AIAA Aerospace Sciences Meeting*, page 1287, 2015.

[162] K. Duraisamy, Z. J. Zhang, and A. P. Singh. New approaches in turbulence and transition modeling using data-driven techniques. In *53rd AIAA Aerospace Sciences Meeting*, page 1284, 2015.

[163] B. Peherstorfer and K. Willcox. Dynamic data-driven reduced-order models. *Computer Methods in Applied Mechanics and Engineering*, 291:21–41, 2015.

[164] J. T. C. Liu. Coherent structures in transitional and turbulent free shear flows. *Annual Review of Fluid Mechanics*, 21(1):285–315, 1989.

[165] A. K. M. F. Hussain. Coherent structures and turbulence. *Journal of Fluid Mechanics*, 173:303–356, 1986.

[166] D. Rempfer and H. F. Fasel. Evolution of three-dimensional coherent structures in a flat-plate boundary layer. *Journal of Fluid Mechanics*, 260:351–375, 1994.

[167] F. Waleffe. Exact coherent structures in channel flow. *Journal of Fluid Mechanics*, 435:93–102, 2001.

[168] H. Wedin and R. R. Kerswell. Exact coherent structures in pipe flow: travelling wave solutions. *Journal of Fluid Mechanics*, 508:333–371, 2004.

[169] F. Waleffe. Three-dimensional coherent states in plane shear flows. *Physical Review Letters*, 81(19):4140, 1998.

[170] M. Oberlack. Symmetries of the Navier-Stokes equations and their implications for subgrid-models in large-eddy simulation of turbulence. In *Fundamental Problematic Issues in Turbulence*, pages 247–255. Springer, 1999.

APPENDIX A

An Invariant MUSCL Scheme for Solution of Euler Equations in 1D

In this appendix, we extend the work presented in Chapter 6 to include the procedure for construction of an invariant form of a standard MUSCL (monotonic upstream-centered scheme for conservation laws) scheme with minmod limiter for the solution of one-dimensional Euler equations. For the conservative form of one-dimensional Euler equation given in Eq. (6.1),

$$\mathbf{U}_t + \mathbf{F}(\mathbf{U})_x = 0 \tag{A.1}$$

the standard form of a slope limited MUSCL scheme, which involves use of piecewise linear reconstructions of cells, can be written as follows:

$$\mathbf{U}_i^{n+1} = \mathbf{U}_i^n + \frac{\tau}{h}\left[\mathbf{F}(\mathbf{U}^*_{i+1/2}) - \mathbf{F}(\mathbf{U}^*_{i-1/2})\right] \tag{A.2}$$

where

$$\mathbf{U}^*_{i+1/2} = \mathbf{U}^*_{i+1/2}(\mathbf{U}^L_{i+1/2}, \mathbf{U}^R_{i+1/2})$$

$$\mathbf{U}^*_{i-1/2} = \mathbf{U}^*_{i-1/2}(\mathbf{U}^L_{i-1/2}, \mathbf{U}^R_{i-1/2})$$

are scheme dependent functions and are given by

$$\mathbf{U}^L_{i+1/2} = \mathbf{U}_i + 0.5\,\phi(r_i)\,(\mathbf{U}_{i+1} - \mathbf{U}_i)$$
$$\mathbf{U}^R_{i+1/2} = \mathbf{U}_{i+1} - 0.5\,\phi(r_{i+1})\,(\mathbf{U}_{i+2} - \mathbf{U}_{i+1})$$

Table A.1
Initial configurations for one-dimensional Euler equations.

	ρ_L	ρ_R	u_L	u_R	p_L	p_R
case 1 :	1.0	1.0	0.0	0.0	7.0	10.0
case 2 :	1.0	2.5	-2.0	-2.0	40.0	40.0

$$\mathbf{U}^L_{i-1/2} = \mathbf{U}_{i-1} + 0.5\,\phi(r_{i-1})\,(\mathbf{U}_i - \mathbf{U}_{i-1})$$
$$\mathbf{U}^R_{i-1/2} = \mathbf{U}_i - 0.5\,\phi(r_i)\,(\mathbf{U}_{i+1} - \mathbf{U}_i)\ .$$

Here, the function $\phi(r_i)$ is the limiter function that limits the slope such that the solution obtained from this scheme is always TVD (total variation diminishing). In this study, we consider a minmod limiter which is given as

$$\phi(r_i) = \begin{cases} 0, & if\ r_i \le 0, \\ r_i, & if\ 0 \le r_i \le 1, \\ 1, & if\ r_i \ge 1, \end{cases}$$

where r_i is

$$r_i = \frac{\mathbf{U}_{i+1} - \mathbf{U}_i}{\mathbf{U}_i - \mathbf{U}_{i-1}}\ .$$

The invariant form of the above MUSCL scheme is simply obtained by implementing the point transformations given in Eq. 6.14 to this scheme as shown in the following:

$$\tilde{\mathbf{U}}^{n+1}_i = \tilde{\mathbf{U}}^n_i + \frac{\tilde{\tau}}{\tilde{h}}\left[\mathbf{F}(\tilde{\mathbf{U}}^*_{i+1/2}) - \mathbf{F}(\tilde{\mathbf{U}}^*_{i-1/2})\right]\ . \tag{A.3}$$

Snapshots of density (ρ), velocity, pressure, and internal energy obtained from the exact analytical solution (slid line) and the invariant MUSCL scheme with minmod limiter, Eq. (A.3), (+) are given in figures A.1 and A.2. The initial conditions used for these figures are noted in table A.1. Similar to the previously considered base numerical schemes (i.e., Lax-Friedrichs scheme, van Leer scheme), the proposed

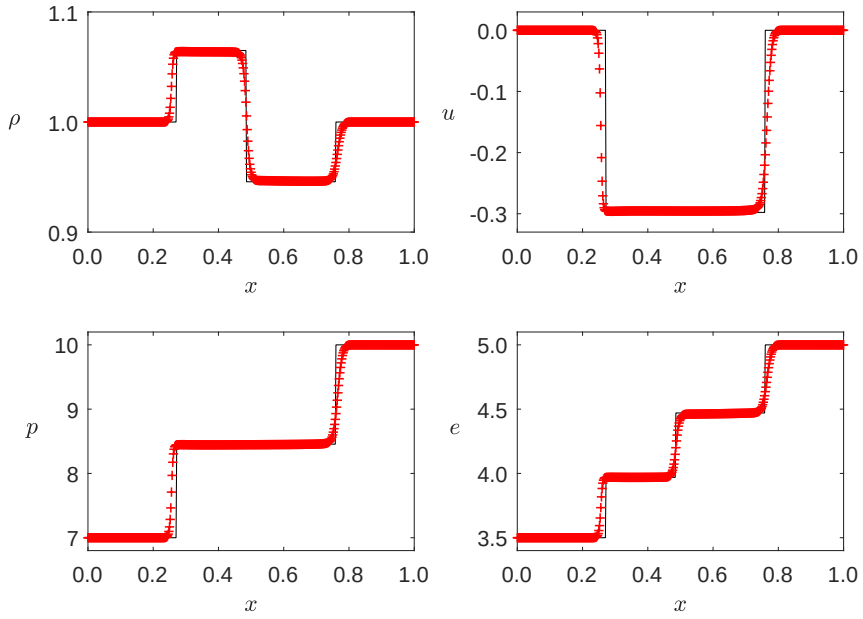

Fig. A.1. Euler equations in 1D (*case* 1). Snapshots of exact solution (solid line) and numerical solution based on the invariant MUSCL scheme with minmod limiter (+). Parameter settings: $h = 0.002$, $CFL = 0.25$, $t = 0.05$.

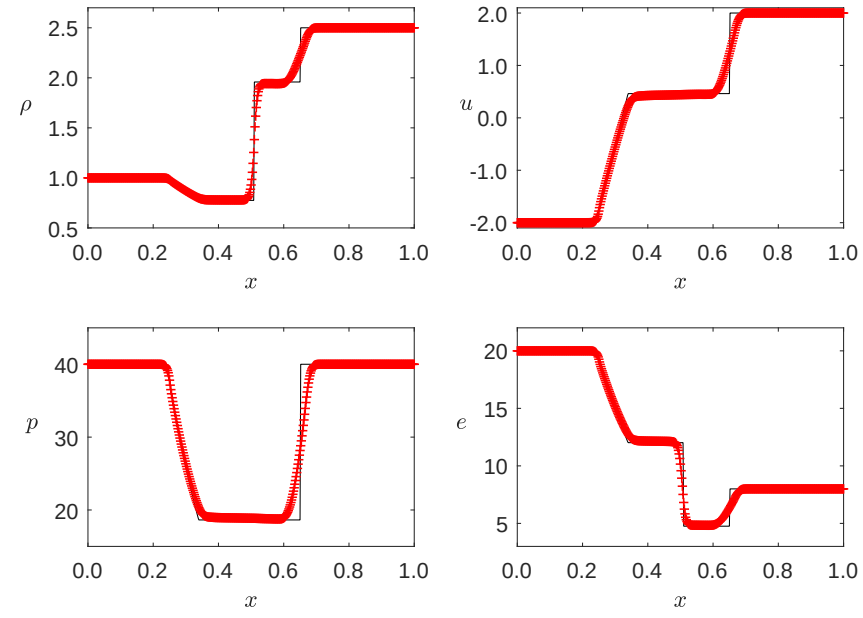

Fig. A.2. Euler equations in 1D (*case* 2). Snapshots of exact solution (solid line) and numerical solution based on the invariant MUSCL scheme with minmod limiter (+). Parameter settings: $h = 0.002$, $CFL = 0.25$, $t = 0.02$.

invariant MUSCL scheme with minmod limiter, given in Eq. (A.3), also accurately captures approximate solutions for one-dimensional Euler equations.

APPENDIX B

Lie Symmetry Groups of Euler Equations in 3D

The conservative form of the three-dimensional Euler equations can be written as

$$\mathbf{U}_t + \mathbf{F}(\mathbf{U})_x + \mathbf{G}(\mathbf{U})_y + \mathbf{H}(\mathbf{U})_z = 0 \tag{B.1}$$

where the vectors **U**, **F**, **G** and **H** represent the conserved variables and fluxes in x-, y- and z-directions, respectively, and are given by

$$\mathbf{U} = \begin{bmatrix} \rho \\ \rho u \\ \rho v \\ \rho w \\ E \end{bmatrix} \quad \mathbf{F} = \begin{bmatrix} \rho u \\ \rho u^2 + p \\ \rho uv \\ \rho uw \\ u(E+p) \end{bmatrix} \quad \mathbf{G} = \begin{bmatrix} \rho v \\ \rho uv \\ \rho v^2 + p \\ \rho vw \\ v(E+p) \end{bmatrix} \quad .\mathbf{H} = \begin{bmatrix} \rho w \\ \rho uw \\ \rho vw \\ \rho w^2 + p \\ w(E+p) \end{bmatrix} .$$

Also, u, v, and w represents fluid velocities in x-, y-, and z-coordinates, respectively, and total energy per unit volume is given by

$$E = \frac{p}{\gamma - 1} + \frac{1}{2}\rho(u^2 + v^2 + w^2) \ .$$

The Lie symmetry groups associated with the three-dimensional compressible Euler equations, Eq. (B.1), are found to be [14]

$$X_1 = \frac{\partial}{\partial t} \ , \qquad X_2 = \frac{\partial}{\partial x} \ , \qquad X_3 = \frac{\partial}{\partial y} \ , \qquad X_4 = \frac{\partial}{\partial z}$$
$$X_5 = t\frac{\partial}{\partial x} + \frac{\partial}{\partial u} \ , \qquad X_6 = t\frac{\partial}{\partial y} + \frac{\partial}{\partial v} \ , \qquad X_7 = t\frac{\partial}{\partial z} + \frac{\partial}{\partial w}$$

$$
\begin{aligned}
X_8 &= y\frac{\partial}{\partial x} - x\frac{\partial}{\partial y} + v\frac{\partial}{\partial u} - u\frac{\partial}{\partial v} \\
X_9 &= z\frac{\partial}{\partial x} - x\frac{\partial}{\partial z} + w\frac{\partial}{\partial u} - u\frac{\partial}{\partial w} \\
X_{10} &= z\frac{\partial}{\partial y} - y\frac{\partial}{\partial z} + w\frac{\partial}{\partial v} - v\frac{\partial}{\partial w} \\
X_{11} &= t\frac{\partial}{\partial t} + x\frac{\partial}{\partial x} + y\frac{\partial}{\partial y} + z\frac{\partial}{\partial z} \\
X_{12} &= t\frac{\partial}{\partial t} - u\frac{\partial}{\partial u} - v\frac{\partial}{\partial v} - w\frac{\partial}{\partial w} + 2\rho\frac{\partial}{\partial \rho} \\
X_{13} &= p\frac{\partial}{\partial p} + \rho\frac{\partial}{\partial \rho} \ .
\end{aligned}
$$

Here, the groups X_1, X_2, X_3, and X_4 represent invariance under translations in time and space, respectively, the groups X_5, X_6 and X_7 represent invariance under Galilean transformation, the groups X_8, X_9, and X_10 represent rotations about z-, y- and x-coordinates, and finally, the groups X_{11}, X_{12}, and X_{13} represent invariance under scaling. Scaling groups (X_{11}, X_{12}, and X_{13}) can be linearly combined to obtain a more general group of the form

$$
X_{14} = x\frac{\partial}{\partial x} + y\frac{\partial}{\partial y} + z\frac{\partial}{\partial z} - t\frac{\partial}{\partial t} + 2u\frac{\partial}{\partial u} + 2v\frac{\partial}{\partial v} + 2w\frac{\partial}{\partial w} + p\frac{\partial}{\partial p} - 3\rho\frac{\partial}{\partial \rho} \ .
$$

Similar to the one- and two-dimensional cases, the three-dimensional Euler equations given in Eq. (6.7) admit the following additional symmetry group

$$
\begin{aligned}
X_{11} = tx\frac{\partial}{\partial x} + ty\frac{\partial}{\partial y} + tz\frac{\partial}{\partial z} + t^2\frac{\partial}{\partial t} + (x - tu)\frac{\partial}{\partial u} + (y - tv)\frac{\partial}{\partial v} \\
+ (z - tw)\frac{\partial}{\partial w} - 5tp\frac{\partial}{\partial p} - 3t\rho\frac{\partial}{\partial \rho}
\end{aligned}
$$

for the special case of $\gamma = 5/3$ which corresponds to isentropic flow of a monatomic gas with three-degrees of freedom. Similar to the previous cases, we ignore the Galilean and rotation groups and determine point transformations based on the

remaining subgroups as follows:

$$
\begin{aligned}
\tilde{t} &= \frac{t+s_1}{\lambda}\, e^{-s_{10}} \\
\tilde{x} &= \frac{x+s_2}{\lambda}\, e^{s_{10}} \\
\tilde{y} &= \frac{y+s_3}{\lambda}\, e^{s_{10}} \\
\tilde{z} &= \frac{z+s_4}{\lambda}\, e^{s_{10}} \\
\tilde{u} &= [\lambda\, u + s_{11}(x+s_2)]\, e^{2s_{10}} \\
\tilde{v} &= [\lambda\, v + s_{11}(y+s_3)]\, e^{2s_{10}} \\
\tilde{w} &= [\lambda\, w + s_{11}(z+s_4)]\, e^{2s_{10}} \\
\tilde{p} &= \lambda^5\, p\, e^{s_{10}} \\
\tilde{\rho} &= \lambda^3\, \rho\, e^{-3s_{10}}\ .
\end{aligned}
\tag{B.2}
$$

Recall that the unknown symmetry parameters in the above point transformations can be determined by considering convenient moving frames as demonstrated in earlier chapters (i.e., Chapters 3, 4, 5 and 6). Once the point transformations are fully defined, one can chose a non-invariant base numerical scheme for the solution of the three-dimensional Euler equations and implement the above point transformations to obtain the invariant form of that particular numerical scheme (similar to the presentation in Chapter 5 for the 1D/2D Euler equations). Detailed studies on performance of such high order invariant schemes for solution of the three-dimensional compressible Euler equations will be pursued as part of future work.

APPENDIX C

Lie Symmetry Groups of Incompressible Navier-Stokes Equations

The governing (Navier-Stokes) equations describing the motion of incompressible fluid flows are given by

$$\begin{aligned} \frac{\partial u_j}{\partial x_j} &= 0, \qquad && \text{(sum over } j = 1,2,3) \\ \frac{\partial u_i}{\partial t} + u_j \frac{\partial u_i}{\partial x_j} + \frac{1}{\rho}\frac{\partial p}{\partial x_i} - \nu \frac{\partial^2 u_i}{\partial x_j \partial x_j} &= 0, \qquad && (i = 1,2,3) \end{aligned} \tag{C.1}$$

where $u_i = (u, v, w)$ represents fluid velocity components, p is the pressure, ρ is the density, and $\nu = \mu/\rho$ is the kinematic viscosity. The Lie symmetry properties of these equations have been extensively studied [14, 20, 21, 155, 156, 170]. Hence it is known that the Navier-Stokes equations admit the following Lie groups:

$$\begin{aligned} X_1 &= \frac{\partial}{\partial t} \\ X_2 &= g[t]\frac{\partial}{\partial p} \\ X_{3,i,j} &= x_j \frac{\partial}{\partial x_i} - x_i \frac{\partial}{\partial x_j} + u_j \frac{\partial}{\partial u_i} - u_i \frac{\partial}{\partial u_j}\ , \qquad && i = 1,2, \quad j > i = 1,2,3 \\ X_{4,i,k} &= a_i[t]\frac{\partial}{\partial x_j} + a_i'[t]\frac{\partial}{\partial u_j} - a_i''[t]\frac{\partial}{\partial p}\ , \qquad && i = j, \text{ and } i = 1,2,3 \\ X_5 &= 2t\frac{\partial}{\partial t} + x_i \frac{\partial}{\partial x_i} - u_i \frac{\partial}{\partial u_i} - 2p\frac{\partial}{\partial p} \qquad && i = 1,2,3 \end{aligned} \tag{C.2}$$

where $a_i[t]$ is a twice differentiable, arbitrary function of time and the notation $(\cdot)'$ represents differentiation with respect to time. For simplicity, let us consider the function $a_i[t]$ (associated with the symmetry group $X_{4,i,k}$) to be a constant for one

case (i.e., $k=1$), and be equal to t for another (i.e., $k=2$). This would indicate two different group operators corresponding to spatial translations for $k=1$ and Galilean transformations for $k=2$. In the above Lie symmetry groups: X_1 represents invariance under translation in time, X_2 represents invariance under translation in pressure (when $g[t]$ is a constant), $X_{i,j}$ represents invariance under rotations, $X_{4,i}$ represent invariance under Galilean transformations, and finally X_5 represents invariance under scaling.

The general form of the point transformations associated with the symmetry group given in Eq. (C.2) are as follows

$$\begin{aligned}
&\tilde{t} = (t+s_1)\, e^{2s_5} \\
&\tilde{x}^i = [x^j + s_{4,i,1} + s_{4,i,2}(t+s_1)]\, e^{s_5} \ , && i=1,2,3 \\
&\tilde{u}^i = (u^i + s_{4,i,2})\, e^{-s_5} \ , && i=1,2,3 \\
&\tilde{p} = (p+s_2)\, e^{-2s_5}
\end{aligned} \tag{C.3}$$

when the rotation groups given in $X_{3,i,j}$ are ignored for simplicity reasons. After determination of the unknown symmetry parameters through convenient selections of moving frames, these point transformations can be implemented in a non-invariant base numerical of scheme of choice to obtain its invariant form as demonstrated throughout various chapter of this dissertation (i.e., Chapters 4, 5 and 6).